DEPARTMENT OF ELECTRONIC & ELECTRICAL ENGINEERING

University of Strathclyde Engineering

PLASMA-WATER INTERFACE REACTIONS CAUSED BY POSITIVE CORONA AND GLOW DISCHARGES

A thesis presented in fulfilment of the requirement for the degree of

Doctor of Philosophy

Zhongshu Zhang, B.Eng(Honours)

2020

Department of Electronic and Electrical Engineering

University of Strathclyde

Glasgow, UK

Declaration of Authenticity and Author's Rights

‘This thesis is the result of the author’s original research. It has been composed by the author and has not been previously submitted for examination which has led to the award of a degree.’

Signed: Zhongshu Zhang

Date: 21/09/2020

Acknowledgement

Firstly, I would like to thank Dr. Tao Wang for providing the opportunity of doing this PhD project. During the past several years, I have always been appreciating his help in this research, as well as the caring in my study and life. We had hundreds of interesting discussions on science and technology, which would be unforgettable experiences in my life.

I would like to express thanks to Prof. Scott MacGregor for the supervision, support and the help. Many thanks to Dr. Igor Timoshkin for his invaluable advice and discussions through my research. Many thanks to Dr. Michelle MacLean for their generous help in the research, especially providing chemical and biometric advice and instruments. I would like to express my gratitude to Dr. Martin Given and Dr. Mark Wilson for their comments and corrections on my academic paper.

Thanks to all the staff in the High-Voltage Workshop: Sean Doak, Andy Carlin, Frank May, and David Griffin for their help in machining reactors and experimental equipment in this research. Many thanks to Mrs. Maureen Cooper for her patient assistance and order of laboratory supplies.

Thanks to all my colleagues in the HVT Research Group. We had many interesting discussions, as well as colourful days in the lab. I would like to express my special thanks to my good friend, Dr. Ying Sun, for the five years we have had together in Glasgow. There are so many warm memories that I would never forget in my life.

I would also like to thank my family for their great help and love in my life. Particularly, I would like to express my appreciation to my wife. Her companionship, help and love, make me full of passion and happiness for life.

Abstract

Plasma in and in contact with water has drawn extensive attention in the field of advanced oxidation processes, due to its advantages of producing various reactive species such as O, OH, HO_2, H_2O_2 and O_3 in water. Plasma-water interface reactions are one of the core challenges in this field since it involves multiple physical and chemical processes leading to complex mechanism of mass/energy transfer and reactive species production at interface. Exploration of the plasma-water interface reactions would promote the wide application of plasma in environmental remediation and plasma medicine.

The objective of this research is to investigate the interface reactions between water cathode and positive plasma produced by two types of gas discharges: corona discharge producing low energy drift positive ions and glow discharge producing energetic positive ions. A nine-needle electrode was developed to initiate d.c. corona discharge in nitrogen and oxygen. The experiments with a mesh cathode above water and a water cathode were conducted to explore the effects of ions and reactive neutral species. Glow discharge was generated between a single-needle anode and water cathode in nitrogen, oxygen and helium. The electrical characteristics of the discharges have been studied. The treated solutions have been investigated, including hydrogen peroxide (H_2O_2) production, pH and conductivity change. The effects of gas flow rate, gas pressure and hydroxyl radical (OH) scavengers on H_2O_2 production were studied.

In corona discharges, the contribution of positive ions and reactive neutral species to H_2O_2 production has been quantified. An analytical model that describes interface processes has been developed. The drift positive ions accumulated on water surface acted as ion-anode, on which the adsorbed hydroxyl radical (•OH) and oxygen radical (•O) were formed. The H_2O_2

production under both nitrogen corona discharge and oxygen corona discharge was proved not from the OH dimerization.

In glow discharge, the amount of hydrogen peroxide (H_2O_2) produced by each positive ion has been proved higher than that in corona discharge, which is thought caused by the large kinetic energy of positive ions. In nitrogen and helium glow discharge, the majority of H_2O_2 production was found to be from OH dimerization. Oxygen glow discharge did not produce OH in water. The effects of ions' kinetic energy and potential energy on the interface reactions were discussed.

List of Abbreviations

ABS	Absorbance
AOPs	Advanced Oxidation Processes
AC	Alternating Current
CO_2	Carbon Dioxide
DBD	Dielectric Barrier Discharge
DMSO	Dimethyl Sulfoxide
eV	Electron Volt
d.c.	Direct Current
GDE	Glow Discharge Electrolysis
H_2O_2	Hydrogen Peroxide
H_2SO_4	Sulfuric Acid
HNO_2	Nitrous Acid
HNO_3	Nitric Acid
HTA	Hydroxyterephthalic Acid
KCl	Potassium Chloride
LF	Low-frequency
MB	Methylene Blue
MB	Methylene Blue
M	Mole per Liter
mM	Mili-mole per Litre
mol	Mole

ns	Nanosecond
NaOH	Sodium Hydroxide
NO	Nitric Oxide
NO_2	Nitrogen Dioxide
n_e	Electron Density
OH	Hydroxyl Radical
ONOOH	Peroxynitrous Acid
PTFE	Polytetrafluoroethylene
PVC	Polyvinyl Chloride
RNO	N,N-dimethyl-p-nitrosoaniline
RF	Radio-frequency
SLPM	Standard Litre per Minute (0 ℃, 1 atm)
TA	Terephthalic Acid
TB	Tert-butanol
T_e	Electron Temperature
UV	Ultraviolet
µs	Microsecond

Contents

1. Introduction

1.1 Motivation

Advanced oxidation processes (AOPs) relying on producing strongly oxidative hydroxyl radicals (OH) have attracted significant attention in water treatment since it was first proposed in 1987 by Glaze et al [1]. Their work reviewed the OH yield in the systems of ozone (O_3) at high pH, ozone/hydrogen peroxide (O_3/H_2O_2) ratios, ozone/ultraviolet radiation (O_3/UV), and H_2O_2/UV. OH radicals can non-selectively and rapidly oxidize multiple types of non-degradable organics (such as aromatics, dyes, pharmaceuticals and pesticides [2]) and volatile organic compounds to water, carbon dioxide and inorganic salt without introducing hazardous by-products in sewage water. Therefore, by generating strong oxidizing free radicals (particularly OH) in situ, which can significantly degrade organic contaminants, AOP is expected to become the ultimate solution for water treatment in the future [11].

In addition to conventional AOPs, the interaction of plasma and liquid water can also produce large quantities of active substances in water, including OH, H_2O_2, O_3, radical oxygen (O), hydroperoxyl radical (HO_2), UV light and shockwaves [3]. Compared with conventional AOPs techniques, plasma-water interactions have the benefits of no chemical consumables, vast array of oxidation processes, superior decomposition rates and simple structures. This implies that plasma induced AOPs have the potential to revolutionise conventional water treatment techniques with extensive applications [3].

To improve the OH yield, a lot of researchers focused on the plasma and water interaction mechanisms. Samukawa et al. reviewed recent research and summarized the processes occurred at the interface of air plasma and water [4] as shown in Figure 1.1. They spatially divided the plasma-water interaction into

three parts: gas phase, interface and bulk liquid. In gas phase, three types of active species are produced by plasma: positive ions, reactive neutral species and UV light. Both the positive ions and UV light interacting with water can ionize or decompose water molecules, producing water ions, aqueous electrons and reactive neutral species (eg. O, H and OH). Simultaneously, the evaporation and electrolysis of water also occurs at the interface. Although some processes have been discovered, a variety of physical and chemical processes, e.g. the transfer mechanisms of charged species, neutrals and radicals between liquid phase and gas phase, have not been fully identified [4]. These unknown mechanisms limit the understanding of plasma-water interactions, and thus the optimization in the application of plasma-induced AOPs.

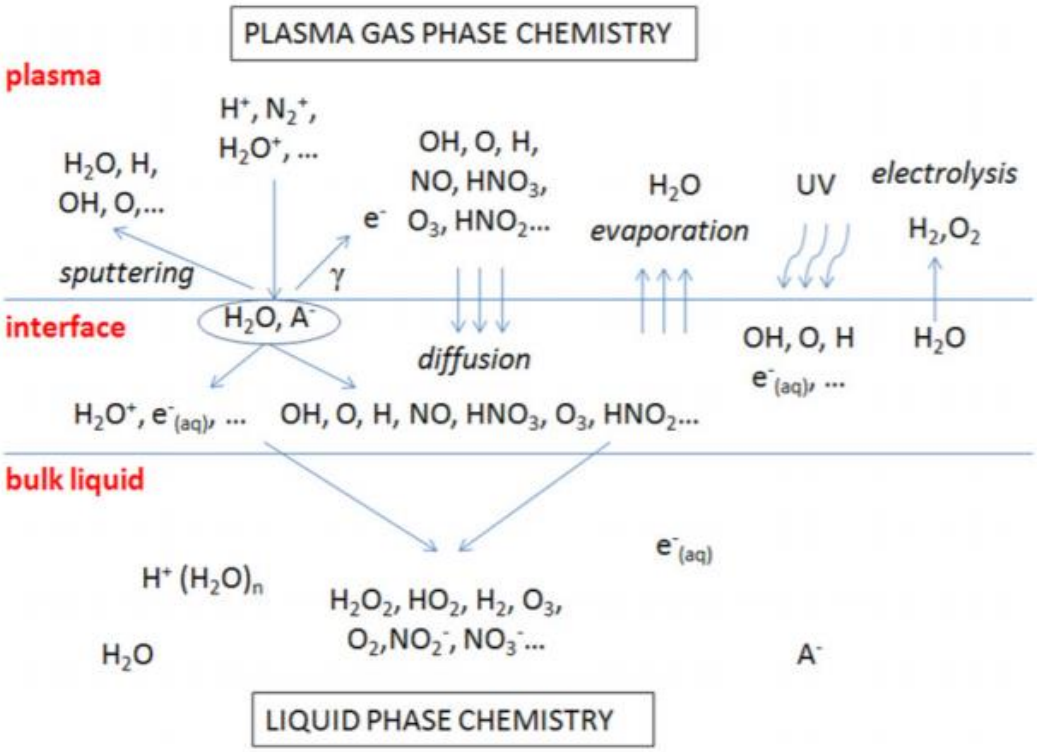

Figure 1.1 Interface processes in the air plasma–liquid cathode interaction [4].

1.2 Objectives

There are two general states for plasma: equilibrium and non-equilibrium. For plasma in equilibrium state, the temperature of electrons, ions and neutrals is almost equal, and normally the background gas temperature reaches thousands of kelvin degree, hence it is also called thermal plasma; for plasma in non-equilibrium state, the electron temperature is much higher than ions and neutrals, and the background gas temperature barely rises, hence it is also called non-thermal plasma [203]. For non-thermal plasma, the energy is mainly used for accelerating electrons, which can ionize and dissociate the background gas to produce radicals that destroy contaminants, without dissipating much energy on gas heating [203]. This research focused on the investigation of non-thermal plasma and water interface reaction mechanisms, especially the effect of the kinetic energy and potential energy of positive ions on the interface reactions. Two discharge types, including corona discharge and glow discharge, were employed, both in contact with water. A novel reactor with nine-needle electrode has been developed to generate d.c. corona discharges in two gases: nitrogen and oxygen; a single-needle electrode has been developed to generate d.c. glow discharges in three gases: nitrogen, oxygen and helium.

For corona discharges, experimental tests with water cathode and mesh cathode have been conducted to investigate the effects of low energy drift positive ions and reactive neutral species on the production of H_2O_2 in water. The interface reactions with accumulated positive ions on water surface as ion anode have been diagrammed. For glow discharges, a series of tests have been conducted to investigate the effects of energetic positive ions on the production of H_2O_2 in water. By comparing the results of corona discharges and glow discharges, the difference of interface reactions caused by low energy and energetic ions has been determined.

The contribution of this study is the investigation of the interface reactions caused by energetic and low energy positive ions, thereby determining the effects of kinetic energy and potential energy of positive ions in the production of OH and H_2O_2. This work also analysed the limiting factors of energy yield of OH and H_2O_2 in water by positive ions. These findings are important for determining the plasma-water interface reaction mechanism and improving the energy efficiency of water treatment by plasma.

1.3 Thesis outline

The thesis is comprised of seven chapters. Chapter 1 introduces the background and the objectives of the research.

The current status of AOPs technology is introduced in chapter 2. The fundamentals of plasma-based water treatment techniques are reviewed. The characteristics and types of plasma in contact with water are discussed, including corona discharge, streamer discharge, glow discharge, gliding arc discharge and dielectric barrier discharge. The chemical and physical reactions in gas phase and aqueous phase, as well as the generation mechanisms of reactive species like O_3, H_2O_2, OH and HO_2 are reviewed.

Chapter 3 introduces the methodologies and experimental setup of the research. There are two types of gas discharges used, one is a corona discharge generated between a nine-needle electrode and water; the other is a glow discharge generated between a single needle electrode and water. The gas flow and control systems are introduced. The electrical systems, including the circuit design and components are detailed. The preparation of solutions, including deionized water, TB, DMSO, sulphuric acid and potassium titanium (IV) oxalate was introduced. The analysis methods for H_2O_2, pH and conductivity of the treated solution are provided.

Chapter 4 shows the experimental results of the interface reactions between water and the ionic wind generated by positive d.c. corona discharge in nitrogen. The effects of plasma treatment time, gas flow rate and OH scavengers (TB and DMSO) on H_2O_2 production are presented. The influences of the mesh cathode on the ionic wind are analysed. The Faraday efficiency and energy yield of H_2O_2 production are discussed. By comparing the results of mesh cathode group and liquid cathode group, the effects of drift positive ions and active neutral species on H_2O_2 production, liquid pH and liquid conductivity are discussed separately. It was found that 1 mol of positive drift ions produced 0.13 mol of hydrogen peroxide in water under atmospheric pressure, equalling the contribution of the active neutral species. A reduced gas pressure tends to increase the contribution from the positive drift ions, with 1 mol of ions producing 0.29 mol of hydrogen peroxide at 100 Torr. The addition of OH scavengers (TB and DMSO) did not reduce H_2O_2 production. The reactions of positive drift ions and water produce adsorbed (·OH) and (·O) at the interface between ionic wind and water; the transfer of reactive neutral species HO_2 and H_2O_2 in gas phase to water lead to the production of aqueous H_2O_2 in nitrogen corona discharge.

Chapter 5 presents the experimental results of the reactions between water and the ionic wind generated by positive d.c. corona discharge in oxygen. It was found that 1 mol of positive drift ions produced 0.2 mol of hydrogen peroxide at atmospheric pressure, while 0.69 mol of hydrogen peroxide was produced by reactive neutral species. When the gas pressure was decreased to 200 Torr, the corresponding hydrogen peroxide production by positive drift ions increased to 0.45 mol. A maximum energy efficiency of 0.307 g/kWh for hydrogen peroxide production was achieved at 200 Torr. The amount of ozone generated did not have much influence on the production of hydrogen peroxide in water.

Chapter 6 introduces the results of the interface reactions between d.c. glow discharge and water. The d.c. glow discharge was generated between single-

needle electrode and the water cathode in nitrogen, oxygen and helium. At atmospheric pressure, the highest Faraday efficiency of H_2O_2 production in deionized water was 1.28 in nitrogen, 0.98 in helium and 1.13 in oxygen. The highest energy yield of H_2O_2 production was 2.33 g/kWh, achieved in nitrogen at 100 Torr. Nitrogen glow discharge reduced the pH of deionized water to 3.6 and increased its conductivity to 250 μS/cm. A reduced gas pressure significantly increased the Faraday efficiency of H_2O_2 production by nitrogen glow discharge, reaching 1.39 at 100 Torr. The addition of OH scavengers (TB and DMSO) significantly reduced H_2O_2 production in water under nitrogen and helium glow discharge but not in oxygen.

Chapter 7 compares and concludes the plasma and water interface reactions using corona and glow discharge in contact with water. In corona discharges in nitrogen and oxygen, both positive drift ions and reactive neutral species produce hydrogen peroxide, not hydroxyl radicals, in water. The hydrogen peroxide produced by glow discharge in nitrogen and helium is mainly from the dimerization of OH species generated in water, but not in oxygen glow discharge.

Future work should focus on the chemical compositions in both gas phase and aqueous phase, which can provide more detail for analysing the plasma and water interface reaction mechanisms. A method to increase the energy efficiency of plasma-induced reactive species production in water is proposed.

2. Literature Review

2.1 Introduction

The application of advanced oxidation processes (AOPs) in water treatment has been extensively researched in the past three decades [5]. The ability of AOPs to degrade organic pollutants is mainly based on the on-site generation of highly reactive hydroxyl radicals, which can non-selectively react with organic compounds in water with a rate constant order of $10^8 – 10^{10}$ $Lmol^{-1}s^{-1}$ [6]. The large reaction rate constant indicates that the effective degradation rate and wide applicability of hydroxyl radicals to various organic contaminants in water. As discussed below, typical conventional AOPs constitute [7-12]:

- UV-based processes (OH produced by UV light irradiation in the presence of H_2O_2 /O_3 /Cl_2)
- Ozone-based processes (OH produced by ozone in the presence of oxidants (H_2O_2)/catalysts (Fe^{2+}, Mn^{2+} etc.)/alkaline environment (Ph>8.5))
- Catalysts-based processes (OH produced by Fenton reaction, photocatalytic process)

The conventional AOPs can achieve oxidation of organic pollutants by producing large amount of OH using ozone, hydrogen peroxide, UV light or photolysis. Nevertheless, the high cost of conventional AOPs caused by consumption of chemicals (e.g. H_2O_2) and energy of producing ozone or UV light limits the large-scale application of AOPs.

In addition to the conventional AOPs, plasma-induced AOPs have drawn attention due to their advantage of no chemical consumption and simultaneously producing various reactive species, i.e. UV light, OH, H, HO_2, H_2O_2, O, O_3, NO,

peroxynitrite ($ONOO^-$), NO^{2-}, and NO^{3-}. Various types of gas discharges have been proposed, including corona discharge, glow discharge, arc discharge and dielectric barrier discharge (DBD). There are numerous electrode configurations for plasma-water reactions, as shown in Figure 2.1. The configuration determines the parameters of plasma and the way it is in contact with water.

Figure 2.1(A) represents a direct liquid phase discharge, which relies on a strong electrical field (on the order of 1 MV/cm [204]) built in microseconds, normally by a pulsed power. Such discharges in liquid can have an electron density up to $10^{26}/m^3$ and a gas temperature of 5000 K [13]. The current of liquid phase discharge is mainly conducted by the motion of ions in the liquid, rather than electron movement [4]. There is no acknowledged principle for the breakdown mechanism in liquid discharge. Some researchers have suggested that the discharges are ignited in the pre-existing bubbles or bubbles produced by the voltage [14]. As discharge in liquid is generated in water or water vapour directly, the reactive species produced can be different from that of discharges in typical gases. By electron collision or thermal dissociation, the water molecules are decomposed to radicals (H, OH and O), which can recombine to form reactive species (HO_2, H_2O_2, H_2 and O_2). These reactive species are produced directly in liquid and can react with organic pollutants rapidly.

Figure 2.1(B) represents a gas phase discharge contacting liquid indirectly, such as gas phase reactive species produced in a plasma jet being carried to a liquid surface. Plasma jets are often generated by DBDs with fast gas flow, which enhances the reactive species production and transport from the gas phase to liquid. Helium and argon are commonly used in plasma jet generation. In plasma jet, the gas discharge is not electrically coupling with the liquid and, as ions and electrons rarely reaching the liquid in this type of discharge, neutral species (metastables, atoms and radicals etc.) are the dominant components in

the interface reactions. A typical pulsed plasma jet has a gas temperature of 300-400 K, an ionization degree of 10^{-5}-10^{-6} and a radical density (e.g. OH, O) of 10^{19}-10^{21} m^{-3} [15].

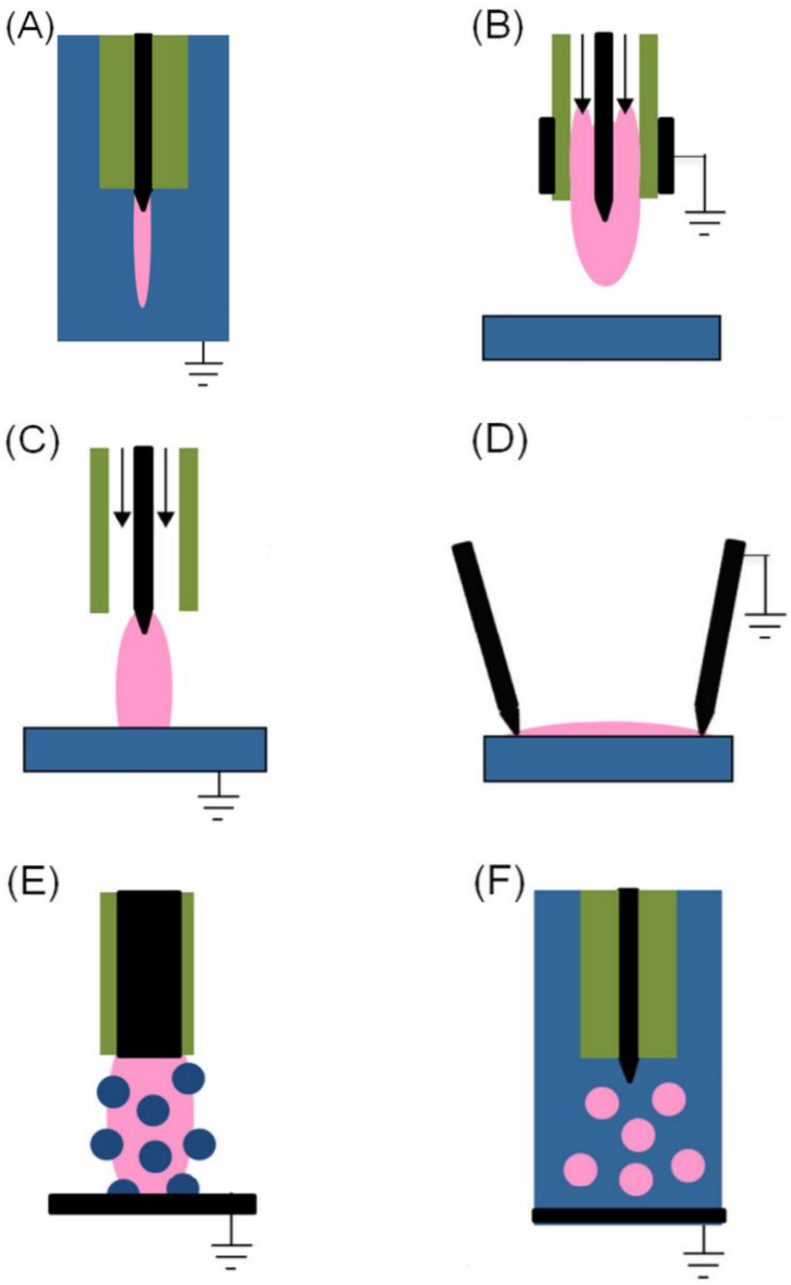

Figure 2.1 Typical electrode configurations for plasma-water reactions. (A) direct discharge in water; (B) plasma jet without direct contact with water; (C) gas phase discharges with water electrode; (D) gas phase discharge along water surface; (E) gas phase discharge with water spray and (F) discharges in bubbles. Blue = liquid, pink = plasma, green = dielectric, black = metal electrodes [4].

Figure 2.1(C) shows a gas phase discharge with the liquid as one electrode. In such cases there is an electrical coupling between the discharge and liquid. In this kind of configuration, one or both electrodes can be liquid. One typical application of this configuration is glow discharge electrolysis. At the plasma-water interface, gases produced by electrolysis and water vapour from the evaporation constitute the vapour layer. When a liquid cathode is used, the evaporation is much more efficient [16]. Xiong et al. investigated the OH density distribution in an atmospheric glow discharge with liquid electrode. They found that the OH density can reach 10^{23} m^{-3} in both water-cathode and water-anode discharges [17]. In water-cathode discharges, the maximum OH density is found in the region close to water surface; while in water-anode discharges, the maximum OH density is found in the region close to the metal electrode [17].

Figure 2.1(D) shows a gas phase discharge along a liquid surface. This configuration provides direct contact between plasma and liquid without electrical coupling relations. A typical configuration is a flashover which is caused by streamer discharge propagating at the gas-liquid interface. The propagation velocity can be up to 10 km/s [18]. As the discharge is along the liquid surface, the reactive species can easily enter the liquid phase.

Figure 2.1(E) and Figure 2.1(F) show multiphase plasmas, which can be generated in gas phase with water spray or in liquid phase with gas bubbling. This configuration can increase the contact area between plasma and water, which can increase the reactive species production. Locke et al. found that the yield of H_2 and H_2O_2 were up to 13 and 81 g/kWh with argon carrier in a pulsed gliding arc discharge with water spray [18]. They speculated that the high energy yield is attributed to the condensed water droplets, which can capture the radicals and significantly prevent the radicals' quenching in gas phase [18]. However, the large contact area between plasma and liquid in this configuration

also contributed to the high energy yield. Discharges in bubbles are normally generated with gas feeding along the high-voltage electrode. The plasma is formed inside the bubble before the bubble leaves the electrode and propagates along the gas-liquid interface [19]. It has been reported that the discharges in bubbles can produce plasmas with electron density up to 10^{22} m^{-3} and electron temperature of 8-10 eV [20]. Reactive species H, O, and OH were detected in the gas discharge in helium, argon, and oxygen bubbles [20, 21]. When with oxygen bubbling, ozone was also detected in water [21].

Although plasma-water reactions have been extensively researched, many critical physical and chemical processes remain unknown. These unknown mechanisms include [4]:

i) The transport of positive and negative ions at the plasma–liquid interface.
ii) The transport of low energy electrons (<1 eV) at the plasma-liquid interface.
iii) The lifetime and the state of hydrated electrons.
iv) The relationship between reactive neutral species related reactions and temperature/pressure.
v) Energy transfer mechanisms at the plasma-liquid interface.
vi) The integrated effects of pH, temperature and electrical field on liquid phase reactions.
vii) Reaction rate between heavy particle and fast atoms/vibrationally excited H_2O and OH.
viii) Comprehensive interpretation of the ignition and ionization processes of liquid discharge.

As explored in this chapter, the complexity of plasma compositions and highly dynamic process at plasma-liquid interface result in numerous challenges in understanding the interface reactions. Investigations of these challenging

questions will benefit the wide applications of plasma in environmental engineering, plasma medicine and material synthesis. This chapter discusses the status of the research on plasma-water reactions, involving various types of gas discharges and typical reactions in gas phase, liquid phase and interface. The production of reactive species is investigated, especially the formation mechanisms. These analyses provide the fundamental knowledge and guidance for the experimental research undertaken in the later chapters.

2.2 Gas Discharge types for plasma-water reactions

2.2.1 Corona discharge for plasma-water reactions

2.2.1.1 Corona discharge in gas phase

In corona discharge, the electric field is not uniform due to the specific geometry [143]. The local electric field around a sharp electrode is much stronger than that in remote locations. In gas phase, as the discharge voltage increases, initially the local electric field near the electrode becomes intense enough to ionize the surrounding gas but not high enough to cause an electrical breakdown between electrodes. According to the geometry, the corona discharge can be defined as positive corona, negative corona, bipolar corona, ac corona and HF corona. The typical electrode configurations of corona discharge applied in water treatment are pin-to-plate, wire-to-cylinder and wire-to-plate.

Compared with other discharges, corona discharge has a drift region with weak electric field connecting the ionization region and the passive electrode. In the drift region, the low density of ions can only acquire small kinetic energy under the weak electric field. The movement of drift ions can generate an ionic wind, which also carries the reactive neutral species. The ions and reactive neutral species can react with water to produce reactive agents, such as O, OH, and HO_2 [22].

Magureanu et al. investigated the production of H_2O_2 and degradation of methylene blue (MB) under pulsed negative corona discharge in oxygen generated using a multi-wire-plate configuration above water [23]. The voltage and current waveforms are shown in Figure 2.2. It was observed that the MB solution was decolourized rapidly after the plasma treatment. The concentration of H_2O_2 increased with plasma treatment time, and reached 200 mg/L in distilled water and 137 mg/L in MB solution after 30-minute treatment [23]. They also found that the concentration of H_2O_2 and MB continued to decrease after the treatment, which demonstrates that the reactive species still react with MB in the post-discharge period.

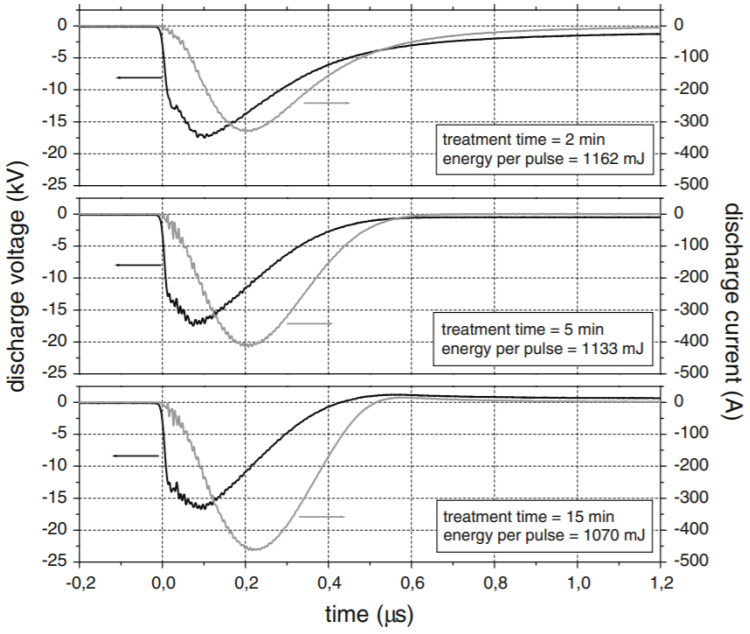

Figure 2.2 Voltage and current waveforms for corona discharge generated by multi-wire-plate geometry above water [23].

Corona discharges can take place in the gas close to water, or directly in water, to produce reactive species. The energy efficiency of ozone generation by pulsed positive corona discharge in air above water is up to 40 g/kWh [24]. In addition to ozone, OH was also detected in the corona discharge above water [25].

2.2.1.2 Corona discharge in liquid phase

Pulsed corona discharge in liquid phase can produce O, H, OH and H_2O_2 [25, 26]. The density of these reactive species can be increased by using positive polarity rather than negative polarity of d.c. voltage, bubbling gases or increasing the discharge voltage [25]. Akiyama stated that streamer discharges in water can produce fast electrons, ozone, reactive species, UV lights and shock waves [27]. Sun applied optical emission spectra to detect the reactive species produced by a pulsed corona discharge generated with a needle-plane electrode in water: hydroxyl radicals, atomic hydrogen and atomic oxygen were detected during discharge [28]. Figure 2.3 illustrates an optical emission spectrum of the pulsed streamer corona discharge in distilled water. They found that the increase of pulse voltage and gas (oxygen and argon) injection leaded to an increase in hydroxyl radical density. When the conductivity of liquid was increased by the addition of either potassium hydroxide (KOH) and potassium chloride (KCl), the hydroxyl radical emission intensity increased initially but then declined [28].

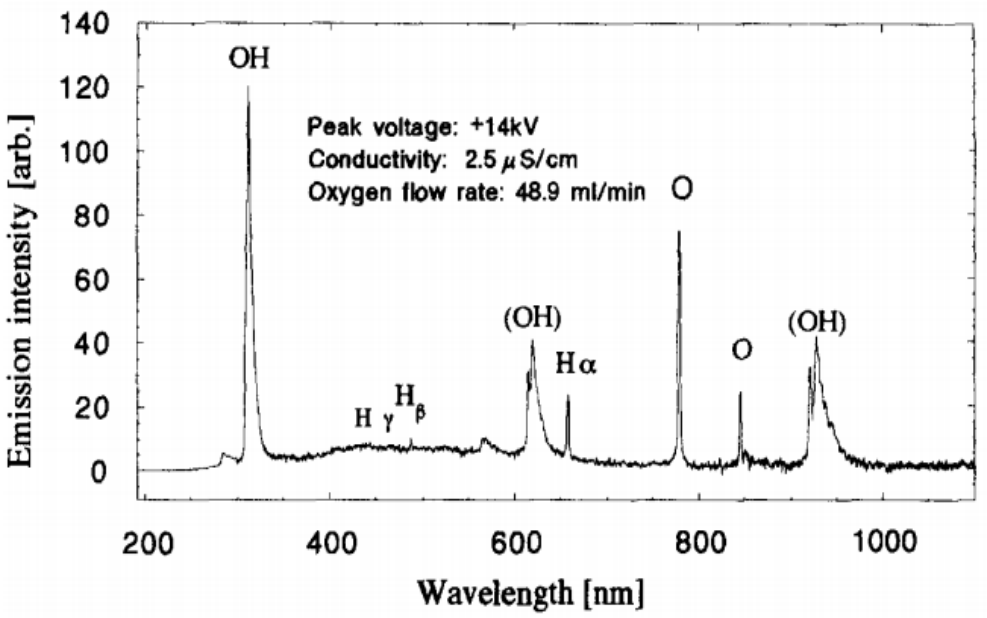

Figure 2.3 Emission intensity of reactive species produced by streamer discharge in distilled water with needle-plate system [28].

Michael et al. investigated the reactive species produced by underwater pulsed positive corona discharge. Their reactor configuration is shown in Figure 2.4, with a typical voltage-current waveform shown in Figure 2.5. In the experiments, 13 mol of H_2O_2, 26 mol of H_2 and 5 mol of O_2 was produced in water with 1 mol of passing electrons [26]. This ratio is much larger than Faraday's law values, demonstrating that the reactive species were produced in the plasma instead of an electrochemical process on the electrode surface. The overall reaction they proposed for the pulsed discharge under water is [26]:

$$6H_2O \rightarrow 4H_2 + 2H_2O_2 + O_2 \qquad \text{(R 2.1)}$$

However, the energy efficiency of hydrogen production by the underwater pulsed discharge did not show results comparable with electrolysis, because the discharge voltage in electrical discharge is much higher than that in electrolysis [26]. The high ratio only indicates that the formation mechanism of H_2O_2, H_2 and O_2 by electrical discharges is different from that by the electrolysis.

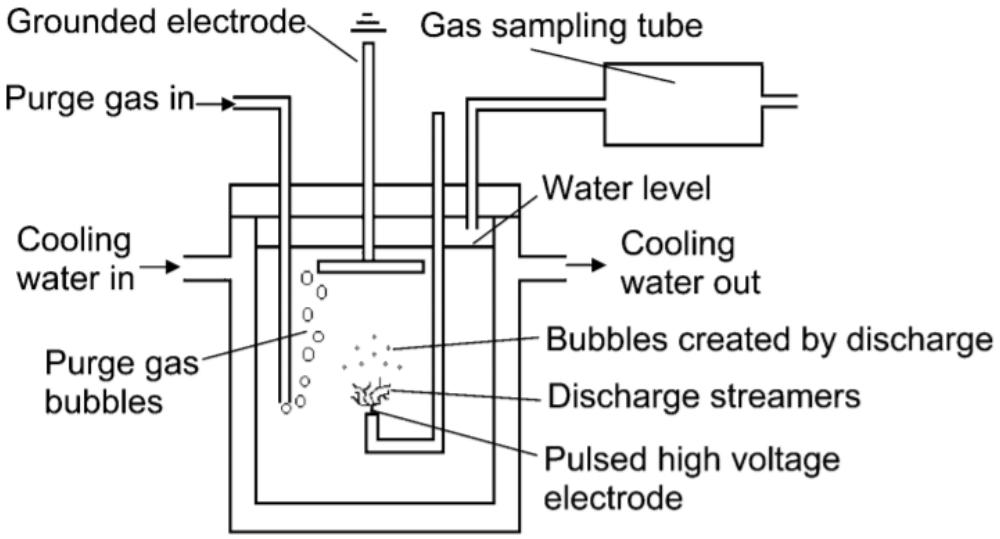

Figure 2.4 Reactor configuration for underwater corona discharge. Note: the purge gas act as a carrier and did not contact with plasma [26].

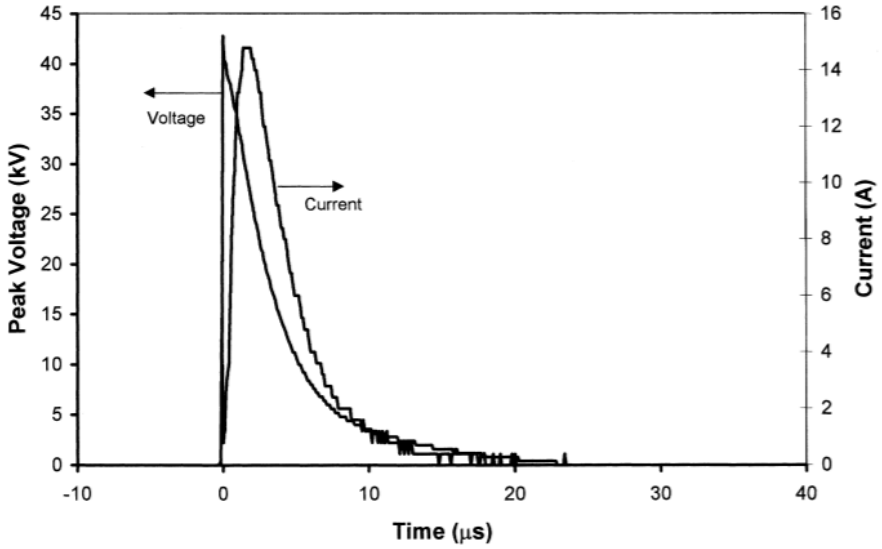

Figure 2.5 Voltage and current waveforms of the pulsed corona discharge under water in 150 mS/cm KCl solution [29].

2.2.2 Glow discharge for plasma-water reactions

The glow discharge is a type of luminous plasma. The luminosity is due to the visible light emission in the excited collisions caused by numerous energetic electrons. The glow discharge in or in contact with water was found effective for water treatment. Many studies have proved that glow discharge in or in contact with water can produce reactive species such as hydroxyl radical, atomic hydrogen and hydrogen peroxide [30-34], which are effective for water decontamination and sterilization.

There are different types of electrode configurations in glow discharge in or in contact with water. Glow discharge electrolysis (GDE) was first reported in electrochemistry in 1887, with a glow-discharge plasma as the anode and a grounded liquid as the cathode [34]. As Figure 2.6 shows, a typical glow discharge has five regions: from anode to cathode, the five regions are anode glow, positive column, negative glow, cathode dark region and cathode spot [34]. Lu et al. observed the AC glow discharge generated with metal-water electrodes and found the structure (negative glow, anode dark space, positive column, negative glow and cathode fall region) was consistent with that of regular glow discharge between metal electrodes [35].

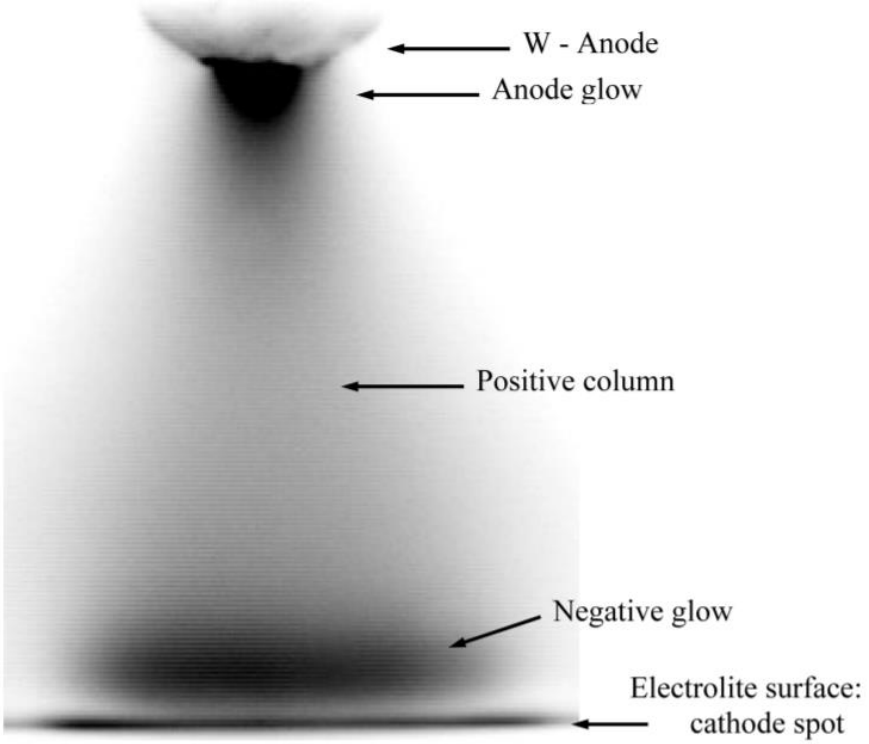

Figure 2.6 CCD camera picture of glow discharge with electrolyte cathode [34].

The plasma-water interaction in glow discharge electrolysis involves charge transport, energy conversion and chemical reactions. Since the water acts as the cathode, the mechanism of secondary electron emission in GDE is different from that with a metallic cathode. The positive ions can be accelerated significantly in the cathode dark space region. When the energised positive ions impact the water cathode, numerous water molecules are ionized by the collision to H_2O^+ and solvated electrons in the surface water [34]. Some of the produced H_2O^+ can recombine with solvated electrons e_{aq} to form water molecules. Simultaneously, some H_2O^+ will dissociate to H^+ and OH. In deionized water, the self-quenching reaction to form H_2O_2 will dominate the OH consumption. O_2 can be produced via hydrogen peroxide decomposition [36]. The secondary electron emission from the water cathode is based on the chemical tunnel effect. In this process the energy required for one electron

emission is 1.56 eV, which is much smaller than 6.1 eV for direct electron emission from water [37].

Verreycken et al. investigated the positive column of atmospheric d.c. glow discharge with pin-water electrode, in which the estimated order of electron temperature and density are 1 eV and 10^{19} m^{-3} [38]. Malik compared 27 types of plasma reactors for treating pollutants in water, found that the energy efficiency of contact glow discharge is at the bottom of the reviewed discharges [39]. This is possibly due to the large percentage of input energy is dissipated in heating the liquid [39].

It has been proved that the reaction between water and glow discharge can produce hydroxyl radicals [38, 40]. Sugama et al. generated low-pressure (20 Torr) glow discharge in saturated water vapor between a disc anode and water cathode using three power sources: i.e., d.c. low-frequency (LF) (100 kHz) and radio-frequency (RF) (13.56 MHz) power sources [40]. They found that the $OH(A^2\Sigma^+ - X^2\Pi)$ emission intensity was the strongest near the water surface, and increases as the discharge power increases, demonstrating efficient OH production near the water surface [40]. However, as Figure 2.7 illustrates, the $OH(A^2\Sigma^+ - X^2\Pi)$ intensity is also high when getting close to the metal electrode in RF discharge. When adding N, N-dimethyl-p-nitrosoaniline (RNO) or methylene blue in water, it was found that the target compound was degraded by OH near the plasma-contact solution surface and the reaction rate was limited by slow diffusion of the compound in the liquid [40].

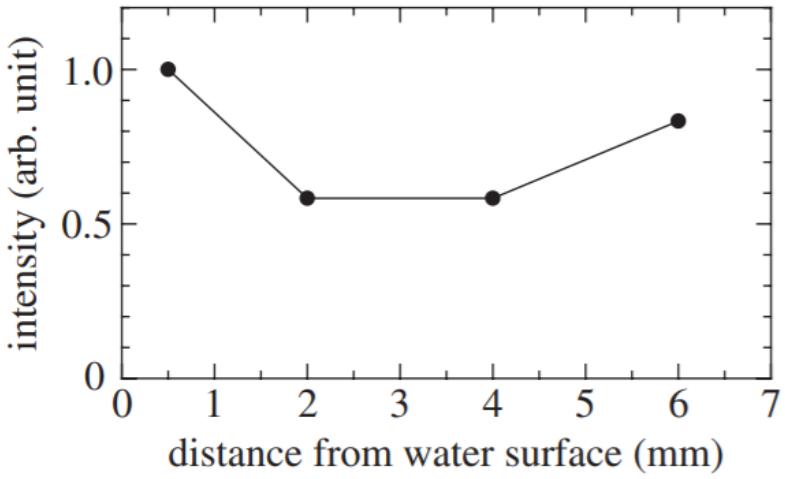

Figure 2.7 Spatial distribution of $OH(A^2\Sigma^+ - X^2\Pi)$ produced by RF glow discharge between water and stainless-steel disc electrode [40].

In addition to the glow discharge over the water surface, a glow discharge can also be generated under water. A typical electrode configuration is illustrated in Figure 2.8. The underwater glow discharge commonly develops from normal electrolysis by a thin wire or needle electrode. The development process of underwater glow discharge can be divided into four stages, with the typical V-I characteristics for a positive electrode as Figure 2.9 shows. The first stage is conventional electrolysis: the currents rises linearly as the discharge voltage on the pin increases from zero to several hundred volts. The electrolysis current can be up to several hundred milli-Amperes (mA). A lot of gas bubbles are produced around the wire or needle tip, which can separate the water from the electrode. In the second stage, as the voltage continues to increase, sporadic discharges are generated in the gas bubbles between the electrode and water. As the discharge voltage increases, the current begins to decrease. Both the voltage and current are fluctuating due to the unstable gas gap in this stage. In the third stage, the current stays constant as voltage continues to increase. A stabilized gas sheath is formed around the electrode. If the voltage continues to increase, the process enters the fourth stage, and a brightly visible glow

discharge appears. In this stage the current increases linearly as the voltage rises [41].

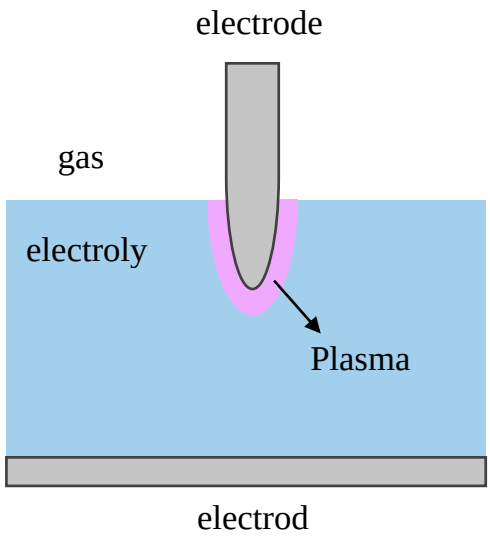

Figure 2.8 Schematic electrode configuration of glow discharge under water.

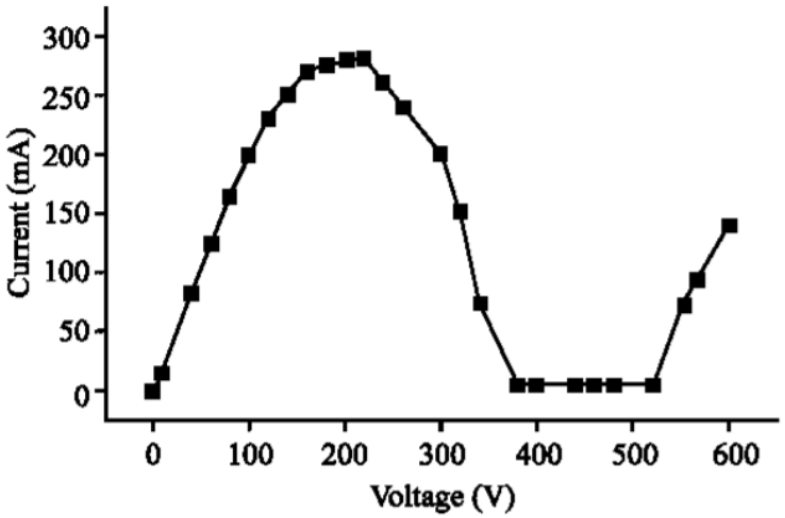

Figure 2.9 Typical V-I characteristics of glow discharge electrolysis [41].

Contact glow discharge electrolysis is a non-equilibrated discharge which has been proved by optical emission spectra to produce radicals such as O, OH and H [33, 42]. These radicals can combine to form H_2, O_2 and H_2O_2 [33, 43], whose yield is reported to be higher than Faraday's law values [43]. Sengupta et al. reported 3.92 mol of H_2 and 1.70 mol of H_2O_2 can be produced by an anodic contact glow discharge electrolysis with 1 mol of electrons passing [43]. Both plasma zone and interface reactions are thought contribute to the yield [43].

2.2.3 Gliding arc discharge for plasma-water reactions

Either a.c. or d.c. power supply can be used to generate gliding arc discharge. The breakdown occurs firstly at the shortest gap between the blade electrodes. Plasma will be formed within 1 microsecond (μs) of breakdown and the voltage drops [44]. In the first stage, the plasma channel is stable and in thermodynamic equilibrium; as the channel keeps gliding to a wider gap region, the plasma state enters non-equilibrium stage and cools down rapidly to a gas temperature of 1000 K, however, the conductivity is maintained due to the high electron temperature (1 eV) [44]. The gliding arc will keep moving to a wider gap until it exceeds the critical length, the heat losses of plasma would be higher than that provided by the power supply, resulting in plasma decay [44]. After the decay, a new breakdown occurs at the shortest gap and the cycle process continues to repeat [44].

The electrode configurations for the reaction between gliding arc discharge and water can be divided into two types: gliding arc discharge over water surface, see Figure 2.10, and gliding arc discharge with water-gas mixture spray, see Figure 2.11. In the gliding arc discharge over water surface, the plasma region was blown toward the water surface by high-speed gas, so that reactive species produced in the gas phase can enter the water. The water can also be an electrode in this case. In the gliding arc discharge with water-gas mixture spray, the sliding arc discharge has larger contact area with water.

The interaction between water and gliding arc discharges has been shown to produce reactive species, such as OH, O_3 and H_2O_2 [45, 46]. Other products, e.g. nitrides, can also be produced in water with nitrogen and air injection [45]. Compared to gliding arc discharge over water surface, the gliding arc discharge with gas-water mixture spray can produce more hydrogen peroxide [45].

The degradation of organic compounds by gliding arc discharge was also investigated. Du et al. applied gliding arc discharge in the gas-liquid mixture spray and achieved the degradation of acid orange 7 [46]. The degradation efficiency varied with feeding gas: oxygen > air > argon > nitrogen [46]. Highest production of hydrogen peroxide and ozone was achieved with oxygen feeding, which may explain the highest degradation rate by feeding oxygen [46].

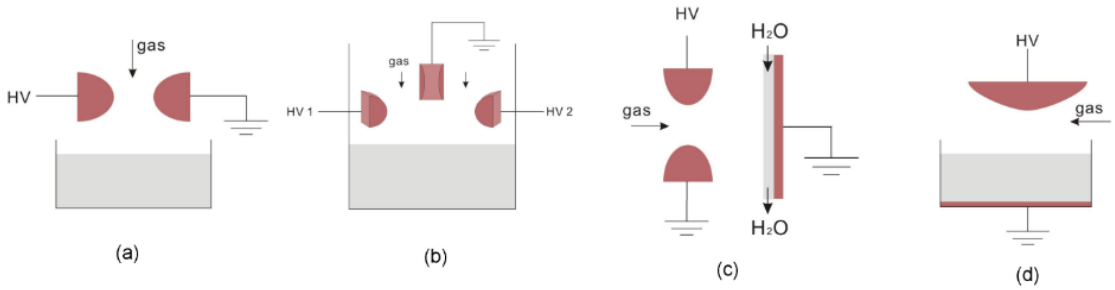

Figure 2.10 Typical electrode configurations of gliding arc discharge over water surface [47].

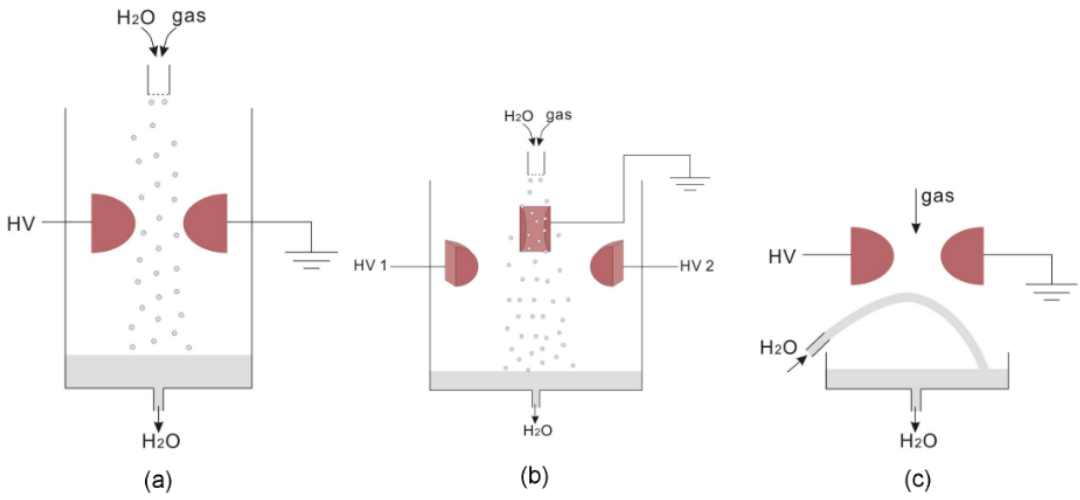

Figure 2.11 Typical electrode configurations of gliding arc discharge with water-gas mixture spray [(a), (b)] and water spray (c) [47].

Burlica et al. found that pulsed sliding arc discharges can increase the yield of hydrogen peroxide and the degradation of organic dyes by hundreds of times compared to AC sliding arc discharges. [48]. In AC gliding arc discharge, the energy yield of hydrogen peroxide was 0.13 g/kWh with argon as the feed gas and 0.21 g/kWh with oxygen as the feed gas; while in pulsed gliding arc discharge, the yield of hydrogen peroxide was 35.7 g/kWh with argon as the feed gas and 54.5 g/kWh with oxygen as the feed gas [48]. Such a huge difference indicated that a large amount of energy was wasted in Joule heating or in destroying produced reactive species in AC gliding arc discharges [48]. The gas composition was found to be critical for hydrogen peroxide production, but has little effect on organic dye removal, indicating that the decolorization was probably caused by electron collisions or thermal processes [48].

2.2.4 Dielectric barrier discharge for plasma-water reactions

Dielectric barrier discharge (DBD) is a type of high-pressure non-thermal gas discharge generated with insulating material between electrodes. Normally, DBD is generated using an AC power supply. Numerous random micro

discharges are produced in the inter-electrode space in DBD. Table 2.1 introduces the characteristics of the micro discharges generated in a 1-mm air gap at 1 bar [49]. The advantage of DBD is that the energetic electrons in the discharges can break the molecular bonds in the gaseous species to produce excited atoms and radicals. DBD are widely applied in industry, including ozone generator, surface and material processing, excimer ultraviolet radiation and treatment of gas pollutants.

Table 2.1 Typical parameters of micro discharges in 1 mm air gap at 1 bar [49].

Parameters	Value
Duration	1-10 ns
Filament radius	100 μm
Peak current	0.1 A
Current density	100-1000 A/cm^2
Ionization degree	10^{-4}
Total charge	0.1-1nC
Electron density	10^{14}-$10^{15}/cm^3$
Electron average energy	1-10 eV
Gas temperature	300 K
Energy density	1-10 mJ/cm^3
Dissipated energy	1 μJ

The interaction between water and DBD has been proved to produce multiple types of reactive species which are capable of water decontamination and sterilization. Laurita et al. analysed the reactive species produced by nanosecond pulsed DBD in air. A decrease of pH and an increase of

conductivity were observed in the treated deionized water. Reactive species, including H_2O_2, NO_2^- and NO_3^- were formed in water [50]. After discharge, H_2O_2 and NO_2^- continued to react in the treated water to form NO_3^- and peroxynitrous acid (ONOOH), of which the latter demonstrated sterilization effect. Part of the formed ONOOH can decompose to OH and NO_2 and then degrade organic compounds, such as phenol [50]. Huang et al. investigated the gas-phase reactive species produced in the reaction between water and DBD with optical emission spectral analysis [51]. The emission intensity of reactive species is shown in Figure 2.12. The main reactive species in the gas phase are O_3, OH^+, N_2O^+, NO and H_2O^+ [51].

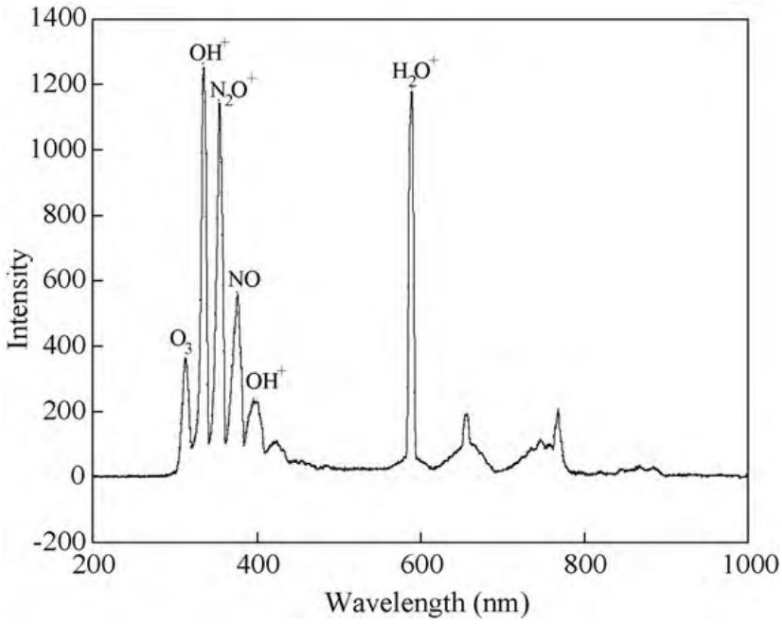

Figure 2.12 Emission spectrum of gas-phase reactive species produced by DBD in atmospheric air [52].

In DBDs, the micro discharges are distributed evenly over the liquid surface, increasing the contact area between plasma and water. The dispersed energetic electrons can increase the production of reactive species, especially UV light, O, and O_3. However, OH and H_2O_2 production by DBD does not show

competitive results compared with other gas discharge types. Locke reviewed DBDs over liquid and found that the energy yield of H_2O_2 production of the reviewed research is in the range of 0.26-2.7 g/kWh [53].

2.3 Plasma-water reactions

As discussed above, gas discharges interacting with water can produce a range of reactive species with a variety of efficiency. Comprehension of the reactions occurring in plasma-water interaction processes is critical for controlling the reaction paths and to improve the yield of reactive species. This section focused on the plasma-water reactions involving different gases.

2.3.1 Plasma-water reactions at interface

Plasm-water reactions at the interface can be classified into three types:

- Reactions caused by positive ions
- Reactions caused by electrons
- Reactions caused by neutral species

For the positive discharges above water cathode, the energized ions bombard the water surface and ionize water molecules [54]:

$$P^+ + xH_2O \rightarrow (x-1)H_2O^* + H_2O^+ + P \qquad \text{(R 2.2)}$$

Where P^+ is the positive ion, H_2O^* is an excited water molecule, H_2O^+ is a positively ionized water molecule and x is the number of impacted water molecules. The excited water molecules are unstable and will decompose to H_2O^+ and electrons:

$$xH_2O^* \rightarrow xH_2O^+ + xe_{aq} \qquad \text{(R 2.3)}$$

Some of the produced x H_2O^+ recombine with hydrated electrons to form H_2O; and some will decompose (assume the number is n, and given that there is one

H_2O^+ directly produced by P^+ as reaction R 2.2 shows, the total number of H_2O^+ is n+1) [54], hence:

$$(n+1)H_2O^+ \rightarrow (n+1)OH + (n+1)H^+ \qquad \text{(R 2.4)}$$

The produced hydrogen ion, H^+, can easily solvate in water. The produced hydrated electrons can be scavenged by H^+ to form H, some of which can transfer to gas phase and provide the secondary electron emission [54]:

$$H \rightarrow e_{aq} + H^+ \qquad \text{(R 2.5)}$$

A schematic description of the interface processes caused by positive ions is shown in Figure 2.13.

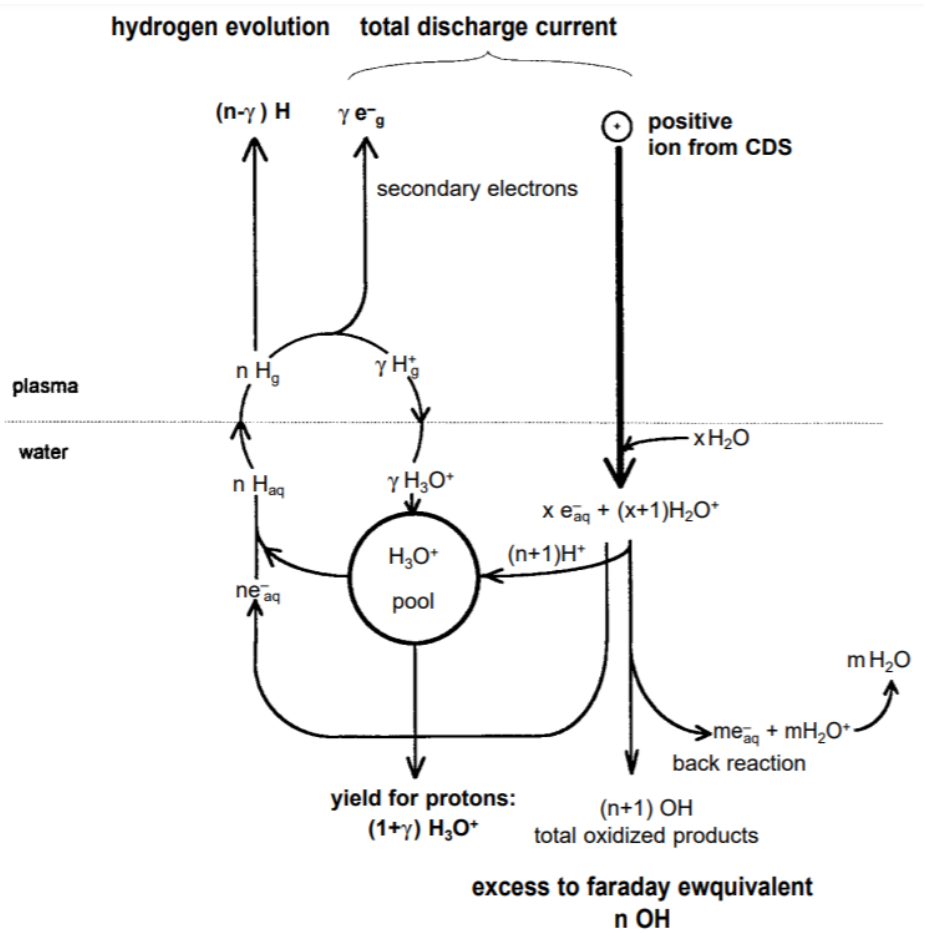

Figure 2.13 Plasma-water interface processes caused by a positive ion. γ is the secondary electron emission coefficient [36].

There are two types of reactions caused by the electrons at plasma-water interface: reactions caused by highly energetic electrons and reactions caused by low energy electrons. The highly energetic electrons impacting interface can cause excitation, dissociation and ionization of water molecules [4, 43]:

$$e + H_2O \rightarrow H_2O^* + e \quad \text{(R 2.6)}$$

$$e + H_2O \rightarrow H + OH + e \quad \text{(R 2.7)}$$

$$e + H_2O \rightarrow H_2O^+ + 2e \quad \text{(R 2.8)}$$

$$e + H_2O \rightarrow H + OH^- \quad \text{(R 2.9)}$$

For the reactions caused by low energy electrons, the electrons enter the aqueous water and form solvated electron e_{eq}, which can recombine with positive ions P_g^+ at the interface to form neutral species P_g (or react with water molecules to produce OH^- and H_2) [4, 55]:

$$e_{gas} \rightarrow e_{aq} \quad \text{(R 2.10)}$$

$$e_{aq} + P_g^+ \rightarrow P_g \quad \text{(R 2.11)}$$

$$2e_{aq} + H_2O \rightarrow 2OH^- + H_2 \quad \text{(R 2.12)}$$

In most cases, the electrons produced by plasma have energies of 1-10 eV. The overall interface reactions caused by positive plasma and negative plasma are shown in Figure 2.14.

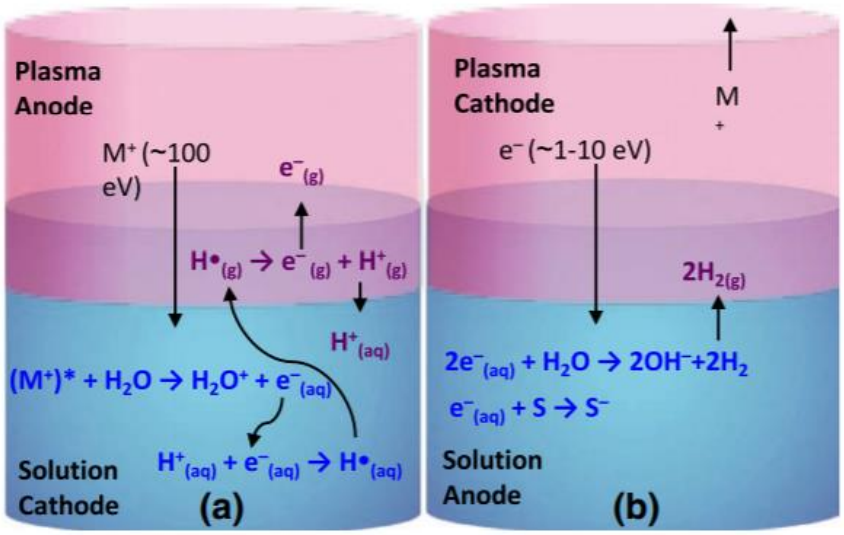

Figure 2.14 Interface reactions caused by positive ions (a) and electrons (b), where M^+ is the positive ion [56].

The neutral species, including excited molecules, excited atoms and radicals, can react with water molecules at the interface. These reaction processes are similar to those occurring in the gas phase. In addition to the chemical reactions, there are some physical processes occurring at the interface, such as evaporation of water and organic molecules transferring form liquid to gas. All these processes occur simultaneously at the interface and may affect each other. As a result, the interface processes are poorly understood and need more analysis.

2.3.2 Plasma-water reactions involving nitrogen

In the gas phase, the energetic electrons from the discharges ionize nitrogen molecules to nitrogen ions:

$$N_2 + e \rightarrow {N_2}^+ + 2e \qquad \text{(R 2.13)}$$

In the presence of water vapor, all the nitrogen ions react with water molecules rapidly to form water ions, which continue to react with water molecules to produce hydroxyl radicals and hydrogen ion [56]:

$$N_2{}^+ + H_2O \rightarrow H_2O^+ + N_2 \quad \text{(R 2.14)}$$

$$H_2O^+ + H_2O \rightarrow H^+ + OH + H_2O \quad \text{(R 2.15)}$$

In addition to ionization process, the molecules can be dissociated or excited by the electrons [52]:

$$N_2 + e \rightarrow N + N + e \quad \text{(R 2.16)}$$

$$N_2 + e \rightarrow N_2^* \quad \text{(R 2.17)}$$

The excited nitrogen molecule $N_2(A)$ or excited nitrogen atom $N(^2D)$ can decompose water molecules [57]:

$$N_2(A) + H_2O \rightarrow OH + H + N_2(X) \quad \text{(R 2.18)}$$

$$N(^2D) + H_2O \rightarrow OH + NH \quad \text{(R 2.19)}$$

In reaction R 2.18, $N_2(X)$ is the ground state nitrogen molecule.

The nitrogen atom can react with a hydroxyl radical to produce NO, which can be further oxidized to nitrous acid (HNO_2) [52]:

$$N + OH \rightarrow NO + H \quad \text{(R 2.20)}$$

$$NO + OH \rightarrow HNO_2 \quad \text{(R 2.21)}$$

The formed HNO_2 can be oxidized to nitric acid (HNO_3) [52]:

$$HNO_2 + OH \rightarrow NO_2 + H_2O \quad \text{(R 2.22)}$$

$$NO_2 + OH \rightarrow HNO_3 \quad \text{(R 2.23)}$$

Reactions R 2.21 - R 2.23 demonstrate that NO, NO_2 and HNO_2 consume OH in the gas phase.

In aqueous phase, the dissolved NO_x react mutually or react with O_2 to generate nitrates and nitrites, which leads to the pH of the solution decreasing. This process normally occurs in the post-discharge stage [58].

$$NO_2 + NO_2 + H_2O \rightarrow {NO_2}^- + {NO_3}^- + 2H^+ \quad \text{(R 2.24)}$$

$$NO + NO_2 + H_2O \rightarrow 2{NO_2}^- + 2H^+ \quad \text{(R 2.25)}$$

The formed ${NO_2}^-$ can recombine with hydrogen ion [58]:

$${NO_2}^- + H^+ \leftrightarrow HNO_2 \quad \text{(R 2.26)}$$

In acidic solutions, the nitrous acid (HNO_2) formed is unstable and will decompose to nitrogen dioxide radical ($NO_2\cdot$) and nitric oxide radical ($NO\cdot$) [58], which can respectively react with dissolved O_2 to form ${NO_3}^-$ and ${NO_2}^-$ in the solution [59, 60]:

$$2HNO_2 \rightarrow NO + NO_2 + H_2O \quad \text{(R 2.27)}$$

$$4NO\cdot + O_2 + 2H_2O \rightarrow 4{NO_2}^- + 4H^+ \quad \text{(R 2.28)}$$

$$4NO_2\cdot + O_2 + 2H_2O \rightarrow 4{NO_3}^- + 4H^+ \quad \text{(R 2.29)}$$

In the presence of H^+, nitrite can react with hydrogen peroxide to produce peroxynitrite [58, 61]. Peroxynitrite (ONOO) and its conjugated acid (ONOOH) are highly oxidizing and cytotoxic because they react with proteins, lipids, and DNA [58, 62]. Peroxynitrite is also thought to be the key factor for sterilization of plasma activated water.

$$H_2O_2 + {NO_2}^- + H^+ \rightarrow ONOOH + H_2O \quad \text{(R 2.30)}$$

Additionally, ONOOH is formed in water via reaction:

$${O_2}^{\cdot -} + NO_2\cdot \rightarrow ONOOH \quad \text{(R 2.31)}$$

The cytotoxicity of peroxynitrite can be decomposed to either hydroxyl radical and nitrogen dioxide radical or nitrate ion and hydrogen ion in acidic environments [58, 63]. Reaction R 2.32 is a reversible reaction and is considered the formation pathway of ONOOH. The ratio of the ONOOH decomposition through reaction R 2.32 and R 2.33 is 30% and 70% respectively.

$$ONOOH \leftrightarrow OH + NO_2 \quad \text{(R 2.32)}$$

$$ONOOH \rightarrow NO_3^- + H^+ \quad \text{(R 2.33)}$$

2.3.3 Plasma-water reactions involving oxygen

In the gas phase, the energetic electrons ionize and dissociate O_2 [52, 57]:

$$O_2 + e \rightarrow O_2^+ + 2e \quad \text{(R 2.34)}$$

$$O_2 + e \rightarrow O + O + e \quad \text{(R 2.35)}$$

With massive oxygen presence, O_2^+ can combine with O_2 to form O_4^+ [65]:

$$O_2^+ + 2O_2 \rightarrow O_4^+ + O_2 \quad \text{(R 2.36)}$$

The potential energy of both O_2^+ (12.06 eV) and O_4^+ (11.66 eV) is lower than the ionization energy of H_2O (12.62 eV) [64], so that their charge does not transfer to H_2O directly. However, Good et al. found that with trace water vapour (concentration of 0.34%) in oxygen, almost all O_2^+ transferred the positive charge to water molecule to form $H^+(H_2O)_n$ within 400 μsec. The proposed charge-transfer mechanism is shown below [65]:

$$O_2^+ + H_2O + O_2 \rightarrow O_2^+(H_2O) + O_2 \quad \text{(R 2.37)}$$

$$O_4^+ + H_2O \rightarrow O_2^+(H_2O) + O_2 \quad \text{(R 2.38)}$$

$$O_2^+(H_2O) + H_2O \leftrightarrow O_2^+(H_2O)_2^* \rightarrow H^+(H_2O) + OH + O_2 \quad \text{(R 2.39)}$$

Then $H^+(H_2O)$ combines with H_2O molecules to produce cluster $H^+(H_2O)_n$.

In addition, as shown below, oxygen atoms can react with oxygen, water and hydrogen in the gas phase [57]:

$$O + O_2 \rightarrow O_3 \quad \text{(R 2.40)}$$

$$O(^1D) + H_2O \rightarrow OH + OH \quad \text{(R 2.41)}$$

$$O + H_2 \rightarrow OH + H \quad \text{(R 2.42)}$$

$$H + O_2 \rightarrow OH + O \quad \text{(R 2.43)}$$

Gas-phase ozone dissolves in aqueous phase

$$O_{3(g)} \rightarrow O_{3(aq)} \quad \text{(R 2.44)}$$

In aqueous phase (alkaline solution, with the presence of OH^-), ozone decomposes to radical species OH and HO_2 [66]:

$$2O_{3(aq)} + H_2O + OH^- \rightarrow OH^{\cdot} + HO_{2^{\cdot}} + 2O_2 + OH^- \quad \text{(R 2.45)}$$

In the presence of hydrogen peroxide, the decomposition speed of ozone can be promoted [67]:

$$O_{3(aq)} + H_2O_2 + OH^- \rightarrow OH + HO_2 + O_2 + OH^- \quad \text{(R 2.46)}$$

Ozone can also be reduced to oxygen by nitrite [67]:

$$O_{3(aq)} + NO_2^- \rightarrow NO_3^- + O_2 \quad \text{(R 2.47)}$$

In oxygen discharge, O_2^+ and O_4^+ are initially produced. Even though the potential energy of O_2^+ and O_4^+ is lower than the ionization energy of H_2O, these species can transfer their charge to H_2O rapidly via reactions R 2.37 - R 2.39 to produce OH, and $H^+(H_2O)$ which is therefore considered as the main positive ions reaching water surface. Reactive neutral species O_3 and $O(^1D)$ are produced, of which the latter can react with water to produce OH.

2.3.4 Plasma-water reactions involving inert gas

The reactions between water and plasma generated in inert gases, such as argon and helium, rather than diatomic nitrogen and oxygen, there are fewer types of neutral species produced in a discharge. The ionization energy of water (12.62 eV) is lower than that of argon (15.76 eV) and helium (24.59 eV) [64]. In the gas phase, energetic electrons can ionize or excite the gas atom, as shown in the following reactions [68, 69]:

$$e + Ar \rightarrow Ar^+ + 2e \quad \text{(R 2.48)}$$

$$e + Ar \rightarrow Ar^* + e \quad \text{(R 2.49)}$$

$$e + He \rightarrow He^+ + 2e \quad \text{(R 2.50)}$$

$$e + He \rightarrow He^* + e \quad \text{(R 2.51)}$$

Ions and excited atoms react with water molecules [68,70-73]:

$$Ar^+ + H_2O \rightarrow H_2O^+ + Ar \quad \text{(R 2.52)}$$

$$Ar^+ + H_2O \rightarrow OH + ArH^+ \quad \text{(R 2.53)}$$

$$ArH^+ + H_2O \rightarrow H_3O^+ + Ar \quad \text{(R 2.54)}$$

$$Ar^* + H_2O \rightarrow OH + H + Ar \quad \text{(R 2.55)}$$

$$He^* + H_2O \rightarrow He + H_2O^+ + e \quad \text{(R 2.56)}$$

$$He^+ + H_2O \rightarrow H_2O^+ + He \quad \text{(R 2.57)}$$

$$HeH^+ + H_2O \rightarrow H_3O^+ + He \quad \text{(R 2.58)}$$

In helium and argon discharge, the monatomic gas molecules are ionized or excited by the electrons. Thereafter, the ions and excited atoms react with water molecules to produce OH and, H_2O^+, of which the latter is thought to be the main positive ions reaching the water cathode.

2.3.5 Plasma-water reactions involving water vapour

In gas phase, fast electrons ionize, excite or decompose water molecules [52, 74]:

$$H_2O + e \rightarrow H_2O^+ + 2e \quad \text{(R 2.59)}$$

$$H_2O + e \rightarrow H_2O^* + e \quad \text{(R 2.60)}$$

$$H_2O + e \rightarrow OH + H^- \quad \text{(R 2.61)}$$

$$H_2O + e \rightarrow OH + H + e \quad \text{(R 2.62)}$$

The water ions generated react with water molecules to produce hydronium or recombine with electrons to give the dissociation reactions below [56, 75, 76]:

$$H_2O^+ + H_2O \rightarrow H_3O^+ + OH \quad \text{(R 2.63)}$$

$$H_3O^+_{gas} + e \rightarrow H_2 + OH \quad \text{(R 2.64)}$$

$$H_2O^+ + e \rightarrow H + OH \quad \text{(R 2.65)}$$

Excited water molecules can decompose by collisions, e.g.:

$$H_2O^* + H_2O \rightarrow OH + H + H_2O \quad \text{(R 2.66)}$$

The H_3O^+ generated in R 2.63 and R 2.64 can combine with an electron or react with H_2O to form cluster $H^+(H_2O)_n$.

At the gas-liquid interface, as indicated in the following two equations, energetic electrons or ions impact on the water surface and dissociate water molecule to H and OH [74, 75].

$$e + H_2O \rightarrow H + OH \quad \text{(R 2.67)}$$

$$H_2O^+_{gas} + H_2O \rightarrow H + OH \quad \text{(R 2.68)}$$

Some of the produced H and OH radicals produced recombine to H_2O:

$$H + OH \rightarrow H_2O \quad \text{(R 2.69)}$$

As indicated in the following equations, H and OH and other radicals react mutually to form H_2, O_2, HO_2 and H_2O_2 [75, 76].

$$H + H \rightarrow H_2 \quad \text{(R 2.70)}$$

$$OH + OH \rightarrow H_2O_2 \quad \text{(R 2.71)}$$

$$OH + HO_2 \rightarrow H_2O + O_2 \quad \text{(R 2.72)}$$

$$HO_2 + HO_2 \rightarrow H_2O_2 + O_2 \quad \text{(R 2.73)}$$

$$OH + H_2O_2 \rightarrow HO_2 + H_2O \quad \text{(R 2.74)}$$

As discussed previously, water molecules can be ionized, excited or dissociated to produce OH in both gas phase and aqueous phase. In addition to the reactions mentioned above, the reactions of water molecules with other species in gas phase can affect the plasma-water interacting process and products. For example, as outlined in [77], introduction of water vapour can substantially reduce ozone production: gas ions such as N_2^+, He^+ and O_2^+ can be rapidly quenched by water vapour to produce H_2O^+. Although water vapour is inevitable in any type of plasma-water interaction, a variation in concentration of water vapour may lead to very different results. Therefore, the analysis in the effects of water vapour is critical for understanding the reaction process.

2.4 Reactive species production

As has been outlined, a variety of reactive species are produced by plasma and plasma-water reactions, including hydroxyl radicals, hydroperoxyl radicals, hydrogen peroxide, ozone, excited molecules and excited atoms via various pathways. The energy efficiency of these reactive species production is one of

the significant factors which determines the industrial application of non-thermal plasma in water treatment. Understanding the reactive species production mechanism in different reactors is indispensable for promoting the energy efficiency of core reactive species production. This section investigates the production of OH, H_2O_2 and O_3.

2.4.1 Hydroxyl radical

Hydroxyl radical are strongly oxidative agents produced in the reactions between plasma and water, having the second highest oxidation potential of 2.8 V [78]. Hydroxyl radicals are the core components in AOPs due to their instantaneous and non-selective reaction with pollutants. Hence, OH production is critical for water treatment efficiency by plasma. However, due to their high reactivity, OH has a short lifetime and is difficult to be diagnosed, which limits the investigation of OH production and formation mechanisms. To date, it was known that OH can be produced in water-involved reactions, caused by electron collision, ion bombardment and ion-molecule charge transfer etc. These processes can occur in both gas phase and aqueous phase at the plasma-water interface. In addition, some reactive neutral species, such as oxygen atom, can also be involved in the reactions producing OH. As shown below, Bruggeman listed the dominant influencing factors for OH production [79]:

a) gas temperature (T_g)
b) electron temperature (T_e) and density (n_e)
c) ionization degree
d) composition of positive and negative ions and their density
e) vibrational temperature (molecule excited states)
f) gas composition when admixtures of water with other gases are used

These factors can influence which formation paths are dominant in OH production in one specific plasma-water interaction process. Different discharge

types lead to different plasma parameters, including T_g, T_e and n_e. The types of gas discharge listed by Bruggeman have ionization degree order of 10^{-2} to 10^{-8}, T_g of 300 K to 6000 K and T_e of around 1-2 eV [79]. It has been shown that the pulsed discharge can produce plasma with much higher electron temperature, around 10 eV [79]. Table 2.2 lists the T_e and n_e in several typical atmospheric discharges [79-86].

Table 2.2 Electron temperature (T_e) and density (n_e) in typical atmospheric discharges.

Discharge type	T_e (eV)	n_e (m^{-3})
Pulsed corona discharge (nsec)	~10	10^{19}-10^{21}
Non-completely thermal arc	0.2-2	10^{20}-10^{21}
Microwave plasma jets	1-2	10^{20}-10^{21}
Filamentary DBD	1-2	10^{20}-10^{22}
Glow DBD	1-2	10^{17}-10^{18}

Under different discharges conditions, the main pathway of OH production is different. In plasma with a T_e = 1 eV, the OH production rate by electron-ion recombination and ion-ion recombination start to be dominant when the ionization degree is higher than 10^{-5} [79]. In situation where the ionization degree is below 10^{-5}, OH production is mainly from electron dissociation of H_2O [79]. $O(^1D)$ also contributes to the OH production in gas discharges [79]. In non-thermal discharge in inert gas, metastable atoms, such as Ar^* and He^*, can be important actors in pathways for OH production [71, 88]. OH production is balanced by OH reduction reactions, e.g. OH can self-quench or react with other radicals/molecules quickly in gas or aqueous phase and a local high density of OH also increases the reduction rates.

To quantitatively investigate the production of OH, several OH diagnostic methods have previously been applied in gas phase and aqueous phase, including optical emission spectroscopy (OES), absorption spectroscopy (ABS), laser-induced fluorescence (LIF), cavity ring-down spectroscopy and indirect chemical diagnostics with OH trappers or scavengers [17, 77, 79, 89-96]. As discussed previously, due to the short lifetime of OH, it is difficult to measure OH production: however, numerous researchers have measured OH density during gas discharge. Table 2.3, from [79], summarises the gas phase OH density measured by various diagnostic methods in a range of atmospheric discharges, with the original data sources provided in the table.

Table 2.3 OH densities and plasma parameters in a range of atmospheric discharges [79].

Discharge mode	Gas	Power (W)	OH density (m^{-3})	Diagnostic method
Gliding arc [97]	Air	≈ 100-500	10^{20}	OES
Pulsed arc [98]	Air	≈ 0.6×10^{-3}/pulse	10^{21}	LIF
AC arc [99]	Air	–	10^{21}	ABS
AC DBD [93]	6700 ppm H_2O in He	≈ 10-50	10^{19}	ABS
Pulsed DBD [101]	27000 ppm H_2O in Ar	0.36 (50ns, 10 Hz)	10^{21}	ABS
Pulsed Streamers [102]	Air	≈ 0.2×10^{-3}/pulse	10^{21}	LIF
Atmospheric pressure glow discharge [103-104]	Air	10-70	10^{19}-10^{20}	OES
Microwave jet [105]	Ar	12	10^{22}	ABS
Microwave jet [106]	Ar	120	10^{20}	ABS

In addition to the OH produced in plasma, some researchers explored OH production in the aqueous phase. Kanazawa et al. measured OH production in aqueous solution treated using a helium atmospheric low-frequency plasma jet. The OH measurement was achieved by TA (terephthalic acid) based chemical dosimetry method. TA can react with OH in aqueous phase to produce HTA (2-hydroxyterephthalic acid) which emits 425 nm light when irradiated with 310 nm light, allowing the analysis of OH concentration through the measurement of HTA absorption. The reaction between TA and OH is presented in Figure 2.15.

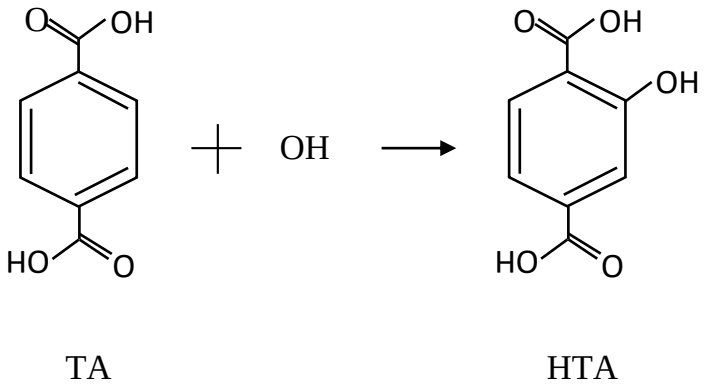

TA HTA

Figure 2.15 TA reacts with OH to produce HTA.

The OH production was estimated as 1.0×10^{-8} M/s to 4.7×10^{-8} M/s depending on the distance from plasma jet to the solution surface. The calculated energy yield for OH is 0.122 - 0.575 g/kWh [107]. Kanazawa et al. used the TA based method to investigate the OH production by positive pulsed discharge generated at an air-water interface; the estimated OH production was 10^{-9} M/s with an energy yield of 0.022 g/kWh [108]. Sahni and Locke applied the pulsed discharge under water and measured the OH production using two different chemical probes of DMSO (dimethyl sulfoxide) and NaTA (disodium salt of terephthalic acid). The maximum energy yield was 0.064 g/kWh achieved at an

discharge voltage of 45 kV [109]. They found that OH production increased linearly as input power rose and believed that hydrogen peroxide was mainly produced by OH dimerization [109].

Hsieh et al. reviewed OH production and energy yield measured by optical methods and chemical probes in different gas discharges [110]. The energy yields of OH measured with optical diagnostic methods ranged from 2.16×10^{-4} g/kWh to 4.70 g/kWh [110]. The maximum OH energy yield, of 4.70 g/kWh, measured with optical diagnostic method, was achieved by a pulsed DBD in a mixture of argon and water vapour [101]. The energy yields of OH measured with chemical probe methods ranged from 2.35×10^{-2} g/kWh to 31.77 g/kWh [110]. The maximum OH energy yield of 31.77 g/kWh was measured with chemical diagnostic methods and achieved by a pulsed discharge with argon as the carrier gas and a flowing liquid film [110].

The optical diagnostic methods have the advantage of non-invasive detection without affecting the chemical reactions. However, in some experiments the application of optical diagnostic methods is limited due to the complex reactor geometry. Chemical probe diagnostic methods have better adaption to the reactor geometry. However, the addition of chemical probes to the reaction vessel affects the chemical reaction pathways and leads to more complex chemistry. The amount of added chemical probe present in the reaction vessel also influences the measured OH production. Therefore, the chemical diagnostic methods require careful design of the applied probes and the measured products.

2.4.2 Hydrogen peroxide

Hydrogen peroxide has been applied to water treatment process for disinfection and sterilization, as it has higher oxidative potential than chlorine (H_2O_2 has a value of 1.78 V [111], Cl_2 has a value of 1.4 V [112]), and does not produce

toxic by-products in oxidation reactions. Plasma in and in contact with water has been proved to produce hydrogen peroxide in gas and liquid. Specifically, dimerization of generated hydroxyl radicals in deionized water contributes to hydrogen peroxide production. Since the measurement of H_2O_2 is easier than that of OH, there has been more research work undertaken for hydrogen peroxide production at plasma-water interface.

As section 2.3 introduced, hydrogen peroxide can be produced by OH dimerization and HO_2 recombination as Section 2.3 introduced. It can also be efficiently produced in plasma electrolysis by the following reactions [53]:

$$H^+ + e \rightarrow H \qquad \text{(R 2.75)}$$

Reaction R 2.75 occurs at a cathode, where hydrogen ions can acquire electrons. In the presence of oxygen, as shown below, the hydrogen atom can combine with an oxygen molecule to form HO_2.

$$H + O_2 \rightarrow HO_2 \qquad \text{(R 2.76)}$$

Through recombination of HO_2 molecules, H_2O_2 is produced.

$$HO_2 + HO_2 \rightarrow H_2O_2 + O_2 \qquad \text{(R 2.77)}$$

The hydrogen peroxide thus formed can be reduced by reaction [113]:

$$H_2O_2 + 2H^+ + 2e^+ \rightarrow 2H_2O \qquad \text{(R 2.78)}$$

The overall formation reaction of H_2O_2 by water dissociation can be summarized as:

$$H_2O + H_2O \rightarrow H_2O_2 + H_2 \qquad \text{(R 2.79)}$$

The total enthalpy required for reaction R 2.64 is 3.2 eV/molecule [83]. The total energy ($E_{H_2O_2}$) required to produce one mol of hydrogen peroxide by water dissociation can be estimated by the reaction enthalpy:

$$E_{H_2O_2} = 3.2\ \text{eV} \times N_A = 3.2\ \text{eV} \times 6.02 \times 10^{23} = 1.9264 \times 10^{24}\ \text{eV} \quad \text{(Eq. 2.1)}$$

The energy value 1.9264×10^{24} eV is equivalent to 0.086 kWh. Hence, according to the thermodynamic limit, the maximum energy yield of hydrogen peroxide would be 395 g/kWh. Locke and Shih summarized the energy yield of hydrogen peroxide by various plasmas [53]. Table 2.4 introduced the representative results in each type of gas discharge from the summary.

Table 2.4 Energy yield of hydrogen peroxide produced by plasma-water reactions [53].

Phase	Discharge type	Power (W)	H_2O_2 Yield (g/kWh)	Reference
Liquid	Radio frequency	1.60E-01	0.64	[114]
Liquid	Pulsed corona (60 Hz)	7.00E-02	1.00	[115]
Liquid	Pulsed corona (60 Hz)	2.28E-02	3.64	[29]
Liquid	Contact glow discharge electrolysis	4.00E-01	1.60	[117]
Bubbles	Multi-electrode (Ar bubble)	2.00E-01	8.40	[117]
Bubbles	Pulsed corona (60 Hz)	3.00E-03	0.75	[115]
Bubbles	Pulsed (oxygen bubble)	9.20E+00	2.10	[118]
Bubbles	d.c. glow discharge	2.20E-2	1.90	[119-120]
Gas over liquid	Pulsed corona (60 Hz) in Ar	5.00E-03	0.70	[115]
Gas over liquid	Pulsed corona (positive) in air	3.80E-05	5.00	[121]
Gas over liquid	Pulsed corona (negative) in air	3.80E-05	1.50	[121]
Gas over liquid	DBD falling film	4.50E-02	2.70	[122]
Gas over liquid	Glow discharge electrolysis	-	1.76	[123]
Droplets	Pulsed gliding arc	2.50E-04	80.00	[18]

In Table 2.4, the majority of the yield ranged from 0-5 g/kWh. The highest energy yield, reported as 80 g/kWh, was achieved by pulsed gliding arc discharge in argon with water spray [18]. A possible reason for the high energy yield is that highly soluble hydrogen peroxide molecules were protected by being absorbed into water droplets: radicals have short lifetime in aqueous water and are therefore less likely to contact and react with the dissolved hydrogen peroxide [53]. The energy yields of hydrogen peroxide achieved in experiments are still quite low compared with the thermodynamic limit of 395 g/kWh.

To determine the key factors affecting hydrogen peroxide production, Lukes et al. investigated three different reactors as illustrated in Figure 2.16. The three reactors were designed to distinguish the effects of gas phase reactions, aqueous phase reactions and gas-liquid interface reactions.

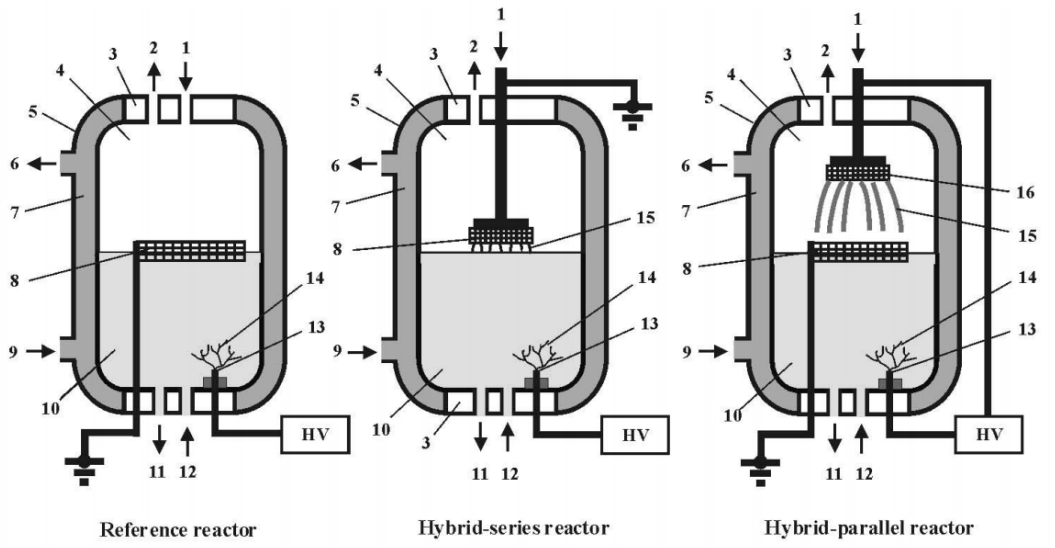

Figure 2.16 Three reactors used in experiments of Lukes et al. 1 and 2: gas inlet and outlet; 3: Teflon cap; 4: gas; 5: glass reactor; 6 and 9: cooling water inlet and outlet; 7: cooling water jacket; 8: ground RVC (reticulated vitreous carbon) electrode; 10: liquid phase; 11 and 12: solution inlet and outlet; 13: liquid phase high-voltage point electrode; 14: liquid phase discharge; 15: gas phase discharge; 16: gas phase high-voltage RVC electrode; HV: pulse power supply [126].

In the reference reactor, only the pulsed discharge in liquid contributed to hydrogen peroxide production.

In the hybrid-series reactor, in addition to the pulsed discharge in liquid, the pulsed discharge between the water anode and RVC cathode above water, which allowed negative ions and electrons to enter liquid and react with water, also contributed to hydrogen peroxide production.

In the hybrid-parallel reactor, in addition to the pulsed discharge in liquid, the gas phase pulsed discharge between two RVC electrodes contributed to hydrogen peroxide production. The positive ions generated by gas discharge lose charge at the RVC electrode without reaching the water. In the hybrid-parallel reactor, the neutral species generated by gas phase discharge can be diffused into liquid.

When using 130 μS/cm potassium chloride (KCl) solution, the hydrogen peroxide production was similar for all three reactors, which demonstrated that the contribution of gas phase discharge and the interface reaction was negligible in this case [126]. Discharges in air or in Ar/O_2 mixture demonstrated similar values of hydrogen peroxide production. Their results indicated that: only the discharge in liquid contributed to the hydrogen peroxide production; electrons and negative ions did not contribute to hydrogen peroxide production; neutral species produced in gas phase discharges did not contribute to hydrogen peroxide production.

To enhance the effect of hydrogen peroxide in the degradation of organic compounds, iron ions (Fe^{2+}/Fe^{3+}) are added to induce Fenton's reactions. Koprivanac et al. found that the addition of Fe^{2+} in a solution significantly increased an organic dyes' degradation rate when subjected to pulsed corona discharge under water [127]. Markovic et al. evaluated three methods for ibuprofen removal from water, namely Fenton's reactions, DBD without Fe^{2+},

and DBD with Fe^{2+}. After 15 minutes, the ibuprofen degradation efficiency were 85% and 99% respectively with DBD method and DBD/ Fe^{2+} method, both were higher than that by Fenton's reactions [128].

2.4.3 Ozone

As a strong oxidant (oxidation potential 2.07 V [129]), ozone has been applied for organic pollutants degradation in water treatment. There are two paths for organic compound oxidation by ozone: direct reaction or indirect reaction. In the direct path, ozone selectively attacks unsaturated bonds and partly degrades the organic compounds; in the indirect path, hydroxyl radicals are produced in radical chain reactions to oxidize organics [130]. At normal temperature, ozone (O_3) is unstable and easily decays to ordinary oxygen (O_2) [131].

Ozone energy yields of up to 450-544 g/kWh have been achieved using non-thermal plasma in pure oxygen in lab conditions [53]. In the presence of water vapour, low levels of ozone are produced since the production of OH suppresses ozone generation in a catalytic cycle which eliminates oxygen atoms, as shown below [132-134]:

$$O + OH \rightarrow H + O_2 \qquad \text{(R 2.80)}$$

$$H + O \rightarrow OH + O_2 \qquad \text{(R 2.81)}$$

Ozone is a significant reactive species produced by plasma-wate reactions. In AOPs, ozone may produce hydroxyl radicals in water, as shown below [135]:

$$3O_3 + OH^- + H^+ \rightarrow 2OH + 4O_2 \qquad \text{(R 2.82)}$$

In the presence of H_2O_2, the generation of OH by O_3 is enhanced [135]:

$$2O_3 + H_2O_2 \rightarrow 2OH + 3O_2 \qquad \text{(R 2.83)}$$

UV light can also enhance the generation of OH by O_3 [135]:

$$O_3 + H_2O + h\upsilon \rightarrow O_2 + H_2O_2 \text{ (h}\upsilon\text{: } \lambda < 300\text{nm)} \quad \text{(R 2.84)}$$

$$2O_3 + H_2O_2 \rightarrow 2OH + 3O_2 \quad \text{(R 2.85)}$$

In under-water discharge, a plasma generated in bubbling oxygen produces ozone [28, 137, 138]. Anpilov et al. studied ozone production by multi-spark discharge under water with gas bubbles using four different bubbling gases: oxygen, air, argon and nitrogen. Ozone production with air was lower than that with oxygen, and an ozone concentration of (1-2)×10^{15} cm^{-3} was achieved in oxygen [139].

In addition to under-water discharge, discharge over water surface can also produce ozone. Lukes et al. studied ozone production by a positive pulsed corona discharge over water in oxygen, O_2/Ar mixture and O_2/N_2 mixture. The level of ozone production for different concentrations of oxygen in Ar/O_2 and O_2/N_2 mixtures is shown in Figure 2.17 [140]. In N_2/O_2 mixture, the ozone production was depressed. This is due to the nitrogen atoms and nitrogen oxides consuming ozone and oxygen atoms via the reactions below [141-144]:

$$O + NO_2 \rightarrow NO + O_2 \quad \text{(R 2.86)}$$

$$O + NO + N_2 \rightarrow NO_2 + N_2 \quad \text{(R 2.87)}$$

$$N + O_3 \rightarrow NO + O_2 \quad \text{(R 2.88)}$$

$$NO + O_3 \rightarrow NO_2 + O_2 \quad \text{(R 2.89)}$$

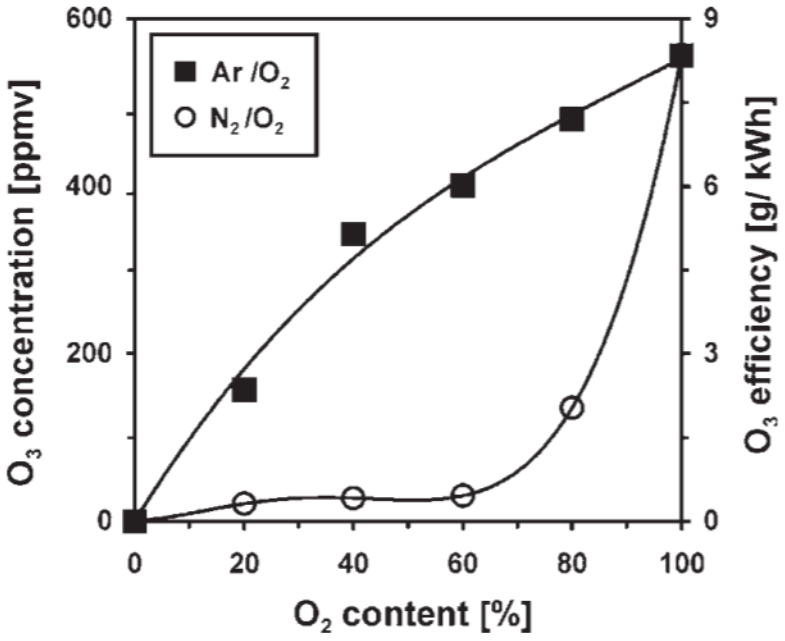

Figure 2.17 The concentration and energy efficiency of ozone production by pulsed corona discharge over water in Ar/O_2 and N_2/O_2 mixtures as a function of oxygen concentration. Total gas flow rate 2.5 L/min, discharge voltage 30 kV, charging capacity 2 nF, electrical power 4.5 W, discharge gap 5 mm, discharge gap 5 mm [140].

In Ar/O_2 mixture, there are no reactions similar to reactions R 2.86 - R 2.89 to depress ozone generation. However, as shown in Figure 2.18 [140], the ozone production with 10–70% argon content was significantly increased, reaching the maximum O_3 energy yield 23 g/kWh with 40% argon. The beneficial effect of argon on ozone production was also reported in other research [145, 146].

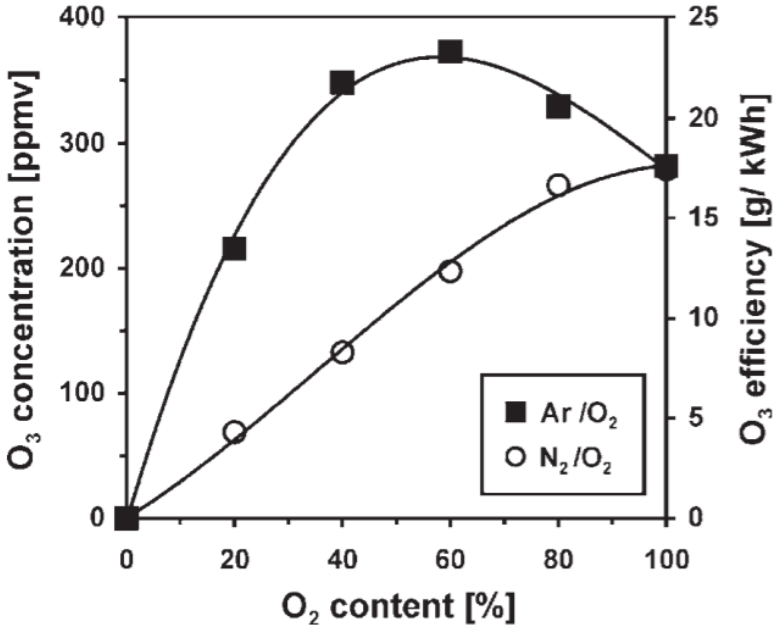

Figure 2.18 The concentration and energy efficiency of ozone produced by pulsed corona discharge over water in Ar/O_2 and N_2/O_2 mixtures as a function of oxygen concentration. Total gas flow rate 2.5 L/min, discharge voltage 30 kV, charging capacity 0.2 nF, electrical power 4.5 W, discharge gap 5 mm [140].

The ozone production is depressed in the presence of water vapour. On one hand, as mentioned in R 2.80, produced OH can react with oxygen atoms to reduce ozone production. On the other hand, water vapour can be decomposed by the electrons and excited molecules (e.g. $N_2(A)$) to H and OH, both of which can destroy ozone rapidly [140]:

$$H + O_3 \rightarrow OH + O_2 \qquad \text{(R 2.90)}$$

$$OH + O_3 \rightarrow HO_2 + O_2 \qquad \text{(R 2.91)}$$

$$HO_2 + O_3 \rightarrow OH + 2O_2 \qquad \text{(R 2.92)}$$

In addition to water molecule decomposition, the reaction of water and oxygen atom $O(^1D)$ can also produce OH, which is also involved in ozone dissociations.

2.5 Conclusions

This chapter reviewed several types of gas discharges in or in contact with water, as well as the reactive species produced in the reaction processes. Compared with the traditional AOPs, one advantage of plasma-water interactions is that they produce various reactive components, including UV light, shock wave, OH, O_3, H_2O_2, HO_2, excited molecules and atoms, which have synergistic effects for water purification and sterilization. Among these reactive species, the core factor is OH, the yield of which was lower than 10 g/kWh in most of the reported research. Although numerous reactions producing OH and other reactive species have been demonstrated, there are some processes affecting the plasma-water interface reactions which remain unclear.

Analysis of the research work to date indicates that the main energy loss occurs as a result of maintaining gas discharge, heating water and self-quenching of radicals. A comparison of ozone generation and plasma-water reactions explains the limitation: in ozone generation, one oxygen molecule can be broken into two oxygen atoms by consuming about 6 eV [83], the oxygen atoms subsequently react with oxygen to form ozone. While in plasma-water reactions, production of a single OH radical always consumes thousands of eV [183]. Although an OH yield of 31.77 g/kWh was reported under laboratory conditions [110], the system is not suitable for large-scale industrial application due to the high cost of carrier gas (argon) and the flowing liquid film in the experiment. However, the hydrogen peroxide produced in water by plasma has been reported up to 80 g/kWh [18], which is thought mainly contributed from OH dimerization.

OH production in water can be from the reactions of positive ions, electrons and reactive neutral species. As reported in Section 2.2, positive gas ions produced in discharges rapidly transfer their charge to gas phase water molecules, with the main positive ions reaching water being clusters of $H^+(H_2O)_n$. On one hand, positive ions reaching the water surface can react with water to produce water

ions, which subsequently decompose to hydrogen ions and hydroxyl radicals. On the other hand, the positive ions with high kinetic energy can decompose or ionize water molecules by bombarding water surface. However, the contribution of ions' kinetic energy and potential energy has not been identified.

The reviews in this chapter provide a fundamental interpretation of present understanding of plasma and water interactions. This knowledge helps in analysing the results in this research, which investigated the plasma-water reactions in positive corona discharges and positive glow discharges. Corona discharges produce positive ions which drift towards the liquid surface and, as such, have low kinetic energy, while glow discharges produce positive ions with high values of kinetic energy impacting on the liquid surface. The results can help analyse the effects of potential energy and kinetic energy on the interface reactions between positive ions and water. In addition to the effect of ions, the effects of reactive neutral species produced by positive corona discharges were also investigated.

3. Experimental System Design and Methodology

3.1 Introduction

For investigating the effects of kinetic energy and potential energy of positive ions on plasma-water reactions, two types of gas discharges were employed in this research: positive corona discharge and positive glow discharge. For a corona discharge, the mean kinetic energy of drift ions reaching water is only 0.01-0.1 eV [147]; While for a water cathode glow discharge, the average kinetic energy of positive ions entering the water was suggested to be greater than 100 eV [148]. Therefore, comparing the effects of positive ions at the plasma water interface in corona discharge and glow discharge can help identify the role of the ions' kinetic energy in the interface reactions.

This chapter presents the experimental system and the methodology for analysing the plasma-water interface reactions. As Figure 3.1 shows, the setup of the experiments can be divided into five sections. The core is the plasma-water reactor designed for corona and glow discharge in contact with water, as discussed in sections 3.2.1 and 3.2.2 respectively, including the reactor chamber, electrode configurations and the sample containers. The gas supply system is introduced in section 3.3, including the gas circuit, and the control of flow rates and gas pressures. The electrical system, introduced in section 3.4, describes the electrical circuit design and the electrical components, and the diagnostics of voltages and discharge currents. Section 3.5 introduces the chemicals and their preparations. Section 3.6 introduced the analysis methods for the treated sample, including the measurements of pH, conductivity and hydrogen peroxide in the treated solutions, and how the reactive species in the off gas (gas flow out from the gas outlet of reactor during discharge) were analysed.

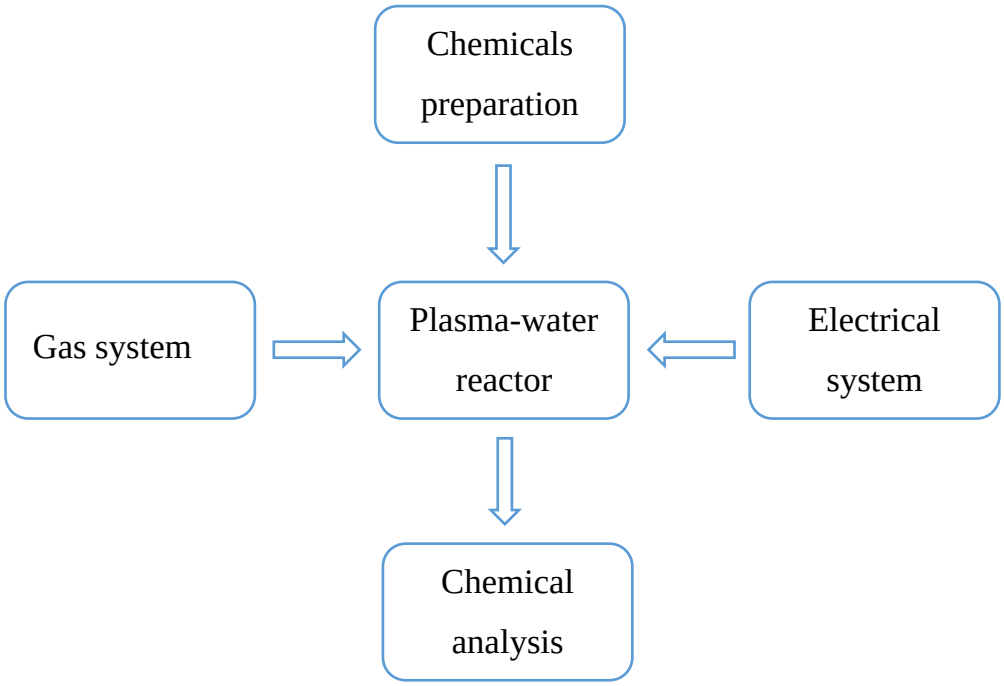

Figure 3.1 Schematic diagram for experimental procedures.

3.2 Plasma-water interaction

3.2.1 Reactor design for corona discharge

The plasma-water reactor for corona discharge is shown in Figure 3.2(a). Positive corona discharge was generated by a nine-needle high-voltage (HV) electrode to produce ionic wind drifting to the sample solution. The current was kept at 30 μA during corona discharge. Single-needle electrode was tested but the maximum d.c. current could only reach 15 μA. The nine-needle electrode can produce twice the amount of ions in comparison to a single-needle electrode, therefore halving the corona discharge time required. The chamber of the gas-tight reactor encompassed an acrylic tube, with an inner diameter of 100 mm and a height of 100 mm. The gas inlet and outlet were situated on the polyvinyl

chloride (PVC) lid. The tip radius of the stainless-steel needles was 0.2 mm. Figure 3.2(b) shows the bottom view of the nine-needle anode.

Inside the reactor, the two sample containers shown in Figure 3.3 were used in the experiments: one with a water cathode and the other with a stainless-steel mesh cathode with the water container underneath. In all the tests of corona discharges, the volume of sample solution is 5 mL.

For experiments with the water cathode, positive corona discharge was generated between the nine-needle anode and the sample solution. The gap between the needle tips and the solution surface was fixed at 10 mm. The solution was grounded through a stainless-steel plate at the bottom of the container. The sample container was fixed and grounded by a brass screw.

For experiments with the mesh cathode, positive corona discharge was generated between the nine-needle anode and the grounded mesh. The mesh was placed 5.3 mm above the solution surface, covering the entire solution. The solution was not grounded. To maintain a consistent corona discharge, the gap between the needle tips and the mesh was set to 10 mm. The positive ions are filtered by the grounded mesh, allowing only neutral species to reach the solution. The mesh cathode is made of stainless-steel grade 316, which has a pore size of 1 mm and a wire diameter of 0.3 mm, a square with side length of 50 mm.

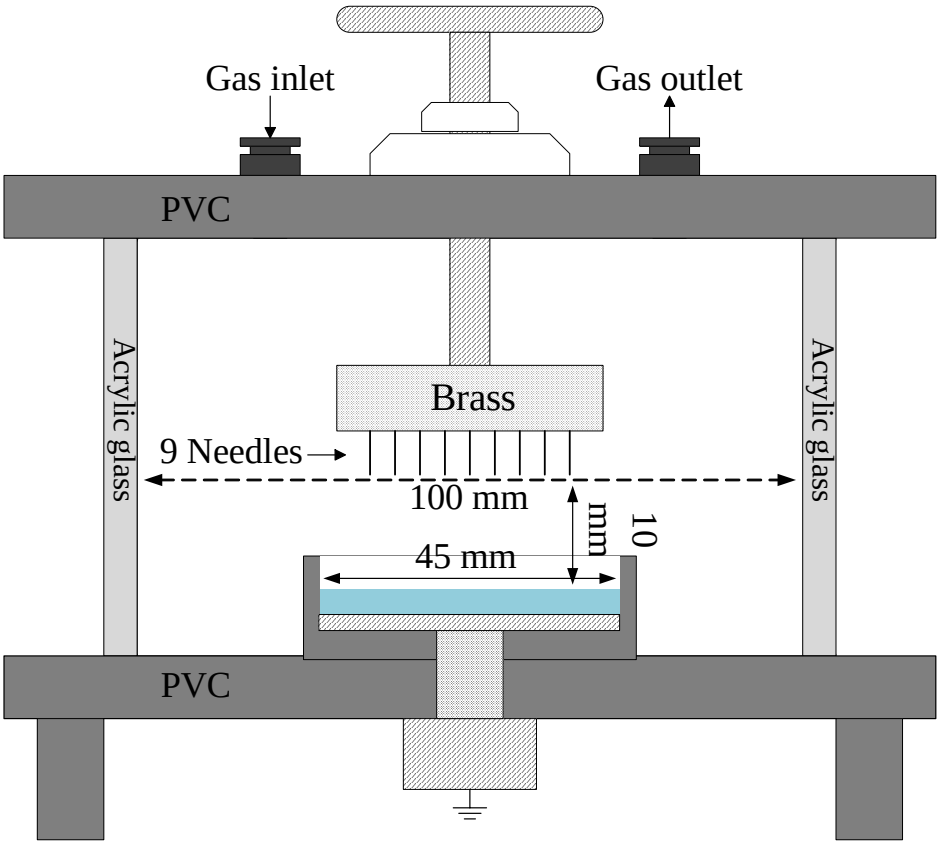

(a)

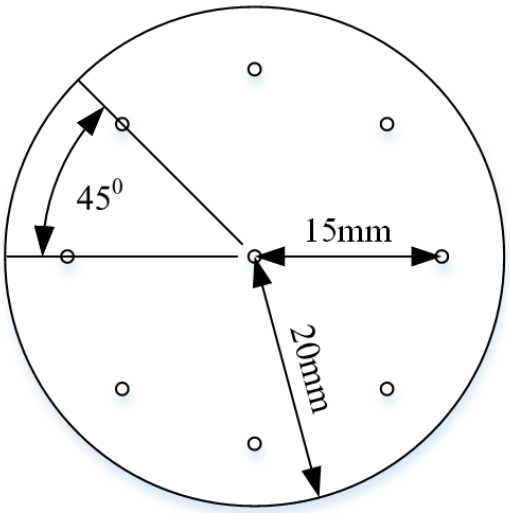

(b)

Figure 3.2 (a) The reactor configuration for corona discharge and (b) the bottom view of the nine-needles electrode.

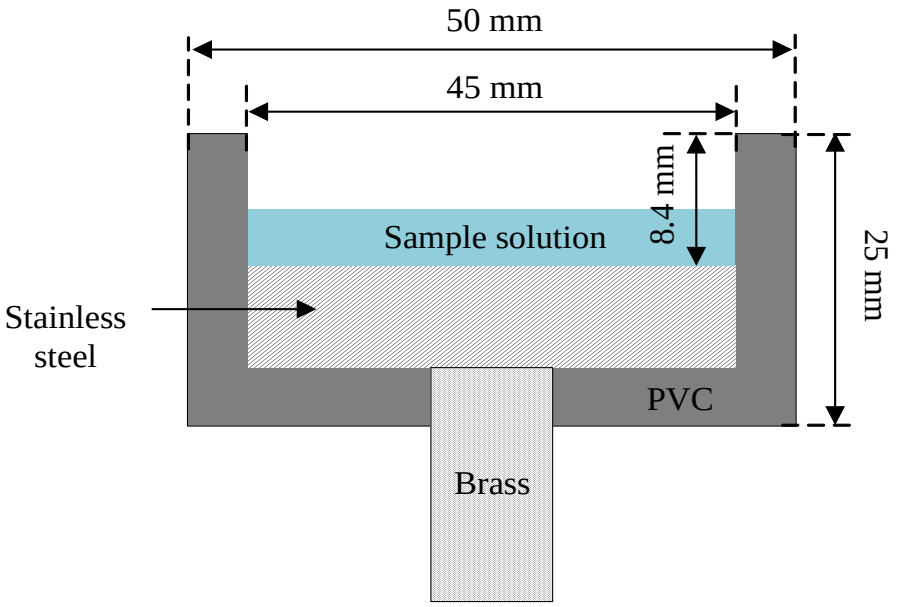

(a)

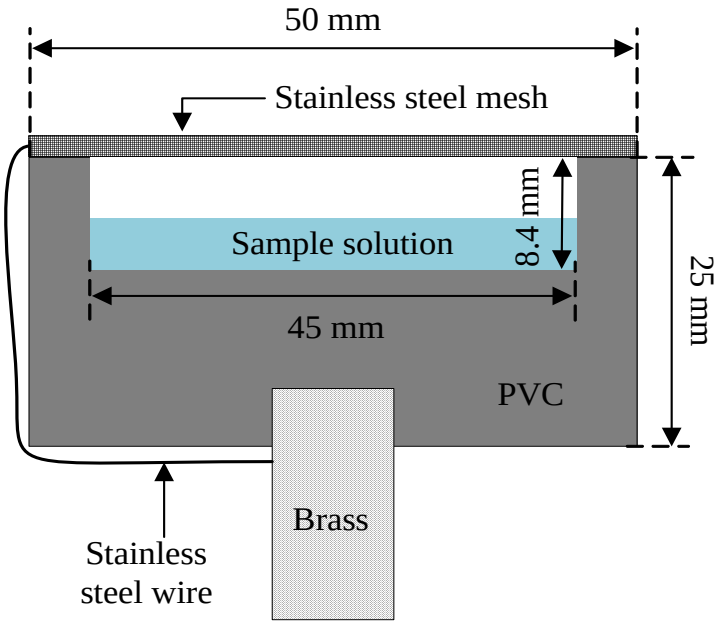

(b)

Figure 3.3 Sample containers with (a) water cathode and (b) with mesh cathode.

3.2.2 Reactor design for glow discharge

The plasma-water reactor for glow discharge is shown in Figure 3.4(a). To minimise differences in plasma-water reaction caused by reactor design, the reactor used for glow discharge is similar to the one used for corona discharge, only the electrode and sample container are different. Positive glow discharge was generated between a single-needle electrode and a water cathode.

The single-needle electrode is configured by one needle embedded at the centre of a brass plate base, as shown in Figure 3.4(b). Each experiment uses a fresh needle, which protrudes 7.4 mm from the brass plate and has a tip radius of 0.2 mm. The single-needle HV electrode was placed directly above the centre of the sample container. The distance from the needle tip to the water surface can be adjusted as required in different gas discharges, the reason for the variation is discussed below.

Figure 3.4(c) shows the configuration of the sample container. The inner diameter is 45 mm and the outer diameter is 50 mm. The depth of the sample container is 20 mm. A stainless-steel plate with thickness of 10 mm is placed at the bottom of the sample container to ground the water. In all the tests of glow discharges, the volume of sample solution is 10 mL.

To acquire a stable glow discharge in each type of gas, the distance from needle tip to water surface, current and discharge time was adjusted in nitrogen, oxygen and helium. Table 3.1 shows the values used for each experimental set-up:

Table 3.1 The parameters of glow discharges in nitrogen, oxygen and helium.

Gas	Distance from needle tip to water	Discharge Current	Discharge Time
Nitrogen	2 mm	3 mA	4 minutes
Oxygen	8 mm	2 mA	5 minutes
Helium	2 mm	3 mA	4 minutes

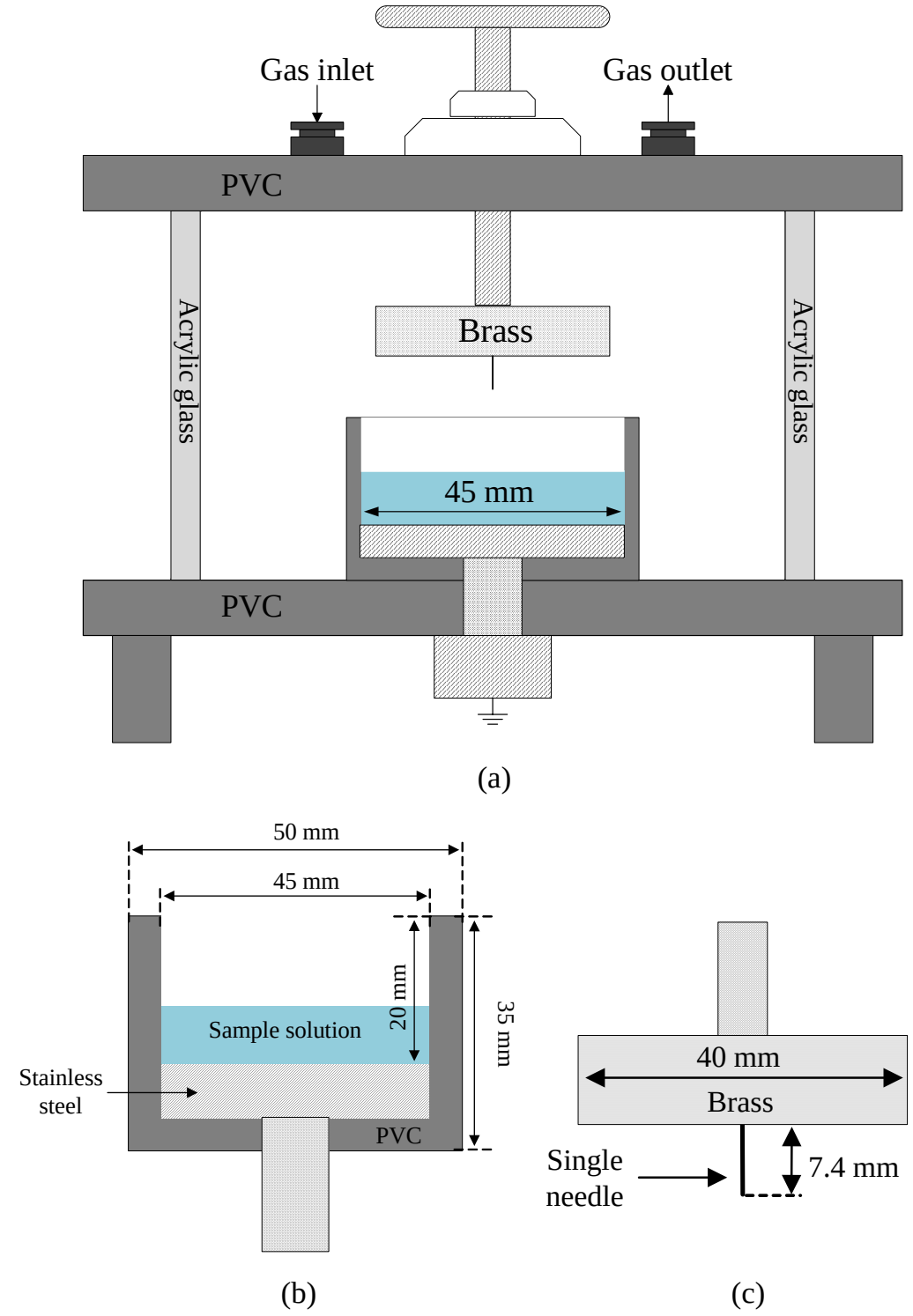

Figure 3.4 (a) The reactor configuration for glow discharge; (b) the sample container; and (c) the single-needle electrode.

3.3 Gas system

3.3.1 Gas control design

Figure 3.5 illustrates the gas control system used for both corona discharge and glow discharge. Polyurethane tubes (6 mm outer diameter and 4 mm inner diameter) were used to connect the gas circuit. The gas preparation before gas discharge is made into three steps:

1st step: keep the valve of mass flow controller closed and evacuate the reactor to below 4 Torr using an Edwards E2M80 rotary-vane pump via the ball valve.

2nd step: set the pressure controller to 760 Torr and close the ball valve to allow the working gas fill the reactor to the atmospheric pressure. The 1st and 2nd steps were repeated three times in each test to reduce the residual air in the plasma reactor.

3rd step: keep the vacuum pump working with the ball valve closed, and the pressure controller and mass flow controller will work at pre-set values. When the gas pressure and flow rate are stable, the gas discharge experiment can be started. During the gas discharge, the pressure controller and mass flow controller automatically adjust to ensure the pre-set gas pressure and flow rate in the plasma reactor.

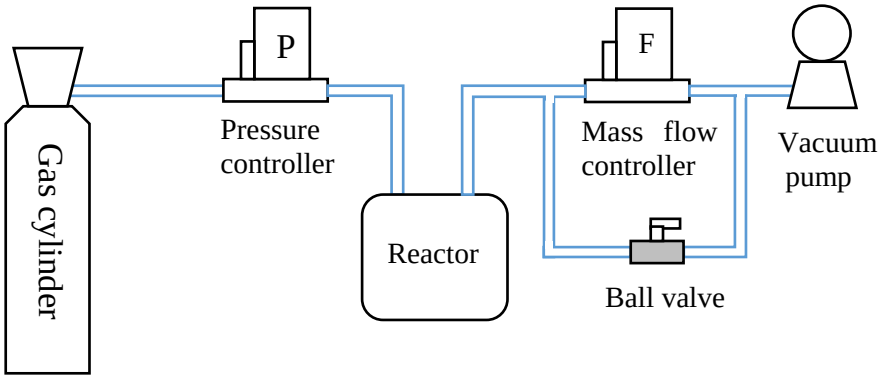

Figure 3.5 The design of the gas control system.

For the corona discharge, nitrogen and oxygen were employed. Helium was not used for the corona discharge, as the d.c. corona discharge current cannot be maintained at 30 μA without a breakdown. For the glow discharge, nitrogen, oxygen and helium were used. The parameters of these gases are listed in Table 3.2.

Table 3.2 Specification of gas supply used in experiment.

Gas type	Supplier	Purity	CAS-No.
Nitrogen (compressed, oxygen free)	BOC	≥99.998%	7727-37-9
Oxygen (compressed)	BOC	99.5%	7782-44-7
Helium (compressed)	BOC	99.996%	7440-59-7

Three models of Alicat mass flow controllers with different flow range were used in the experiments to control the gas flow rate. The specifications of mass flow controllers are listed in Table 9.1 in Appendix. In corona discharges, gas flow rates of 0.002, 0.02, 0.2, 0.5 and 1.0 slpm were investigated. In glow discharge, gas flow rates of 0.2, 0.5, 1, 2 and 5 slpm were investigated.

The gas pressure of the plasma reactor was measured and controlled by an Alicat pressure controller. The specifications of the pressure controller used in the experiments are listed in Table 9.2 in Appendix. Gas pressures of 760, 500, 300, 200 and 100 Torr were tested in nitrogen corona discharge and glow discharge (N_2, O_2, He). For the oxygen corona discharge, gas pressures of 760, 500, 300 and 200 Torr were tested. The pressure of 100 Torr was not tested in oxygen corona discharge as the 30 μA d.c. corona discharge current cannot be maintained under this pressure.

3.3.2 Off gas diagnostics

As Figure 3.6 shows, an ozone analyser was applied to measure the ozone concentration in the atmospheric oxygen discharge. Different from the system described in Figure 3.5, in this system, the mass flow controller was put at the gas-in side and the pressure controller was put at the gas-out side, which is for avoiding the corrosive off gas (which contains ozone) flowing through the mass flow controller. In this system, the pressure controller was working as a pressure meter, without gas flowing through it. The experiments were conducted at atmospheric pressure.

The gas preparation procedure is slightly different from that in Figure 3.5. In the gas filling stage, keep the ball valve closed and the pressure controller's valve open; evacuate the reactor with the vacuum pump to below 4 Torr; set the mass flow controller and let the gas fill the reactor. As before, the gas filling process is repeated for three times before closing the pressure controller's valve and setting the mass flow controller to the pre-set value. When the gas pressure of plasma reactor reaches 760 Torr, open the ball valve. When the gas flow is stable, start the gas discharge. The ozone concentration was tested with a gas flow rate of 0.2, 0.5 and 1.0 slpm. As the recommended flow rate of the ozone analyser is between 0.1 to 1 slpm, ozone concentration was not tested for the gas flow rate of 0.002 and 0.02 slpm.

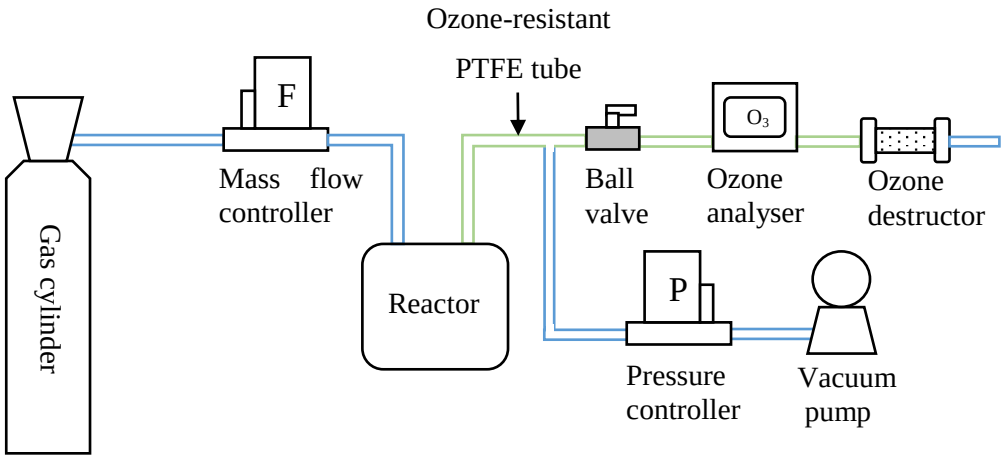

Figure 3.6 The design of the gas control system for atmospheric oxygen discharge.

Ozone-resistant PTFE tubes were used to connect the plasma reactor with the ozone destructor. The pressure controller was positioned between the vacuum pump and the plasma reactor to control its pressure. The specifications of the ozone analyser are listed in Table 9.3.

To investigate the composition and lifetime of the active neutral species, the off gas was analysed with a gas-washing bottle, as shown in Figure 3.7. The gas washing bottle is filled with 20 mL deionized water. In the experiments, the off gas was collected during the whole discharge time range. And the gas flow was maintained for another three minutes after the gas discharge extinguished for collecting the residual gas in the reactor. Then the pH value, conductivity and hydrogen peroxide of the water in gas-washing bottle were tested.

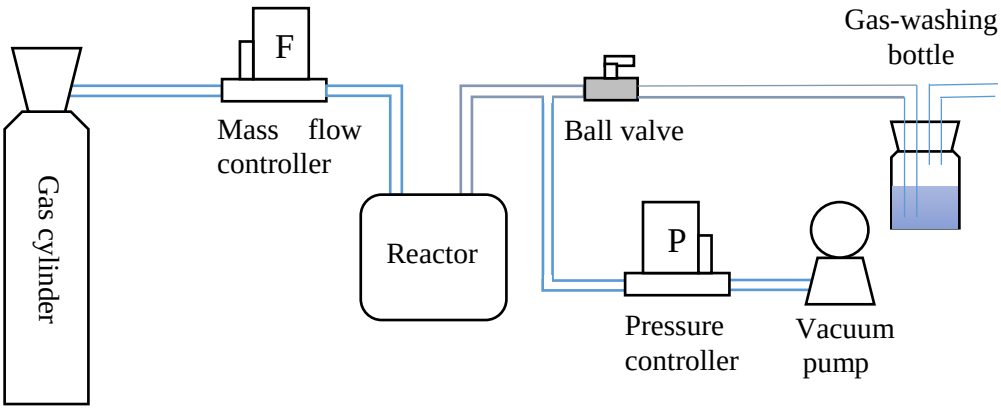

Figure 3.7 The design of gas control system with gas-washing bottle for atmospheric discharge.

3.4 Electrical system

3.4.1 Electrical circuit design

The novel design of electric circuit for corona discharge is shown in Figure 3.8, which can achieve a stable 30-μA d.c. cathode current. The corona discharge was generated using a nine-needle electrode, supplied by a Glassman, PS/EJ20R30 d.c. power supply with a voltage range of 0-20 kV and a current range of 0-30 mA as introduced in Table 9.4. Electrodes with fewer needles (single-needle and seven-needle electrodes) were also tested, and the discharge current using them could not reach 30 μA without causing pulses. A lower discharge current would require longer discharge time to ensure sufficient H_2O_2 concentration in the treated solutions to ensure the accuracy of measurement. The current limiting resistors are R_1 and R_2; the current-viewing resistor (CVR) is R_3. R_2 is connected between the reactor and the CVR to prevent the CVR from taking excessive partial voltage, which may damage the probe and oscilloscope. The voltage applied to the needle electrode was measured by a

Tektronix P6015A high voltage probe. The voltage on the CVR was measured by a Teledyne LeCroy PP008 probe. Voltages were recorded using a Teledyne LeCroy Waverunner 610Zi oscilloscope.

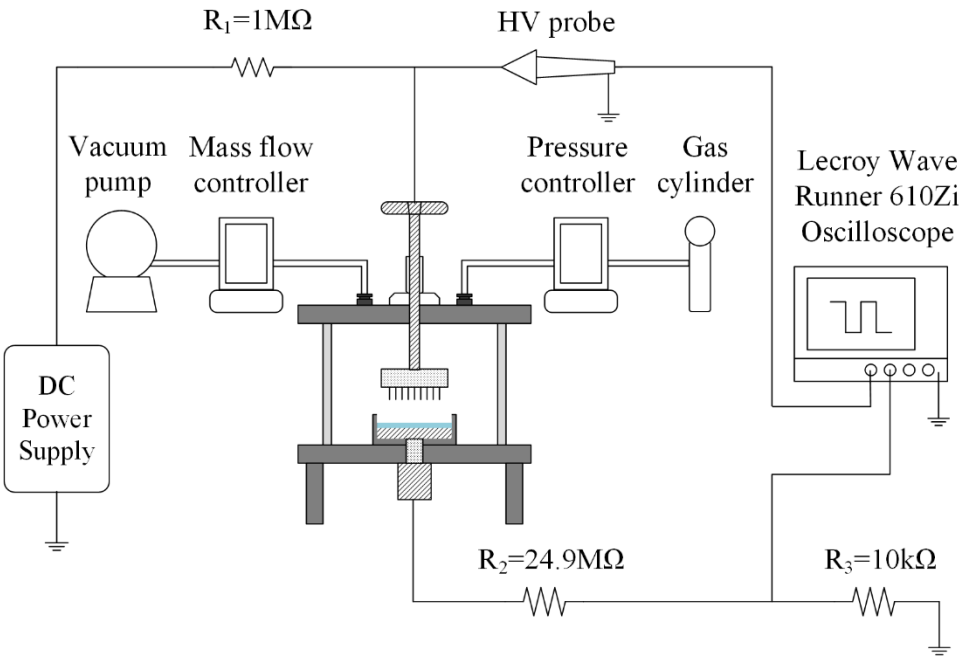

Figure 3.8 Electrical circuit design for corona discharge.

The electric circuit designed for glow discharge is shown in Figure 3.9. The glow discharge was generated using the same power supply as that in the corona discharge but with a single-needle electrode. In this case, the current limiting resistor R_2 is 2 MΩ and the current-viewing resistor R_3 is 1 kΩ, both are lower than those used for corona discharge, which is due to the glow discharge currents are higher and in the order of mA. The other components are the same as those in the corona discharge.

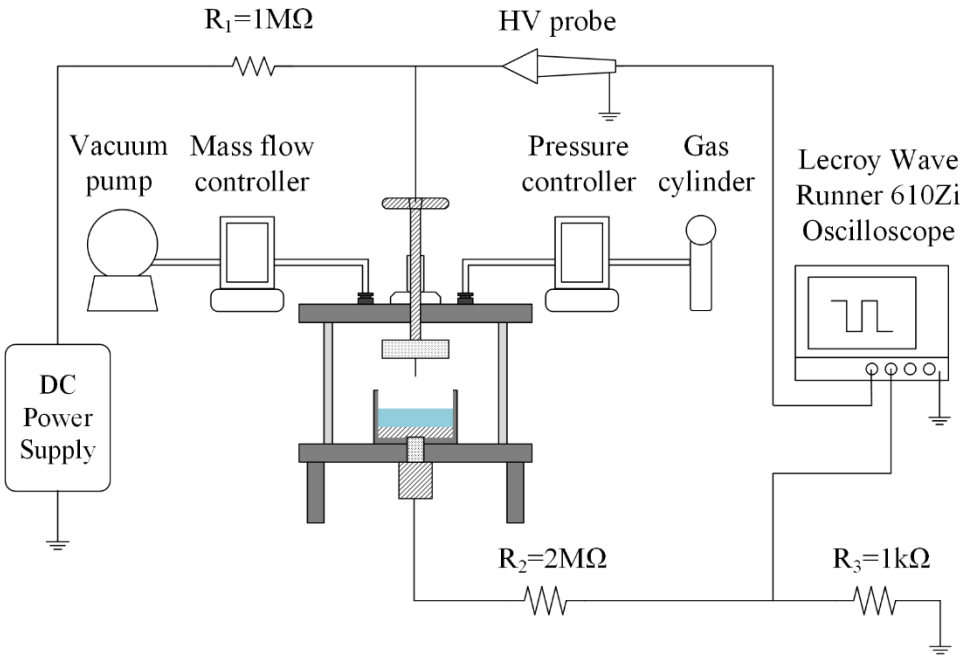

Figure 3.9 Electrical circuit design for glow discharge.

3.4.2 Electrical equipment

As stated above, a Glassman d.c. power supply was employed in the experiments. The power supply specifications are listed in Table 9.4.

A high voltage probe "Tektronix P6015A" was employed to monitor the applied voltage in the HV electrode. The voltage probe specifications are listed in Table 9.5.

The corona discharge is designed to run at a constant 30 μA without any pulsed current. As the pulses in the corona current will lead to inaccuracy in the calculation of ions quantity. The pulsed current was monitored using a 50-Ω coaxial cable (RG405) connected to the oscilloscope 50-Ω terminal. Table 9.6 lists the cable specification. Figure 3.10 shows the electrical circuit with the 50-Ω coaxial cable. No pulsed current was observed in the corona current under the corona discharge configuration.

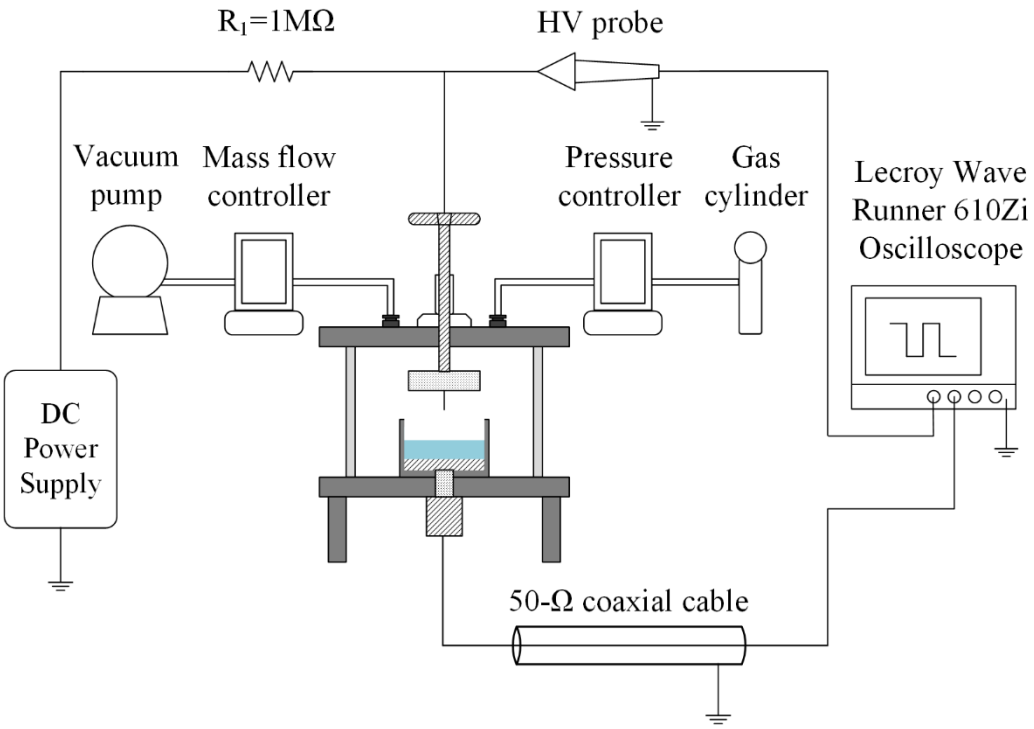

Figure 3.10 Electrical circuit design 50-Ω coaxial cable.

During the gas discharge, the voltage across the CVR was measured by a Teledyne LeCroy PP008 probe, the voltage was then converted to a current value according to the resistance. The specifications of the Teledyne probe are listed in Table 9.7.

The voltage signals were input into Teledyne LeCroy Waverunner 610Zi oscilloscope. The specifications are listed in Table 9.8.

3.5 Chemical analysis

3.5.1 H_2O_2 measurement

The concentration of hydrogen peroxide in liquid was determined by a spectrophotometric method using potassium titanium (IV) oxalate solution. This is a fast and sensitive approach which is able to measure the hydrogen

peroxide concentration as low as 10 μM [5]. Hydrogen peroxide can react with Ti^{4+} to form complex TiO_2^{2+} giving a yellow-orange colour in the solution and has a strong absorption at the wavelength of 390 nm. According to the Beer-Lambert law, the absorbance of solution is proportional to the solution concentration. The relationship is defined as:

$$\text{Abs} = \log_{10}\frac{I_0}{I} = \varepsilon \times l \times c \qquad \text{(Eq. 3.1)}$$

Where:

Abs	Absorbance of the solution for light
I_0	Intensity of input light
I	Intensity of output light
ε	Molar absorption coefficient ($M^{-1}cm^{-1}$)
l	Light path length in the solution (cm)
c	concentration of absorbing sample (M)

In the analysis, quartz cuvette which has cross section of 1 cm × 1 cm, capacity of 4 mL and path length of 1 cm, as shown in Figure 3.11, are placed in the ultraviolet-visible (UV-vis) spectrophotometer (Evolution 201, made by Thermo Scientific). The specifications of the instrument are listed in Table 9.11.

The preparation of the sample for analysis is as follows: after each gas discharge experiment, remove 3 mL of the treated sample solution from the container and mix it with 0.3 mL of 0.1 M Ti^{4+} solution and 0.3 mL of 1 M H_2SO_4 solution in the cuvette. After 1 minute, measure the absorption of the mixed solution at 390 nm using Thermo scientific evolution UV-Visible 201.

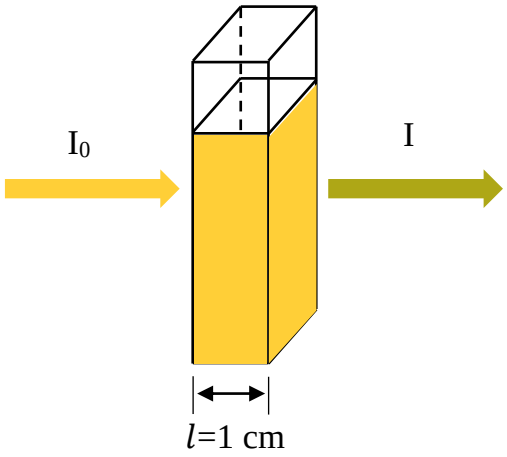

Figure 3.11 Determination of H_2O_2 concentration in the treated sample solution

A standard curve, representing the relationship between H_2O_2 concentration and absorbance, was made using standard solutions: the resulting data is presented in Figure 3.12. Each specific concentration of hydrogen peroxide solution was made by diluting a solution of known H_2O_2 concentration (30 wt%, CAS 7722-84-1, Sigma-Aldrich) in deionized water. As can be seen in the data in Figure 3.12, five concentrations of H_2O_2 were prepared: 0.01 mM, 0.05 mM, 0.1 mM, 0.5 mM and 1.0 mM. The H_2O_2 concentration was verified by potassium permanganate titration method. According to the standard curve, the concentration of H_2O_2 can be calculated from the measured absorbance:

$$c[H_2O_2] = 1.21 \times \text{Abs} \qquad \text{(Eq. 3.2)}$$

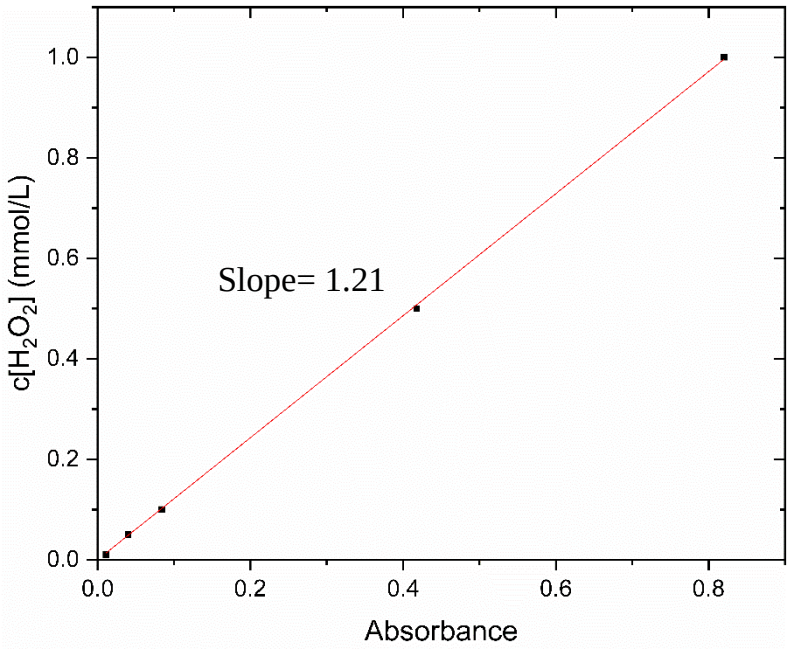

Figure 3.12 Standard curve for hydrogen peroxide concentration measurement.

3.5.2 pH and conductivity measurement

After the gas discharge, 3 mL treated sample solution was diluted with 12 mL deionized water to provide sufficient volume to measure pH and conductivity. The measured value was converted to the pH and conductivity for the treated sample solution. The measurement was conducted within 5 minutes after each gas discharge experiment.

For the water in gas-washing bottle, 15 mL water was removed from the bottle after each gas discharge for the pH and conductivity measurement.

The pH of the treated solution was measured using a Thermo Scientific Orion Star A211 pH meter. The instrument specifications are listed in Table 9.12.

3.5.3 Nitrate and nitrite measurement

The concentration of nitrite and nitrate in the solution was measured by a colorimetric test kit (Sigma-Aldrich, Cat. No. 11746081001). The nitrite reacts with sulfanilamide and N-(1-naphthyl)-ethylene-diamine dihydrochloride to form a diazo dye, exhibiting red colour with a peak absorbance at 540 nm that can be measured by a spectrophotometer. The treated samples were divided into two groups, in one group the nitrite is measured; in the other group, the nitrate was reduced to nitrite by nicotinamide adenine dinucleotide phosphate (NADPH) in the presence of the enzyme nitrate reductase (NR), and the total nitrite was measured. By comparing the difference of nitrite concentration, the nitrate concentration can be determined.

The conductivity of the treated solution was measured using a Thermo Scientific Orion Star A325 conductivity meter. The instrument specifications are listed in Table 9.13.

3.6 Chemical preparation

In each test, a volume of sample solution was filled into the sample container using a pipette. Three models of pipettes, manufactured by Gilson, were employed to dispense the measured volume of liquid. The specifications of the pipettes are listed in Table 9.9.

3.6.1 Deionized water preparation

The deionized water was obtained from a Milli-Q Integral 15 Water Purification System. The conductivity of the deionized water was measured to be lower than 1μS/cm, which indicates there are few ions in the water. The characteristics of water from the Milli-Q Integral 15 Water Purification System are listed in Table 9.10.

3.6.2 Tert-butanol solution preparation

0.01 M, 0.05M and 0.1 M tert-butanol (TB) solutions were used in the experiments to scavenge OH, thereby determines if H_2O_2 was produced by dimerization of OH. The tert-butanol solution was made by mixing tert-butanol (ACS reagent, ⩾99.7%, CAS 75-65-0, Sigma-Aldrich) in the deionized water, obtained from the water purification system described above. The volumes of tert-butanol and deionized water in TB solutions are given in Table 3.3.

Table 3.3 The volume of TB and deionized water in TB solutions.

Solution	TB volume	Deionized water volume
0.1 M TB	1.9 mL	198.1 mL
0.05 M TB	0.95 mL	199.05 mL
0.01 M TB	0.19 mL	199.81 mL

3.6.3 Dimethyl sulfoxide solution preparation

0.01 M, 0.05M and 0.1 M dimethyl sulfoxide (DMSO) solutions were used in the experiments to verify if the H_2O_2 was produced from OH dimerization. The DMSO solution was made by mixing dimethyl sulfoxide (ACS reagent, ⩾ 99.9%, CAS 67-68-5, Sigma-Aldrich) in deionized water. The volumes of DMSO and deionized water in the solutions are given in Table 3.4.

Table 3.4 The volume of DMSO and deionized water in DMSO solutions.

Solution	DMSO volume	Deionized water volume
0.1 M DMSO	0.71 mL	99.29 mL
0.05 M DMSO	0.355 mL	99.645 mL
0.01 M DMSO	0.071 mL	99.929 mL

3.6.4 Sulphuric acid solution preparation

The measurement of H_2O_2 by titanium ions requires an acidic environment. The sulphuric acid was prepared for acidize the treated solution to measure H_2O_2.

The 1 M H_2SO_4 was made by diluting 5.64 mL of concentrated sulphuric acid (AR reagent, > 95.0%, CAS 7664-93-9, Fisher Scientific) with 94.36 mL of deionized water.

3.6.5 Potassium titanium (IV) oxalate solution preparation

The 0.1 M potassium titanium (IV) oxalate solution was used for measuring hydrogen peroxide concentration, prepared by dissolving 3.93 g of $K_2TiO(C_2O_4)_2 \cdot 2H_2O$ (Technical, ⩾90%, Ti basis. Sigma-Aldrich) in 100 mL of deionized water.

3.7 Procedures

The procedures of the tests can be divided into the following stages:

i) Set up the gas and electrical systems according to the design.
ii) Open the reactor lid, and inject the sample solution into the sample container with pipette, close the reactor lid.

iii) Evacuate the reactor to a gas pressure below 4 Torr, and then inject the working gas to 760 Torr; repeat this process for three times to reduce the residual air.

iv) Conduct the gas discharge experiment and record the parameters.

v) After the gas discharge, remove the treated sample and prepare for analysis.

Each test was repeated for more than three times to ensure the consistency of the results, and the average value is reported. In corona discharge, it was observed that the discharge occurred on all the nine needles.

3.8 Conclusions

This chapter introduced the experimental systems and the preparation of the chemicals employed in this work. The experimental systems are divided into two sections: gas systems and electrical systems. The gas systems include the design of gas control system and the diagnostics of gas parameters, such as gas pressure, gas flow rate and ozone concentration. The design of gas control varies in order to meet the requirements of a specific test. The electrical systems include the design of electrical circuit and electrode topology. The current limiting resistors were employed for acquisition of stable d.c. cathode current and protecting the probe on current-viewing resistor. In corona discharges, nine-needle electrode and was employed for acquiring sufficient d.c. cathode current. In glow discharges, single-needle electrode was employed for acquiring ~ mA d.c. cathode current. The discharge voltage, current and time were measured; the input power and passing electric charge were calculated. The employed chemicals include deionized water, sulphuric acid solution, potassium titanium (IV) oxalate solution, TB solution and DMSO solution. The production of H_2O_2, nitrate and nitrite, pH and conductivity of treated solution were measured. The

parameters of the equipment employed in this work are listed. The procedures for general tests have been introduced.

4. Interface Reactions between Water and Positive Corona Discharge in N_2

4.1 Introduction

4.1.1 Motivation

Interface reactions between water and corona discharge have been proved able to effectively deactivate microorganisms and remove organic compounds in water [149-151]. Corona discharge over water produces a variety of reactive species, including ions, O_3, OH, excited molecules and atoms that enter the water and oxidize the pollutants directly or indirectly [24, 140]. Hoeben et al. achieved phenol decomposition in water by applying pulsed corona discharge above water surface [24].

The production of reactive species by corona discharge is affected by the gas compositions. It has been reported that the presence of nitrogen in the air reduces the efficiency of decontamination and sterilization in water [24, 154]. However, few reports have investigated the interface reactions between water and plasma generated by nitrogen corona discharge. The role of low energy positive ions in the interface reactions have not been well described. Different from glow discharges, the positive ions produced by corona discharge have little kinetic energy to ionize or dissociate multiple water molecules at the interface. Therefore, the charge transport process is completely driven by the potential energy of the positive ions.

4.1.2 Objectives

This chapter presents investigations into the reactions between water and the ionic wind generated by a positive corona discharge in nitrogen. The tests with water cathode and mesh cathode were conducted. The effects of low energy positive ions and reactive neutral species on the interface reactions were evaluated. Hydrogen peroxide production by positive ions and reactive neutral species was investigated under the following conditions:

i) Plasma treatment time from 30 to 150 minutes in 30-minute increments.
ii) Gas flow rates of 0.002, 0.02, 0.2, 0.5, 1 slpm.
iii) Gas pressures of 100, 200, 300, 500, 760 Torr.
iv) Deionized water, TB solution and DMSO solution.

The Faraday efficiency of the hydrogen peroxide production was investigated, which indicates the amount of H_2O_2 molecules produced with one ion reaching cathode. The change of pH and conductivity of the treated water was studied to help analyse the interface reaction mechanisms. The reactions caused by positive ions and reactive neutral species at the interface are discussed.

4.2 Voltage and current characteristics

The corona current was kept constant at 30 μA in all nitrogen corona discharges. No impulse current was observed when measuring with a 50-Ω coaxial cable. The applied voltage needs to be controlled to guarantee a constant 30 μA current, if the applied voltage is increased by several hundred volts, the impulse current will appear in the current waveforms.

As shown in Figure 3.8, the Tektronix P6015A high voltage probe detects the applied voltage on the needle electrode. Based on a discharge current of 30 μA, the discharge voltage (voltage from needle to cathode) was calculated by

subtracting the partial voltage V_{R2} on R_2 (24.9 MΩ) and partial voltage V_{R3} on R_3 (10 kΩ) from the detected voltage by Tektronix P6015A high voltage probe. Since the average d.c. current was kept constant at 30 μA (with a current fluctuation less than 1 μA), the total partial voltage (V_{tot}) was:

$$V_{tot} = V_{R2} + V_{R3} = 30\ \mu A * (24.9\ M\Omega + 10\ k\Omega) = 0.75\ kV \quad \text{(Eq. 4.1)}$$

For each test, the mean value of voltage read from the oscilloscope during the discharge is recorded as the discharge voltage. The relationship between the discharge voltage and the treatment time, gas flow rate, gas pressure and addition of TB or DMSO was investigated. This information is significant for analysing the discharge status and the change of solution characteristics after treatment.

Figure 4.1 shows the variation in discharge voltage for treatment times of 30, 60, 90, 120 and 150 minutes. There is no obvious variation in the discharge voltage as the treatment time increases, though the conductivity of deionized water increased with time.

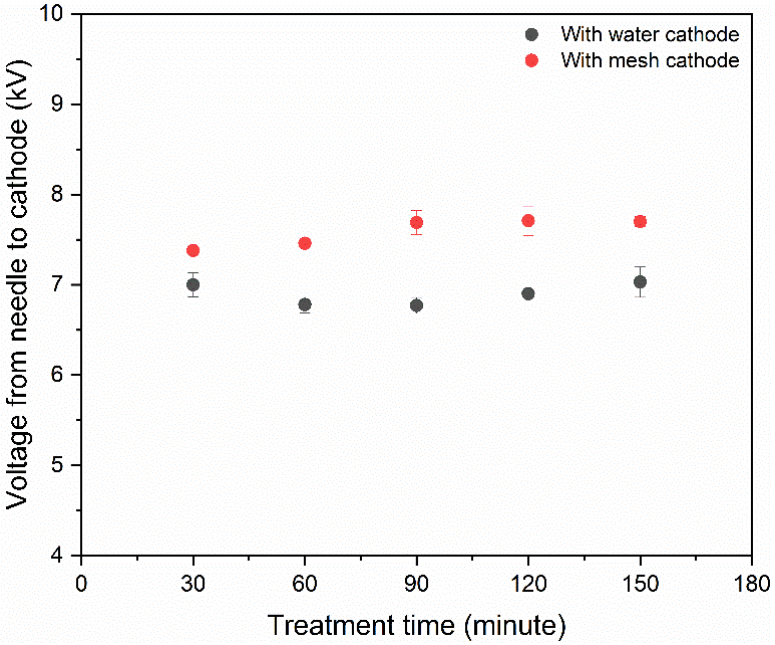

Figure 4.1 Nitrogen corona discharge voltage at 760 Torr with treatment time of 30, 60, 90, 120 and 150 minutes. The sample is deionized water. The gas flow rate is 0.5 slpm.

Figure 4.2 shows the discharge voltage measured at the gas flow rate of 0.002, 0.02, 0.2, 0.5 and 1.0 slpm. As the gas flow rate increased from 0.002 to 1.0 slpm, the discharge voltage shows a slight decrease in both the water cathode and mesh cathode tests.

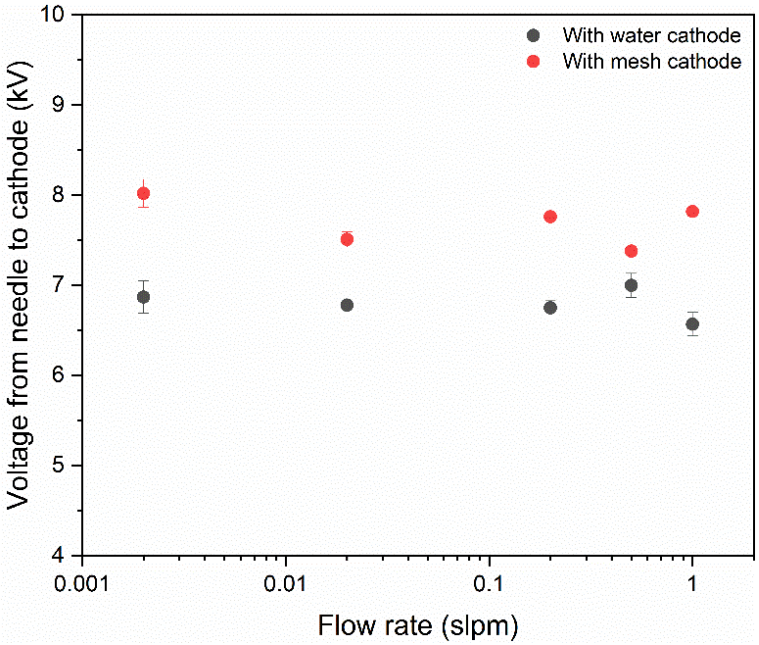

Figure 4.2 Nitrogen corona discharge voltage at 760 Torr with gas flow rate of 0.002, 0.02, 0.2, 0.5 and 1slpm. The sample is deionized water. The treatment time is 30 minutes.

Figure 4.3 shows the discharge voltage for gas pressures of 100, 200, 300, 500 and 760 Torr. As the gas pressure decreased, to maintain an average corona current of 30 µA the voltage applied to the needles need to be reduced. In water cathode tests, the voltage decreased from 6.87 kV to 3.11 kV as the gas pressure decreased from 760 to 100 Torr. In mesh cathode tests, the discharge voltage refers to the voltage from needle tips to the mesh. The discharge voltage in mesh cathode test was higher than that of water cathode tests under the same gas pressure. Since the mesh thickness is 0.6 mm, the real discharge gap could be larger than 10 mm for the mesh cathode. The water resistance is approximately

20 kΩ at a conductivity of 1 µS/cm. Since the current is 30 µA, the partial voltage across the water is around 600 mV at the beginning of gas discharge, which is negligible compared to the gap voltage. As the gas discharge proceeded, the water conductivity increased and the partial voltage dropped. At 100 Torr, the gap voltage for the water cathode and mesh cathode was very close. As the gas pressure was raised, the voltage difference between the two cathode types also increased, reaching a maximum of 1.11 kV at 760 Torr. As presented in Figure 4.3, the voltage in the mesh cathode test decreased from 7.98 to 3.23 kV when the gas pressure decreased from 760 to 100 Torr. The decrease of voltage was due to the lower pressure causing a reduction in the corona discharge voltage [206].

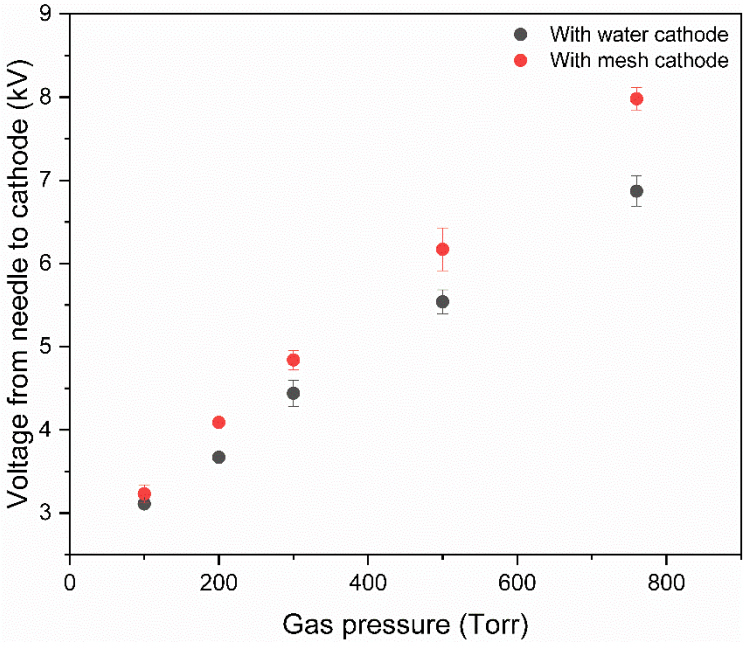

Figure 4.3 Nitrogen corona discharge voltage with gas pressure of 100, 200, 300, 500 and 760 Torr. The sample is deionized water. The treatment time is 30 minutes and the gas flow rate is 0.002 slpm.

Figure 4.4 shows the discharge voltage in water cathode tests at 300 Torr when different solution samples are used. Although the addition of DMSO to

deionized water did not change the discharge voltage, the presence of TB increased the discharge voltage. This is possibly due to the traces of TB vaporized into the gas phase and affecting the discharge gas composition, which resulted in an increase of the discharge voltage.

At an ambient temperature of 20 ℃, the vapour pressure of TB is 4.1 kPa [155], while the vapour pressure of DMSO is only 0.0594 kPa [156]. The extreme low vapour pressure may explain why the DMSO did not change the discharge voltage.

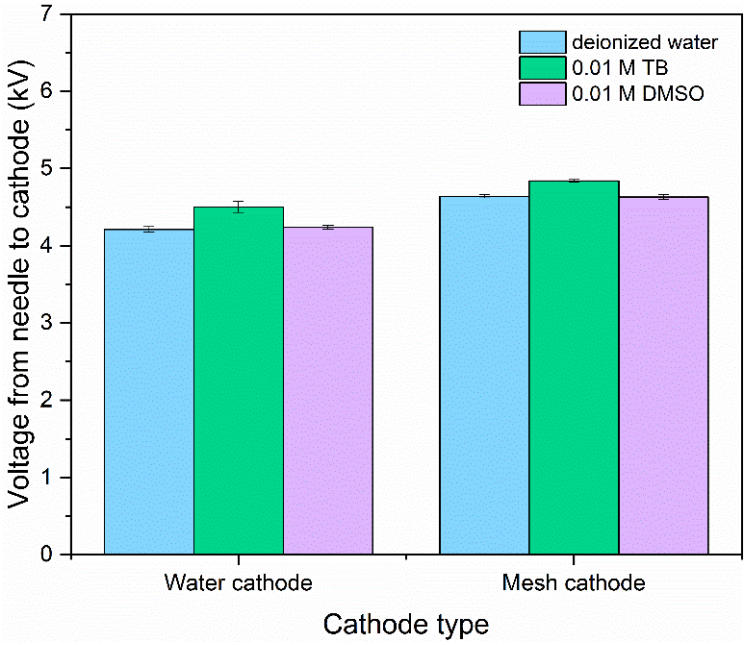

Figure 4.4 Nitrogen corona discharge voltage for water cathode tests at 300 Torr with deionized water, 0.01 M TB solution and 0.01 M DMSO solution. The treatment time is 30 minutes and the gas flow rate is 0.5 slpm.

4.3 Interface reactions between water and positive ionic winds

The production of H_2O_2 in water with treatment time was investigated at 30, 60, 90, 120 and 150 minutes. H_2O_2 production almost increased linearly with treatment time from 30 to 150 minutes in both water and mesh cathode tests. The hydrogen peroxide production in water cathode test was higher than that in mesh cathode tests. The difference in H_2O_2 production between the water cathode and mesh cathode test was thought to be caused by the action of positive ions. In the mesh cathode test, positive ions could not reach the water surface to initiate any ions-induced interface reactions. Hence, with a mesh cathode, only reactive neutral species in the ionic wind contributed to the H_2O_2 production in water.

4.3.1 H_2O_2 production with different gas flow rates

H_2O_2 production with gas flow rates of 0.002 slpm, 0.02 slpm, 0.2 slpm, 0.5 slpm and 1.0 slpm at atmospheric pressure was investigated. The treatment time was 30 minutes.

As Figure 4.5 shows, H_2O_2 production did not display a clear trend with the change of gas flow rate. There was a minimum H_2O_2 production of 0.112 μmol at the flow rate of 0.5 slpm with water cathode. In contrast, with a mesh cathode, the H_2O_2 production reached a maximum value of 0.088 μmol at 0.5 slpm but when the gas flow rate rose from 0.5 slpm to 1.0 slpm, H_2O_2 production experienced a significant reduction. This can be explained by considering that at higher gas flow rate the concentration of reactive neutral species and water vapor would decrease.

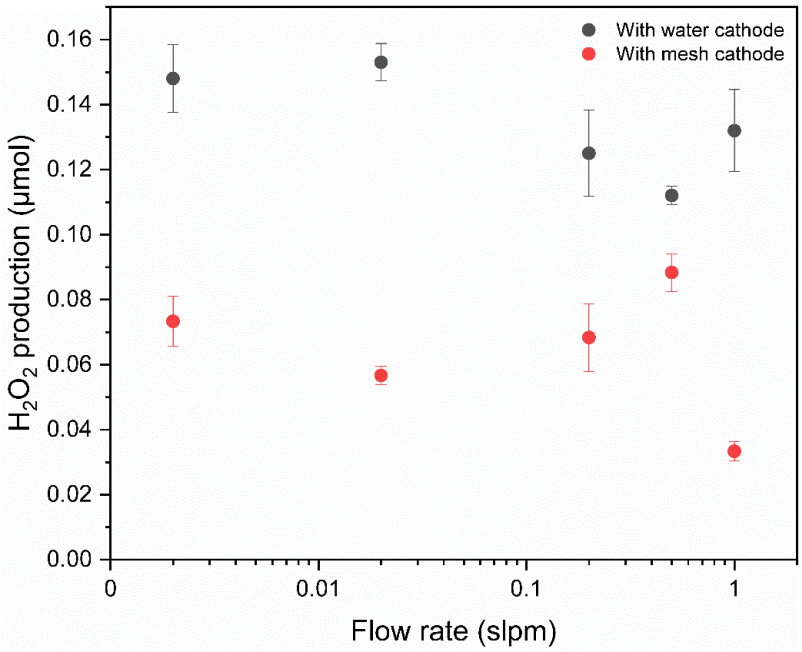

Figure 4.5 H_2O_2 production by nitrogen corona discharge at 760 Torr with a gas flow rate of 0.002, 0.02, 0.2, 0.5 and 1.0 slpm. The treatment time is 30 minutes.

4.3.2 H_2O_2 production with different gas pressures

Figure 4.6 presents the results for hydrogen peroxide production in deionized water at gas pressures of 100, 200, 300, 500, and 760 Torr. The gas flow rate was set at 0.002 slpm and the treatment time was 30 minutes. In water cathode tests, the H_2O_2 production decreased from 0.250 μmol to 0.148 μmol as the pressure increased from 100 to 500 Torr. H_2O_2 production was 0.148 μmol at 500 and 760 Torr. Given that the cathode is water, the measured H_2O_2 in the water were produced by two pathways: positive drift ions and reactive neutral species.

As shown in Figure 4.6, H_2O_2 production in mesh cathode tests was much lower than that in the tests with a water cathode. As discussed previously, in mesh cathode tests, only reactive neutral species could reach and react with water to produce H_2O_2. A slight decrease in H_2O_2 production was found as the pressure

increased from 100 to 500 Torr, with a maximum of 0.085 μmol obtained at 100 Torr. However, at 760 Torr, the production of H_2O_2 is greater than that at 500 Torr. There was no clear relationship between the gas pressure and H_2O_2 production in mesh cathode tests.

The difference in H_2O_2 production between the tests with water and mesh cathode was thought to be caused by positive drift ions. The increase of H_2O_2 production with a water cathode was mainly contributed by positive drift ions as the gas pressure decreased, i.e. as the gas pressure decreased from 760 to 100 Torr, the average reduced electric field increased by 3 times approximately, and this would result in the positive drift ions attaining higher kinetic energy.

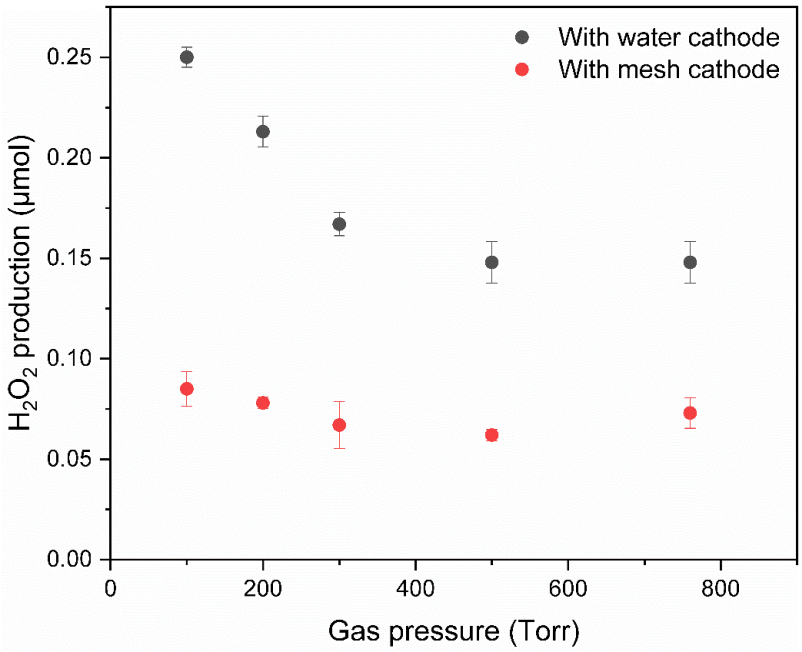

Figure 4.6 H_2O_2 production by nitrogen corona discharge at gas pressure of 100, 200, 300, 500 and 760 Torr. The treatment time is 30 minutes and the gas flow rate is 0.002 slpm.

Figure 4.3 and Figure 4.6 indicate that a decrease of gas pressure led to two results: higher hydrogen peroxide production in water cathode tests and lower

discharge voltages for both water and mesh cathode tests. Figure 4.7 shows the relationship between H_2O_2 yield and gas pressure.

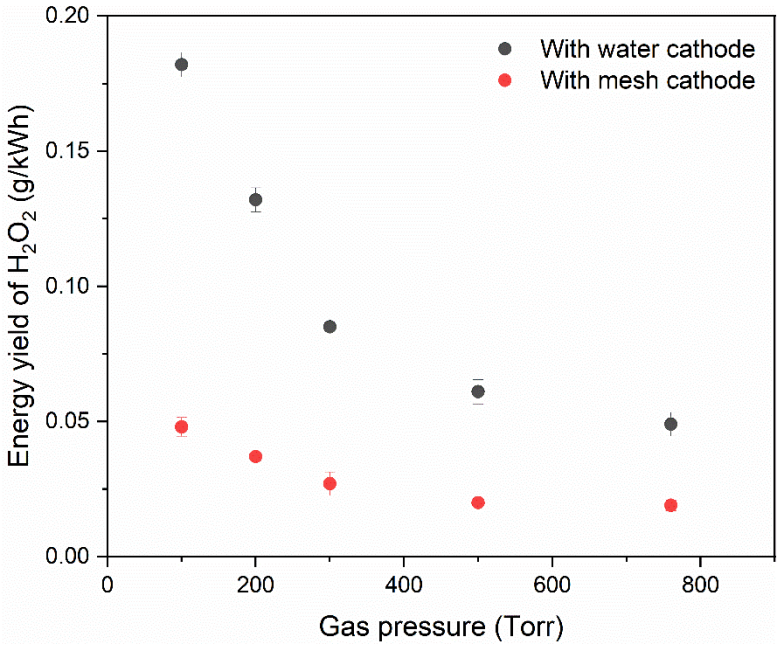

Figure 4.7 Energy yield of H_2O_2 for nitrogen corona discharge at gas pressure of 100, 200, 300, 500 and 760 Torr. The treatment time is 30 minutes and the gas flow rate is 0.002 slpm.

As Figure 4.7 shows, the H_2O_2 production increased as the gas pressure decreased from 760 to 100 Torr. In water cathode tests, the maximum H_2O_2 was obtained at 100 Torr, corresponding to a yield of 0.178 g/kWh, approximately 3 times of that at 760 Torr. In mesh cathode tests, the maximum H_2O_2 yield was 0.048 g/kWh, obtained at 100 Torr, approximately 2.5 times of that at 760 Torr.

4.3.3 H_2O_2 production with OH scavengers in water

To investigate whether hydrogen dioxide generation was from the dimerization of hydroxyl radicals, two types of OH scavengers were employed in the

following experiment: tert-butanol ($\mathrm{tert-C_4H_9OH}$) and dimethyl sulfoxide ($\mathrm{(CH_3)_2SO}$). The reactions between OH and these two scavengers are:

$$\mathrm{OH + tert-C_4H_9OH \rightarrow CH_2C(CH_3)_2OH + H_2O} \quad \text{(R 4.1)}$$

$$\mathrm{OH + (CH_3)_2SO \rightarrow (CH_3)_2SO(OH)} \quad \text{(R 4.2)}$$

Three sample solutions were tested: deionized water, 0.01 M TB solution, and 0.01 M DMSO solution. Each sample was treated for 30 minutes at a gas pressure of 300 Torr and a gas flow rate of 0.5 slpm. The test was not conducted at 760 Torr because the d.c. current could not reach 30 μA with TB solution.

In the water cathode tests, as Figure 4.8 shows, H_2O_2 production increased by 64.7% and 40.1% respectively with the addition of TB and DMSO. In the mesh cathode tests, as previously discussed, only reactive neutral species reached the solution and, hydrogen peroxide production increased by 43.5% with the addition of TB, while the addition of DMSO had minimal effects on H_2O_2 production.

The addition of OH scavengers did not reduce the H_2O_2 production for either the water cathode or mesh cathode test, implying that neither positive drift ions nor reactive neutral species reacted to produce OH in the solution as a major pathway. Higher concentrations of TB and DMSO solution (0.05 M and 0.1 M) were tested but the identical results were obtained.

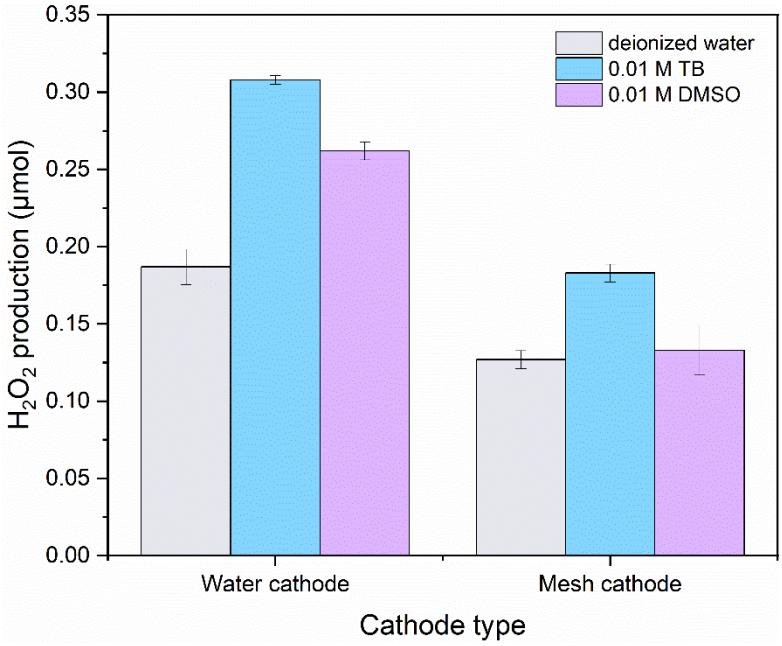

Figure 4.8 H_2O_2 production by nitrogen corona discharge at 300 Torr in deionized water, 0.01 M TB solution and 0.01 M DMSO solution. The treatment time is 30 minutes and the gas flow rate is 0.5 slpm.

4.3.4 pH and conductivity of treated deionized water

Using the same discharge regime, 5mL deionized water was treated for 60 minutes with a nitrogen flow rate of 0.2 slpm at 760 Torr.

As shown in Table 4.1, the original conductivity of the deionized water was lower than 1 μS/cm. After the treatment of 30 minutes, the conductivity of the water increased to 38.0 μS/cm and 41.3 μS/cm for the water cathode and the mesh cathode, respectively. The original pH of the deionized water was about 6.40. After treatment, the pH decreased to 4.38 for the water cathode, and 4.60 for the mesh cathode.

The conductivity and pH of the treated deionized water for the two types of cathode are very close, indicating that the reactive neutral species are the dominant factors leading to the change of water conductivity and pH. With the

water cathode, the concentration of NO_2^- and NO_3^- was measured to be 0.035 mM and 0.123 mM; with the mesh cathode, the concentration of NO_2^- and NO_3^- was 0.043 mM and 0.137 mM. The pH calculated based upon the concentration of NO_2^- and NO_3^- is 3.80 for the water cathode tests and 3.74 for the mesh cathode tests, which proves that the decrease of pH was mainly caused by the production of nitrite and nitrate in the solution. Cadorin et al. also found that water pH dropped to 3 following the treatment of corona discharge in nitrogen [157]. Takahashi et al. also reported that NO_2^- and NO_3^- were produced in water after plasma treatment in a N_2/O_2 gas mixture [158].

Table 4.1 pH and conductivity change of deionized water after 60-minute by nitrogen corona discharge at 760 Torr. The gas flow rate is 0.2 slpm.

Cathode type	pH and Conductivity (μS/cm)			
	$pH_{original}$	$pH_{after\ treatment}$	$Cond_{original}$	$Cond_{after\ treatment}$
Water cathode	6.40	4.38	0.847	38.0
Mesh cathode	6.40	4.60	0.895	41.3

4.3.5 Off gas analysis

To investigate the formation of gas phase reactive species in the reactor, the off gas was passed through a gas-washing bottle containing deionized water. The experimental set-up was presented in Figure 3.7. The experiment parameters are listed in Table 4.2. A volume of 20 mL deionized water was filled in the gas-washing bottle.

Table 4.2 Experimental parameter for off gas analysis.

Pressure (Torr)	Flow rate (slpm)	Sample	Water volume (mL)
760	0.5	Deionized H_2O	20

Three mesh configurations were used to analyse the off gas as Figure 4.9 shows. The barrier in Figure 4.9 (c) is a 1-mm thick Polytetrafluoroethylene (PTFE) square plate, with a side length of 60 mm.

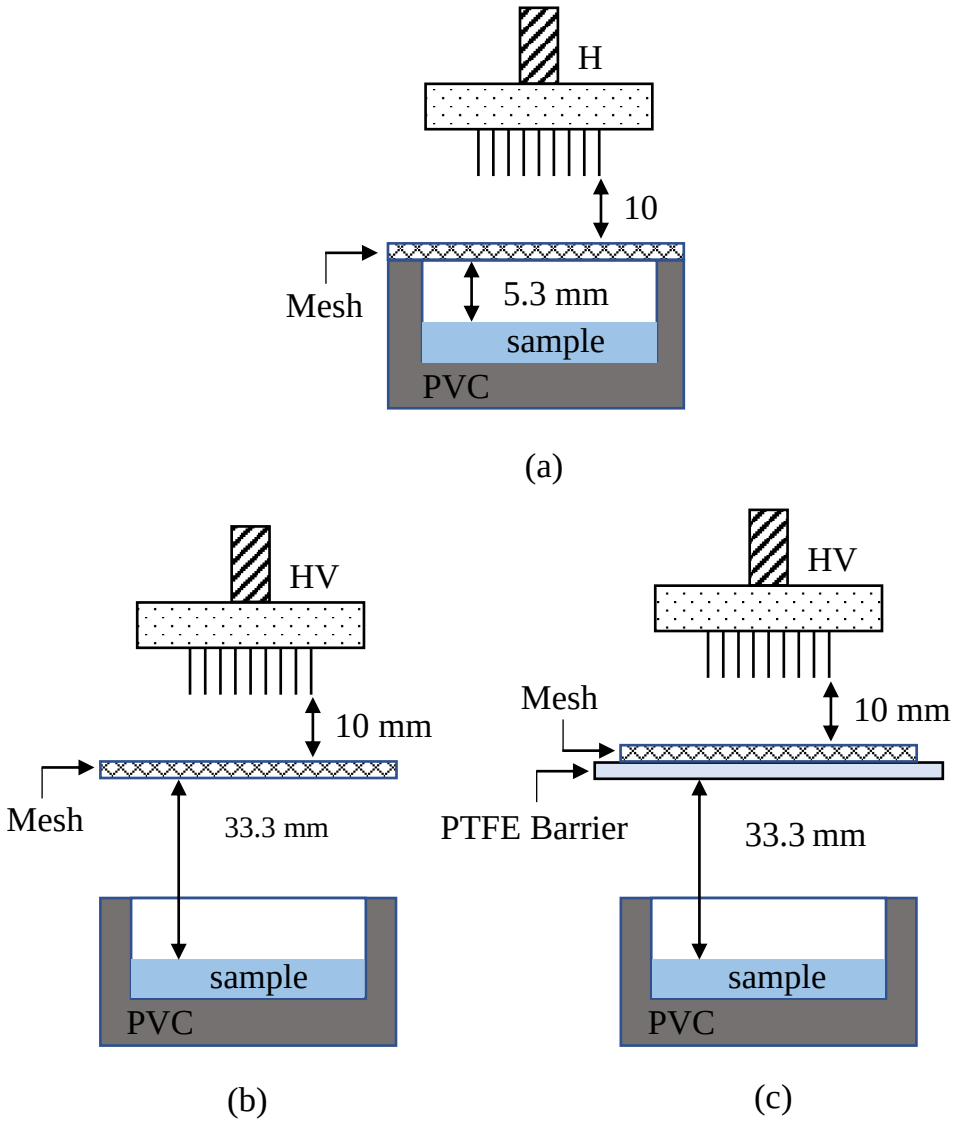

Figure 4.9 Mesh configurations employed for off gas analysis in nitrogen corona discharge: (a) mesh-water distance 5.3 mm without the PTFE barrier; (b) mesh-water distance 33.3 mm without the PTFE barrier; (c) mesh-water distance 33.3 mm with the PTFE barrier.

As Table 4.3 shows, H_2O_2 production in the gas-washing bottle water is much lower than that found in the sample solution in the plasma water reactor. In the test with a mesh to water distance of 5.3 mm, the H_2O_2 production in gas-washing bottle did not change with the treatment time from 30 to 60 minutes.

Since the H_2O_2 concentration in the gas-washing bottle is too low to be measured accurately. The results suggested that the reactive neutral species rarely exist in the off gas. The length of the tube connecting reactor and gas-washing bottle was about 1 m. The cross section of tube inner area is 0.12 cm^2. With gas flow rate of 0.5 slpm, the travel time t_{rg} for gas from reactor to gas-washing bottle cab be calculated as:

$$t_{rg} = 60\ \text{sec} \div \left(\frac{0.5\times10^3\ \text{cm}^3}{0.12\ \text{cm}^2\times100\ \text{cm}}\right) \approx 1.4\ \text{sec} \qquad \text{(Eq. 4.2)}$$

There was few H_2O_2 produced in gas-washing bottle, which indicates the lifetime of reactive neutral species should be less than 1.4 seconds.

Table 4.3 H_2O_2 production in reactor and in gas-washing bottle in different configurations with a mesh cathode.

Mesh configuration	Mesh-water distance (mm)	Treatment time (min)	H_2O_2 production in reactor (μmol)	H_2O_2 production in gas-washing bottle (μmol)
Fig. 4.10 (a)	5.3	30	0.088	0.020
Fig. 4.10 (a)	5.3	60	0.180	0.010
Fig. 4.10 (b)	33.3	60	0.103	0.012
Fig. 4.10 (c)	33.3	60	0.016	0.006

The pH and conductivity of the water in the gas-washing bottle were also measured, as recorded in Table 4.4. The deionized water in the gas-washing bottle has a pH value of 6.00 and conductivity of <1 μS/cm initially. After the treatment, there was a slight decrease in pH in both no-barrier tests and with-barrier tests, indicating that acids were formed in the gas washing bottle. The presence of the PTFE barrier increased further the water conductivity and pH drop in the gas-washing bottle. The PTFE barrier might reduce the ionic wind

reaching the water surface directly, which resulted in more nitrogen oxides in the off gas flowing into gas-washing bottle.

Table 4.4 pH and conductivity of the water in gas-washing bottle.

Mesh configuration	Mesh-water distance (mm)	Treatment time (mins)	pH after treatment	Conductivity after treatment (μS/cm)
Fig 4.10 (b)	33.3	60	5.70	1.658
Fig 4.10 (c)	33.3	60	5.43	3.260

4.4 The influence of mesh on the ionic wind

As discussed previously, it is assumed that the grounded mesh cathode filtered the positive ions from the ionic wind and only the reactive neutral species can reach water surface when using a mesh cathode. To validate the concept, the influence of the mesh cathode was investigated. On one hand, the mesh cathode could have attenuated the ionic wind, thereby reducing the number of reactive neutral species reaching water surface. On the other hand, a mesh cathode may react with reactive neutral species and thereby reducing the number of reactive neutral species reaching water surface. The influences of the mesh cathode on the ion wind were investigated below.

4.4.1 The influence of mesh openings

The open area of the mesh determines the attenuation effect on the ionic wind. To explore the effect of mesh open area, two types of stainless-steel square weaved mesh were put in comparison. Table 4.5 lists the parameters of the two meshes and the corresponding hydrogen peroxide production. The meshes were investigated at a gas pressure of 760 Torr and a gas flow rate of 0.2 slpm. In

each case, the mesh cathode was located 5.3 mm above the water surface, as shown in Figure 4.9 (a). The discharge time was 30 minutes.

Table 4.5 The hydrogen peroxide production with two types of meshes.

Mesh type	Opening	Wire width	Thickness	Open area percent	H_2O_2 production (μmol)
A	2 mm	0.3 mm	1 mm	59.2%	0.068
B	10 mm	2 mm	3 mm	69.4%	0.083

Results indicate that a higher percentage of open area causes the hydrogen peroxide production to increase slightly. However, the larger open area also resulted in a lower discharge voltage, 8.51 kV with mesh A and 8.18 kV with mesh B.

4.4.2 The influence of mesh-water distance

The impact of mesh-water distance on hydrogen peroxide production was investigated. The gas pressure was set to 760 Torr, and the mesh-water distance of 5.3 mm and 33.3 mm were investigated. To maintain the same electrical field in these experiments, the distance from needle tip to the mesh was set to 10 mm in both tests. As Table 4.6 shows, when the mesh-water distance was increased from 5 mm to 33.3 mm, H_2O_2 production was reduced by 42.8%. A possible reason for this is that as the distance increased, the travel time of reactive neutral species reaching water surface also increased. As a result of the increased travel time, some short-lived reactive neutral species would degrade to form stable species, which resulted in the decrease of hydrogen peroxide production. With increased mesh-water distance, more reactive neutral species would diffuse rather than reaching water surface directly, which resulted in less hydrogen peroxide production.

Table 4.6 Comparison of H_2O_2 production with mesh-water distances of 5.3 mm and 33.3 mm.

Mesh-water distance (mm)	Mesh configuration	Flow rate (slpm)	Treatment time (mins)	H_2O_2 production (μmol)
5.3	single-layer mesh	0.5	60	0.180
33.3	single-layer mesh	0.5	60	0.103

4.4.3 Comparison of single-layer and double-layer mesh cathode

A single-layer mesh cathode and a double-layer mesh cathode, as shown in Figure 4.10 (a) and Figure 4.10 (b) respectively, were compared to investigate the mesh influences. The meshes used in this section were of the type defined as mesh A as described in Table 4.5. The dimensions of the single mesh arrangement are the same as those given in Figure 4.9 (a), ensuring the comparability with previous data. As Figure 4.10 (b) shows, the double-layer mesh cathode was configured as the two meshes separated by 1 mm: both meshes were grounded; the distance from needle tip to the surface of upper mesh was 10 mm and distance from the bottom of lower mesh to water surface was 5.3 mm.

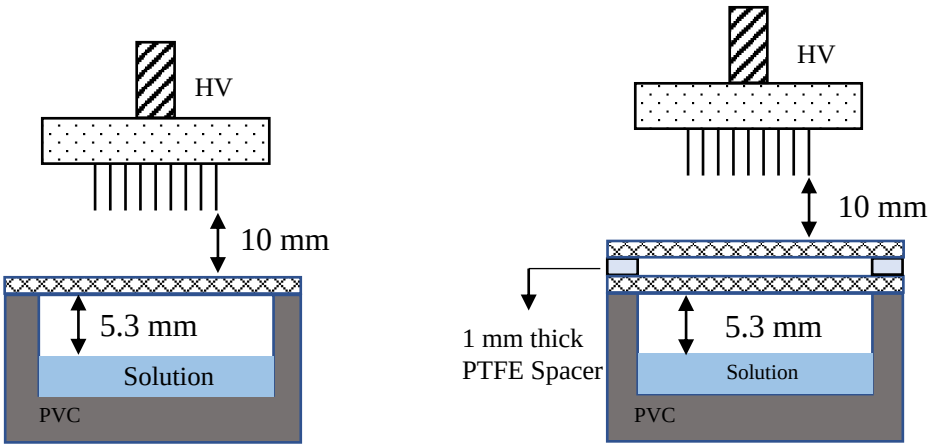

Figure 4.10 Electrode configurations with (a) single-layer mesh cathode and (b) double-layer mesh cathode for nitrogen corona discharge

The H_2O_2 production results for both cathode arrangements are listed in Table 4.7. The hydrogen peroxide production for both single and double-layer mesh cathode was comparable, which indicated that the addition of the second mesh had little effect on the transfer of reactive neutral species. This supports the previous concept that the grounded mesh removed the charged particles and only reactive neutral species could reach water surface, giving rise to the reactions producing H_2O_2. This result suggests that the addition of a second mesh does not significantly influence the production of hydrogen peroxide, allowing simpler design of plasma water reactor to be considered.

Table 4.7 H_2O_2 production with a single-layer and a double-layer mesh cathode.

Mesh-water distance (mm)	Mesh configuration	Flow rate (slpm)	Treatment time (mins)	H_2O_2 production (μmol)
5.3	single-layer	0.5	60	0.180
	double-layer	0.5	60	0.190

4.4.4 The influence of a PTFE barrier underneath the mesh cathode

To investigate the contribution of direct wind impact and diffused reactive neutral species, a further electrode configuration was developed, i.e. a PTFE barrier was placed underneath the mesh. The PTFE barrier is a square with side length of 55 mm and thickness of 1 mm, covering the whole mesh. Figure 4.11 illustrates the configuration with and without a PTFE barrier. The distance from the PTFE barrier to water surface is 33.3 mm, as shown in Figure 4.11 (b). In the tests without the PTFE barrier, as shown in Figure 4.11 (a), the distance from mesh to water surface is 33.3 mm. The other parameters for the tests are listed in Table 4.8.

Table 4.8 Experimental parameters of configurations with and without the PTFE barrier.

Configuration	Gas pressure (Torr)	Flow rate (slpm)	Treatment time (mins)	H_2O_2 production (μmol)
Without PTFE barrier	760	0.5	60	0.180
With PTFE barrier	760	0.5	60	0.016

The reactive neutral species were generated in nitrogen corona discharge. Given the test arrangements, in Figure 4.11 (a) and 4.11 (b), there are two possible paths for reactive neutral species to reach water surface. In Figure 4.11 (a), as discussed, it is probable that reactive neutral species were carried by the ionic wind to the water surface directly. In Figure 4.11 (b) the reactive neutral species diffuse through the atmosphere in the reactor before they reach the water surface.

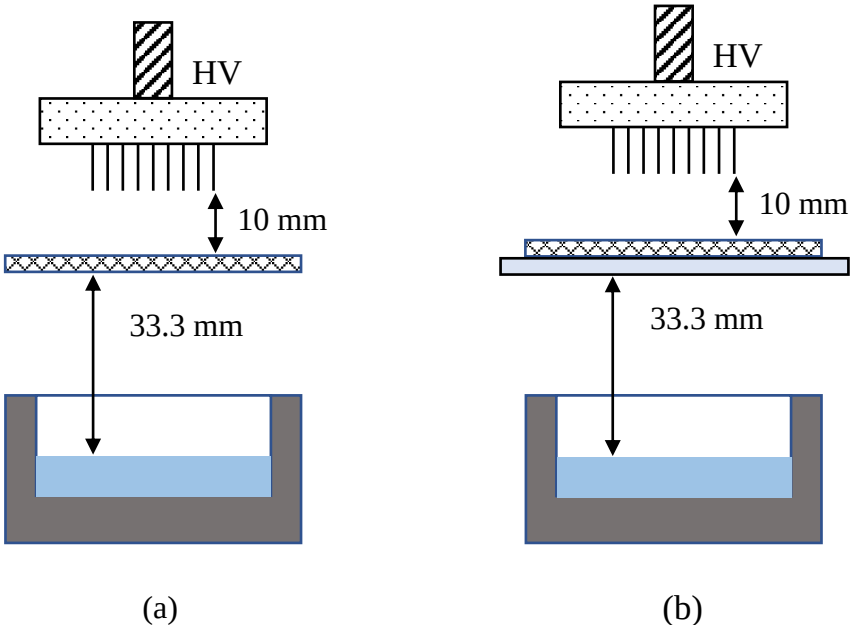

Figure 4.11 Electrode configurations without the PTFE barrier (a) and with the PTFE barrier (b) for nitrogen corona discharge.

Table 4.8 shows that with the PTFE barrier underneath the mesh, H_2O_2 production was reduced by 91.1%, which indicated that most of the hydrogen peroxide was produced by ionic wind carried reactive neutral species. The PTFE barrier blocks ionic wind, thereby increasing the travel time of reactive neutrals before reaching the surface which, as discussed above, allows the species to lose their excited state and become less likely to induce reactions at the water surface. However, in both of tests, there were also diffused reactive neutral species flow out of the reactor. When the off gas was injected into gas-washing bottle, there was few H_2O_2 in the water in gas-washing bottle. These results indicated that the lifetime of reactive neutral species is less than 1.4 seconds.

Other research has indicated that the velocity of ionic wind generated by d.c. corona discharge is between tenths of meters per second and several meters per second [159, 162, 163]. When there is no PTFE barrier, it takes about 10^{-3}–10^{-1}

seconds for the reactive neutral species to reach water surface. With the PTFE barrier, there is no direct path for the reactive species to reach water and H_2O_2 production decreased significantly, which indicated that most of reactive neutral species have decayed before reaching the water surface.

4.5 Faraday efficiency of H_2O_2 production

In this section the Faraday efficiency of H_2O_2 production is analysed to investigate the interface reactions between drift positive ions and water. In the plasma water reactor without mesh cathode, corona discharge in nitrogen generated positive ions and reactive neutral species, both of which reached water surface and initiated the interface reactions. The quantity ratio of the hydrogen peroxide molecules produced in water to the positive ions reaching water surface is used to indicate the Faraday efficiency in this analysis. The number of positive ions $\mathrm{Num_{ion}}$ is calculated as:

$$\mathrm{Num_{ion}} = \frac{\mathrm{Q}}{\mathrm{e}} = \frac{\mathrm{I \times t}}{\mathrm{e}} \qquad \text{(Eq. 4.3)}$$

Q is the total charge injected in period t and e is the unit charge, which is $1.6 \times 10^{-19}\mathrm{C}$. As previously discussed, with water vapour in the reactor, all the positive ions reaching water surface would be $H^+(H_2O)_n$, therefore, one positive ion has one unit charge. Since the corona current was kept at 30 μA, for 30-minute gas discharge, the number of positive ions reaching water is:

$$\mathrm{Num_{ion}} = \frac{(30\times10^{-6}\mathrm{A})\times(30\times60\mathrm{secs})}{1.6\times10^{-19}\mathrm{C}} = 3.375 \times 10^{17} \qquad \text{(Eq. 4.4)}$$

After treatment, the number of hydrogen peroxide molecules produced is:

$$\mathrm{Num_{H_2O_2}} = \mathrm{M_{H_2O_2}} \times \mathrm{N_A} \qquad \text{(Eq. 4.5)}$$

$\mathrm{M_{H_2O_2}}$ is the molar amount of hydrogen peroxide produced, N_A is the Avogadro constant. The Faraday efficiency $\mathrm{R_{H_2O_2/Q}}$ is

$$R_{H_2O_2/Q} = \frac{Num_{H_2O_2}}{Num_{ion}} \quad \text{(Eq. 4.6)}$$

4.5.1 Faraday efficiency with different gas pressures

As section 4.3.6 stated, the decrease of gas pressure significantly increased the hydrogen peroxide production in water cathode tests. In mesh cathode tests, positive ions cannot reach the water surface. As the gas pressure decreased, the hydrogen peroxide production did not increase. These results indicate that each positive ion produces more hydrogen peroxide at lower gas pressure. The Faraday efficiency at different pressures is shown in Table 4.9. The ion contribution is calculated by subtracting the Faraday efficiency obtained using mesh cathode from that of a water cathode. The gas flow rate was set to 0.002 slpm and the treatment time was 30 minutes.

Table 4.9 Faraday efficiency of H_2O_2 production with different gas pressures (The treatment time is 30 minutes and the gas flow rate is 0.002 slpm).

Cathode type	Faraday efficiency (H_2O_2/Q)				
	100 Torr	200 Torr	300 Torr	500 Torr	760 Torr
Water cathode	0.44	0.38	0.29	0.26	0.26
Mesh cathode	0.15	0.14	0.12	0.11	0.13
Ions' contribution	0.29	0.24	0.17	0.15	0.13

As Table 4.9 shows, the Faraday efficiency of hydrogen peroxide production did not present obvious change in mesh cathode tests as the gas pressure decreased.

In water cathode tests, the Faraday efficiency increased from 0.26 to 0.44 as the gas pressure decreased from 500 to 100 Torr. The increase in Faraday efficiency

was caused by the contribution of positive ions reaching water surface. As Table 4.9 shows, the ions' contribution increased from 0.13 to 0.29 as the gas pressure decreased from 760 to 100 Torr. The significant increase of Faraday efficiency in water cathode tests occurred when the gas pressure dropped from 300 to 200 Torr, with an increase of 31.0%.

As the gas pressure decreased from 760 to 100 Torr, the density of gas molecules dropped by 7.6 times, which means the mean free path of ions increased by 7.6 times. As Figure 4.3 illustrated, the discharge voltage dropped by 2.2 times in water cathode tests as the gas pressure dropped from 760 to 100 Torr. Therefore, the reduced electric field increased by 3.5 times, which resulted in higher kinetic energy of positive ions, which might increase the reaction rate of hydrogen peroxide production at the interface. The competitive reactions, for instance, oxygen evolution, might be suppressed. These hypotheses need to be further investigated.

4.5.2 Faraday efficiency in H_2O, TB and DMSO solutions

Both TB and DMSO are OH scavengers. If the H_2O_2 was produced from dimerization of OH in water in previous experiments, the addition of TB or DMSO in the solution will quench OH, therefore reducing or extinguishing the production of H_2O_2. It was found, on the contrary, when adding TB in the deionized water, the Faraday efficiency of H_2O_2 production increased by 0.21 in water cathode tests and 0.10 in mesh cathode tests. The ions' contribution was doubled with the addition of TB. The contribution of reactive neutral species also increased significantly with the addition of TB.

Similarly, the addition of DMSO increased the Faraday efficiency of H_2O_2 production by 0.13 in water cathode tests. But in mesh cathode tests, the addition of DMSO had little influence on the Faraday efficiency. This suggested that the intermediate products of the reaction between reactive neutral species

and water cannot react with DMSO. The H_2O_2 production by ions was doubled with DMSO in the solution, similar to the effect of adding TB. Hence it was suggested that the intermediate products of the reaction between positive ions and water can react with both TB and DMSO to produce twice as much H_2O_2 as that of the deionized water.

Table 4.10 Faraday efficiency of H_2O_2 production in deionized water, 0.01 M TB and 0.01 M DMSO at 300 Torr with gas flow rate of 0.5 slpm.

Cathode type	Faraday efficiency (H_2O_2/Q)		
	Deionized water	0.01 M65 TB solution	0.01 M DMSO solution
Water cathode	0.34	0.55	0.47
Mesh cathode	0.23	0.33	0.24
Ions' contribution	0.11	0.22	0.23

4.6 Analysis of interface reactions

4.6.1 Reactions between water and positive ions

It has been demonstrated above that the positive ions and reactive neutral species generated in nitrogen corona discharge are carried by ionic wind to the water surface and participate in the interface reactions. In the process, both positive ions and reactive neutral species contributed to the hydrogen peroxide production in water. In this section, the reaction mechanisms at the interface were analysed.4.6.1 Reactions between water and drift positive ions

With water in the reactor, when the humidity is saturated at room temperature of 20 ℃, water vapor accounts for about 2.3% of the gas volume [160]. The

nitrogen ions, initially produced by corona discharge, quickly transfer the positive charge to water molecules. Good demonstrated that almost all of the positive ions are transformed to $H^+(H_2O)_n$ after 1 ms of discharge in nitrogen containing traces of water (water vapour ratio is 7.5 ‰) [57]. The corona discharge generated N_2^+ would react with nitrogen molecules to form N_4^+ within 100 μs [57]:

$$N_2^+ + N_2 \rightarrow N_4^+ \quad \text{(R 4.3)}$$

N_2^+ and the newly formed N_4^+ react with water molecules [57]:

$$N_2^+ + H_2O \rightarrow H_2O^+ + N_2 \quad \text{(R 4.4)}$$

$$N_4^+ + H_2O \rightarrow H_2O^+ + 2N_2 \quad \text{(R 4.5)}$$

The H_2O^+ rapidly reacts with H_2O to produce OH and H_3O^+, of which the latter continues clustering reactions to form $H^+(H_2O)_n$:

$$H_2O^+ + H_2O \rightarrow H_3O^+ + OH \quad \text{(R 4.6)}$$

$$H_3O^+ + H_2O \rightarrow H^+(H_2O)_2 \quad \text{(R 4.7)}$$

……

$$H^+(H_2O)_{n-1} + H_2O \rightarrow H^+(H_2O)_n \quad \text{(R 4.8)}$$

Figure 4.12, from [57], illustrates the density of different ions in nitrogen after the discharge. All the positive ions were transferred to $H^+(H_2O)_n$ within 100 microseconds. The velocity of ionic wind generated by corona discharge was reported between tenths of meters per second and several meter per second [162, 163]. Since the distance between the needle tip and water cathode was 10 mm, the travel time for the reactive neutral species in ionic wind to reach the water surface was in the range of 1-100 milliseconds. Therefore, all the positive ions would transform to $H^+(H_2O)_n$ before reaching the water surface.

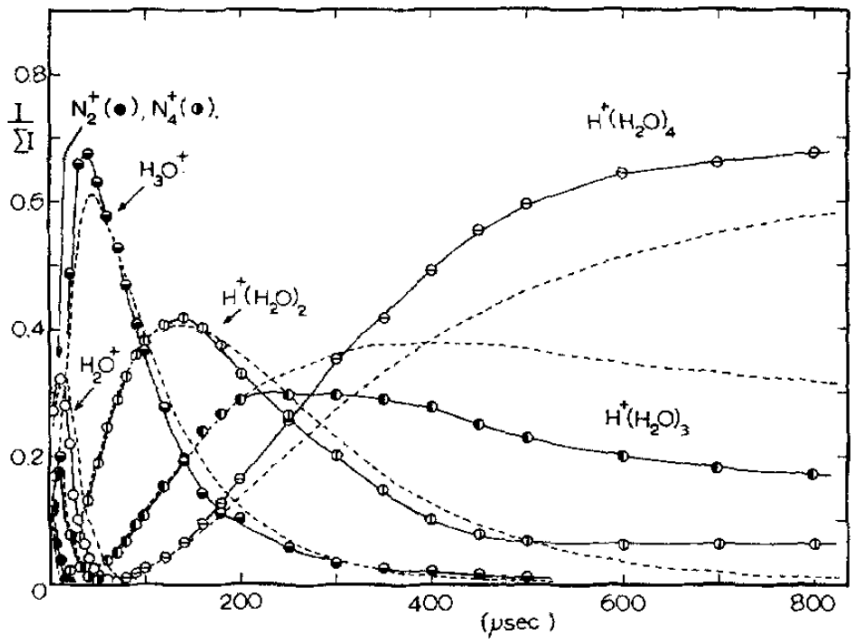

Figure 4.12 Normalized ion-intensity curves for ions in nitrogen containing traces of water vapour after 10 μs electron pulse. [N_2] = 6.4×10^6, [H_2O] = 4.8× 10 molecule/cc, 300^{o}K. Successive intensity maxima indicate the sequence [57].

According to the analysis above, the positive ions that eventually reach the water surface are $H^+(H_2O)_n$ clusters. The interface reactions between the positive ions and water also involve electrochemical processes, with bulk of positive drift ions $mH^+(H_2O)_n$ acting as the ion anode on the water surface.

The ion anode here is like a non-reactive anode material employed in traditional electrolysis. It has been reported that, in traditional electrolysis with specific electrode materials like Boron-doped diamond and Ti/SnO_2, hydroxyl radicals (OH) and reactive oxygen (O) can be adsorbed on the anode surface, which is probably similar to the effect of the ion anode in this case, as these electrode materials are non-reactive and have weak adsorption to OH, leading to low O_2 evolution but high OH production [164]. The adsorbed hydroxyl radicals

M(·OH) and the adsorbed reactive oxygen M(·O) can oxidize organic pollutants in the water [166].

Figure 4.13 illustrates the interface reactions between positive ions and water. A water molecule loses an electron to the ion anode and forms H^+ and (m-1)$H^+(H_2O)_n$(·OH). The adsorbed (·OH) may lose one electron to the ion anode and form H^+ and the adsorbed (·O), while the adsorbed oxygen (·O) can recombine to produce O_2. Alternatively, the adsorbed (·OH) may recombine to produce H_2O_2. In this research, 1 mol of positive ions produce only 0.13 mol of hydrogen peroxide in water at atmospheric pressure (760 Torr). This ratio increased to 0.29 when gas pressure decreased to 100 Torr, which is lower than that predicted by Faraday's law, suggesting that the production of H_2O_2 was concomitant with O_2 evolution.

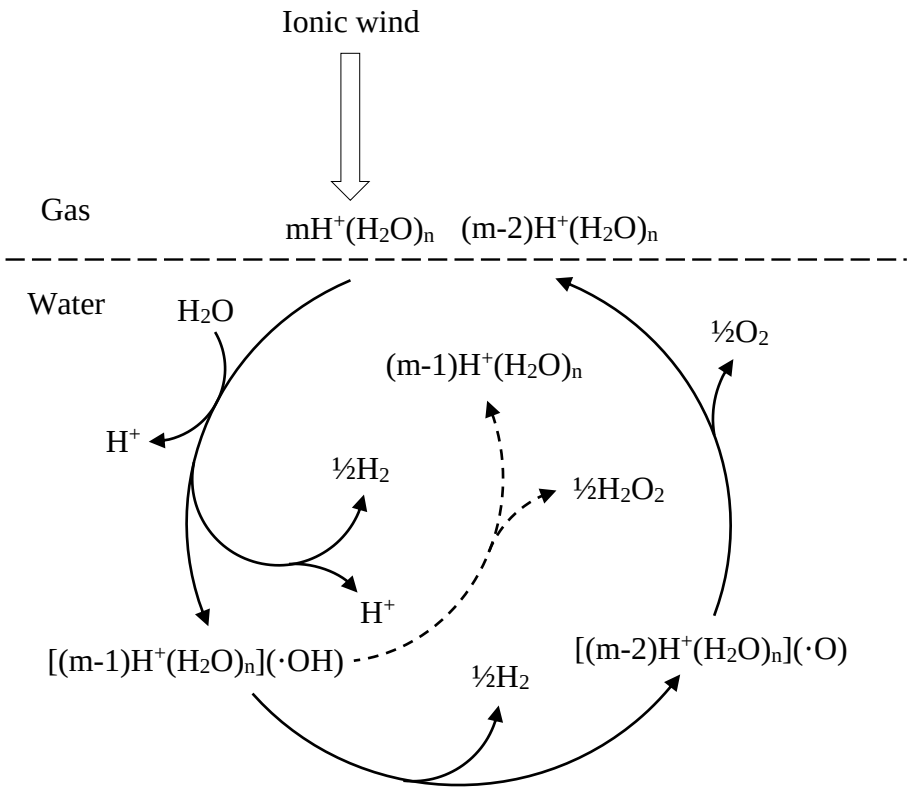

Figure 4.13 Interface reactions of positive drift ions $mH^+(H_2O)_n$ as the ion anode for nitrogen corona discharge. m is the number of $H^+(H_2O)_n$.

The hydrogen peroxide production by positive drift ions was doubled when TB or DMSO was added as shown in Table 4.10. No free radicals produced by the plasma-water reactions were found to react with both TB and DMSO to produce H_2O_2. One hypothesis is that the adsorbed hydroxyl radicals $H^+(H_2O)_n(\cdot OH)$ and active oxygen $H^+(H_2O)_n(\cdot O)$ can synergistically react with TB or DMSO in water to produce twice as much hydrogen peroxide as in the deionized water without the addition of scavengers.

Zhao et al. investigated the production of hydrogen peroxide production in water by pulsed positive discharges in nitrogen above the water cathode, with a pin-plate electrode configuration. They found that the amount of hydrogen

peroxide generated decreased significantly with the addition of TB to deionized water [167]. They suggest that a decrease of hydrogen peroxide demonstrates that OH is the precursor of hydrogen peroxide. However, in the present study, the addition of TB and DMSO did not reduce the production of hydrogen peroxide for either water cathode tests or mesh cathode tests. This implies that hydroxyl radicals were not the major reactive products in the reactions between water and positive drift ions of low kinetic energy.

4.6.2 Reactions between water and reactive neutral species

It has been reported that hydroxyl radicals, excited nitrogen molecules, nitrogen atoms, etc. can be generated by corona discharge in N_2/H_2O mixture [168, 169]. One of the excited states of nitrogen molecule is $N_2(A^3\sum_u^+)$ state. As the lifetime of $N_2(A^3\sum_u^+)$ is reported to be longer than 10 ms [170], which may be longer than the travel time of ionic wind. Hence this excited state of nitrogen molecule can be carried to the water surface and participate in the interface reactions. Fresnet et al. explained the process [17]:

$$e^* + N_2(X) \rightarrow e + N_2(A^3\sum_u^+) \qquad \text{(R 4.9)}$$

$$N_2(A^3\sum_u^+) + H_2O \rightarrow N_2(X) + H + OH \qquad \text{(R 4.10)}$$

$N_2(X)$ is the ground state nitrogen molecule and e* is the energetic electron.

In this research, with the addition of TB, the production of H_2O_2 by reactive neutral species was increased. With the addition of DMSO, the production of H_2O_2 by reactive neutral species was almost the same as that in the deionized water. Based on this result, HO_2 was probably the major reactive neutral species, since it can react with TB to produce H_2O_2, but not DMSO.

$$HO_2 + \text{tert} - C_4H_9OH \rightarrow (CH_3)2C(OH)CH_2 + H_2O_2 \qquad \text{(R 4.11)}$$

The self-reaction of HO_2 can also generate H_2O_2:

$$HO_2 + HO_2 + H_2O \rightarrow H_2O_2 + O_2 + H_2O \quad \text{(R 4.12)}$$

With the same amount of HO_2 transported to the water, Reaction R 4.11 can produce twice the amount of H_2O_2, in comparison to Reaction R 4.12. However, the addition of TB did not double the H_2O_2 production. Hence, the H_2O_2 must not all come from the dimerization of HO_2 in the deionized water. This implies that part of the H_2O_2 produced in the deionized water might come from the gas phase H_2O_2 that was produced in the corona discharge and transported to the water. Although HO_2 can react with H_2O_2 to form O_2 in the aqueous phase, the dimerization of HO_2 has a much higher reaction rate.

4.7 Conclusions

The interface reactions between water and positive ionic wind generated by nitrogen corona discharge were investigated. The effects of treatment time, gas pressure, gas flow rate and OH scavengers (TB and DMSO) on H_2O_2 production have been explored. The effects of low energy ions and reactive neutral species at interface have been determined: both of them reacted with water to produce H_2O_2. Experiments show that the production of H_2O_2 in water increased linearly with treatment time, drift positive ions accounted for 50% of the total H_2O_2 production at atmospheric pressure, and the figure increased at lower gas pressure. The best energy yield of H_2O_2 production by drift ions in deionized water was achieved at 100 Torr, with 1 mol ions producing 0.29 mol H_2O_2. Since the energy transferred to the interface is mainly the potential energy of ions, this is equivalent to 47 eV to produce one H_2O_2 molecule, or an energy yield of 29 g/kWh, However, taking into consideration that the energy input was mostly dissipated in the corona discharge, the overall energy efficiency was still low.

A novel reaction mechanism between positive drift ions and water has been developed. At the interface, accumulated positive ions may act as an ion anode,

on which the adsorbed hydroxyl radicals and the adsorbed oxygen are formed, accompanying the evolution of oxygen and hydrogen. As outlined above, the adsorbed oxidative agents can form H_2O_2 in deionized water, or react with TB or DMSO to produce H_2O_2. In addition, the reactive neutral species led to the production of H_2O_2 in water, as the result of recombination of HO_2 and the transportation of gas phase H_2O_2 into water.

The water pH and conductivity changes observed were proven to be mainly caused by the formation of nitrate and nitrite in water, which were produced by the reactions between water and reactive neutral species. In mesh cathode tests, the ionic species are removed from the ionic wind prior to impact with the liquid surface, after 60-minute corona discharge at 760 Torr, the water pH dropped to 4.60 and the water conductivity increased to 41.3 μS/cm. In water cathode tests, the concentration of NO_2^- and NO_3^- was measured to be 0.035 mM and 0.123 mM; with mesh cathode, the concentration of NO_2^- and NO_3^- was 0.043 mM and 0.137 mM.

The interaction of the off gas and water produced little hydrogen peroxide, or change of water pH and conductivity.

The influence of the mesh structure on the experimental results was also analysed. It was found that a mesh with larger open area (59.2% to 69.4%) resulted in a slight increase of the hydrogen peroxide production (from 0.068 to 0.083 μmol). A double-layer mesh did not cause a decrease of hydrogen peroxide production. These results indicated that the changes in mesh dimension did not significantly affect the reactive neutral species reaching water surface. However, a longer distance between mesh and water or the presence of the PTFE barrier underneath the mesh can significantly decrease the hydrogen peroxide production, suggesting that the amount of reactive neutral species reaching water and the lifetime of reactive neutral species are vital for the production of hydrogen peroxide in water.

5. Interface Reactions between Water and Positive Corona Discharge in O_2

5.1 Introduction

5.1.1 Motivation

The ionic wind generated by positive corona discharge in nitrogen has been proved able to produce hydrogen peroxide in water, with a maximum yield of 0.178 g/kWh. Both positive ions and reactive neutral species contributed to hydrogen peroxide production.

Compared with corona discharge in nitrogen, corona discharge in oxygen can produce more types of reactive neutral species, such as O, $^1O_2$, and O_3, which react with water to form OH and HO_2 [22]. Hence, oxygen corona discharge has potential to achieve higher energy yield of OH and H_2O_2. However, different from nitrogen ions, the potential energy of both O_2^+ (12.06 eV) and O_4^+ (11.66 eV) is lower than the ionization energy of H_2O (12.62 eV) [64], which may lead to different reaction mechanism at the interface. Hence, investigating the reactions between water and oxygen corona discharge can provide a contrast to the results obtained in nitrogen corona discharge.

5.1.2 Objectives

This chapter explored the reaction mechanisms between water and the ionic wind generated by oxygen corona discharge. The hydrogen peroxide production by positive ions and reactive neutral species were investigated. The effect of treatment time, gas flow rate, gas pressure, and OH scavengers on H_2O_2 production has been explored. The pH and conductivity change in water after treatment has been analysed.

The interface reactions caused by positive ions and reactive neutral species generated by oxygen corona discharges has been discussed. The composition of reactive neutral species (such as O, HO_2, H_2O_2, O_3) generated by oxygen corona discharges were analysed. The difference of influence of mesh on ionic wind between nitrogen and oxygen corona discharges has been demonstrated.

5.2 Voltage and current characteristics

The corona d.c. current was kept constant at 30 μA in all tests. At the beginning of oxygen corona discharge, there were irregular current pulses with an amplitude of tens of μA. After several minutes of discharge, the current and voltage waveforms became constant, which should be due to the increase of water conductivity as the corona discharge progressed. In nitrogen corona discharge, there was no voltage settling period observed, this is possibly due to the fact that the water conductivity increased much faster. Compared to the treatment time applied in the test, the settling period was short and the effect to the experiments was assumed negligible.

As the discharge progressed, the needle voltage decreased slightly and settled at a constant value after several minutes. After this period, no pulse current was observed when measuring with a 50-Ω coaxial cable as shown in Figure 3.10. The discharge voltage characteristics with treatment time, gas flow rate, gas pressure and sample solution were investigated.

From experiments using water and mesh electrode, Figure 5.1 shows the discharge voltage with different treatment time, measured at 760 Torr and a gas flow rate of 0.2 slpm. There is no significant change of discharge voltage as the treatment time increased from 30 to 150 minutes.

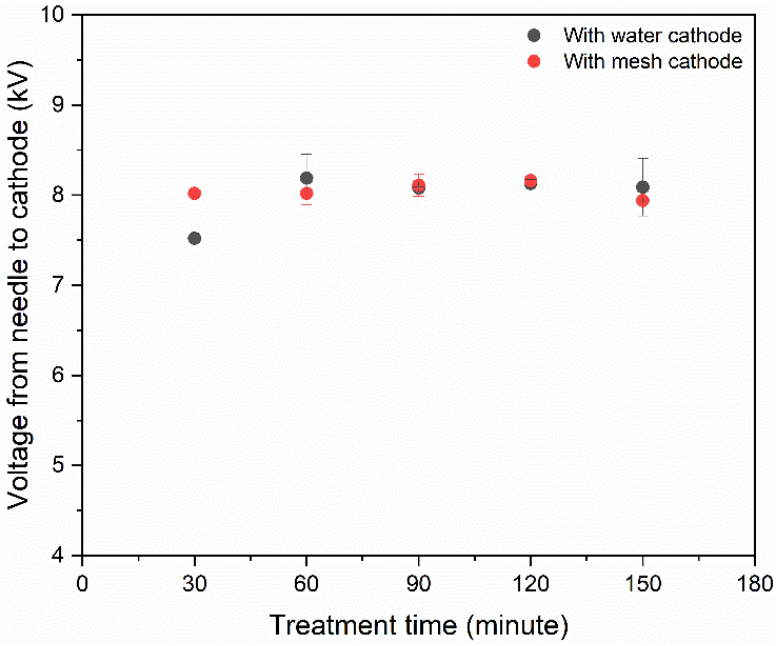

Figure 5.1 Oxygen corona discharge voltage at 760 Torr with treatment time of 30, 60, 90, 120 and 150 minutes. The sample is deionized water. The gas flow rate is 0.2 slpm.

Figure 5.2 shows the discharge voltage measured at different gas flow rates at 760 Torr. The discharge voltage in water cathode and mesh cathode tests were almost the same at gas flow rate of 0.002 and 0.02 slpm, however, when the gas flow rate was increased above 0.2 slpm, the discharge voltage with mesh cathode became higher than that with water cathode and the difference grew as the gas flow rate increased.

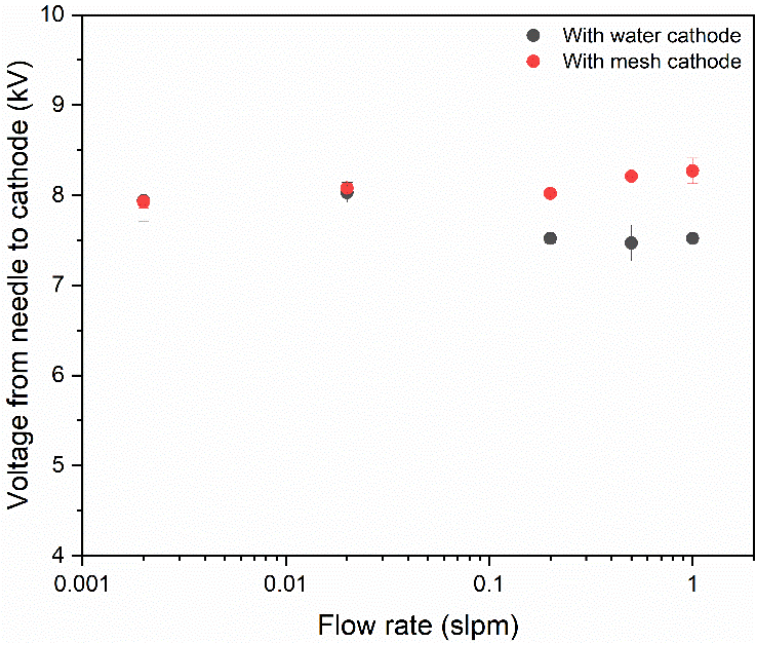

Figure 5.2 Oxygen corona discharge voltage at 760 Torr with gas flow rate of 0.002, 0.02, 0.2, 0.5 and 1slpm. The sample is deionized water. The treatment time is 30 minutes.

Figure 5.3 shows the discharge voltage measured at different gas pressures. As the gas pressure increased from 200 to 760 Torr, the discharge voltage increased from 4.14 to 7.54 kV in water cathode tests and from 3.69 to 8.01 kV in mesh cathode tests. For mesh cathode tests, the discharge voltage was close for corona discharge in nitrogen and oxygen at the same gas pressure; however, for water cathode tests, the discharge voltage in oxygen was higher than that in nitrogen. For example, at 760 Torr, the discharge voltage was 7.54 kV for oxygen and 6.87 kV for nitrogen in water cathode tests. In nitrogen corona discharge, the conductivity of treated water was higher than that in oxygen corona discharge. However, the water conductivity difference cannot cause a difference of several hundred volts in the discharge voltage since the current was only 30 µA. The water resistance can be calculated as:

$$R_{DI} = \frac{l}{\sigma S}$$

In the equation, σ is the water conductivity, assumed to be 0.5 μS/cm for deionized water. l is the thickness of water, 0.314 cm. S is the cross-section area of water, 15.90 cm^2. Hence,

$$R_{DI} = \frac{0.314\ cm}{0.5\ \mu S/cm \times 15.90\ cm^2} \approx 40\ k\Omega$$

The corona current was assumed to be uniformly distributed on the water surface.

Since the corona current was 30 μA, the voltage drop at the deionized water was calculated to be 1.2 V, which is negligible compared to discharge voltage. Hence the voltage difference was considered caused by the difference discharge characteristics in nitrogen and oxygen.

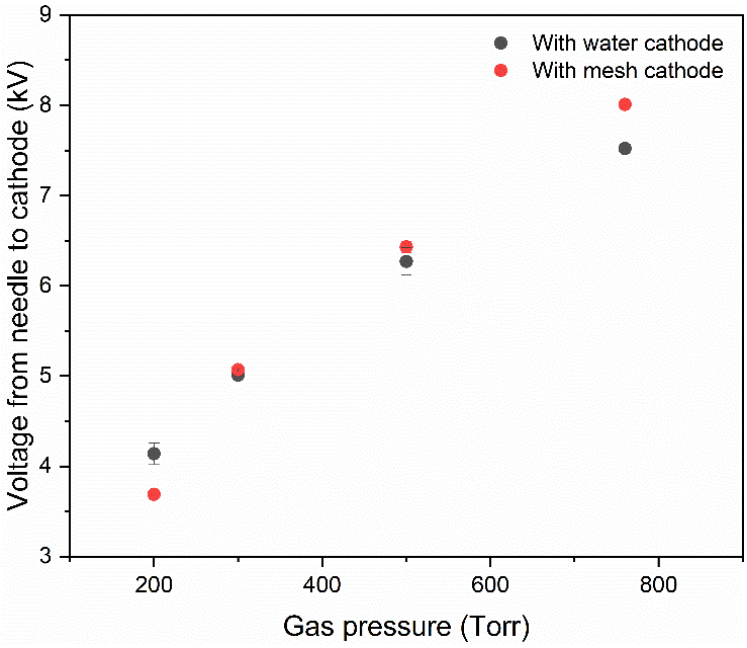

Figure 5.3 Oxygen corona discharge voltage with gas pressure of 200, 300, 500 and 760 Torr. The sample is deionized water. The treatment time is 30 minutes and the gas flow rate is 0.2 slpm.

Figure 5.4 shows the discharge voltage at 760 Torr measured with different sample solutions. There was no significant difference in discharge voltage for water and mesh cathode. Since the mesh thickness is 0.6 mm, the practical discharge gap could be larger than 10 mm for mesh cathode, which resulted in higher discharge voltage.

The addition of TB or DMSO did not cause significant change of discharge voltage. Although the conductivity of treated TB solution was much higher than that of treated deionized water, which did not cause difference in discharge voltage. These results also demonstrated that the partial voltage on liquid resistance was negligible compared with discharge voltage.

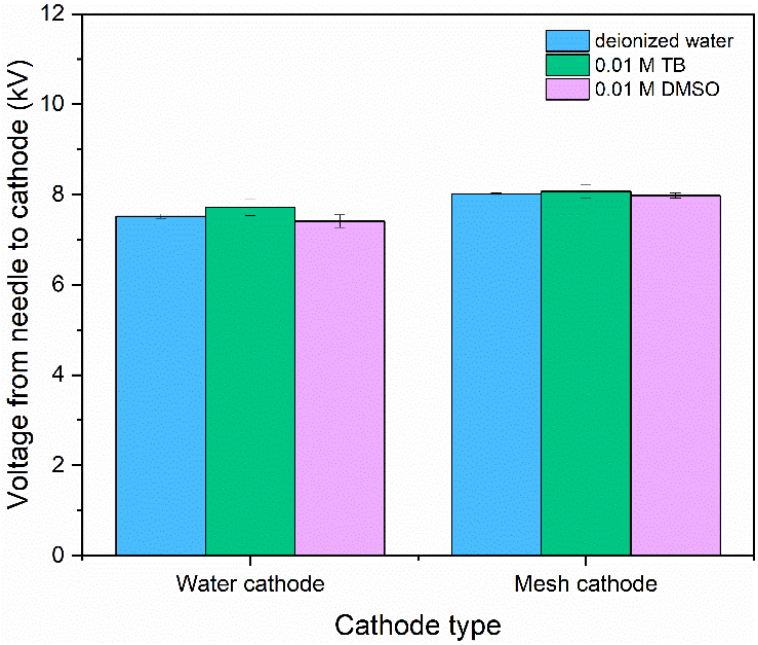

Figure 5.4 Oxygen corona discharge voltage at 760 Torr with sample of deionized water, 0.01 M TB solution and 0.01 M DMSO solution. The treatment time is 30 minutes and the gas flow rate is 0.5 slpm.

5.3 Interface reactions between water and positive ionic winds

The production of H_2O_2 in water by oxygen corona discharge with treatment time of 30, 60, 90, 120 and 150 minutes was investigated. In the tested time range, the production of H_2O_2 increased linearly as treatment time increased.

In oxygen corona discharge, the initial positive ions are O_2^+ [65]. Then O_2^+ reacts with water vapour to produce positive ion clusters $H^+(H_2O)_n$. It has been reported that all the oxygen ions would be transformed to $H^+(H_2O)_4$ clusters after 300 microseconds when with 0.34% water vapour in oxygen as Figure 5.5 shows [65]. With aqueous water in the reactor, the water vapor concentration at saturation is estimated to be 2.3% [160]. The travel time of positive ions in the reactor was estimated to be in the range of 1-100 ms, therefore all the positive ions would be transformed to $H^+(H_2O)_n$ before reaching water surface in oxygen corona discharge, which is the same as that in nitrogen corona discharges. In summary, with trace of water, all the positive ions reaching water surface would be $H^+(H_2O)_n$ in both nitrogen and oxygen corona discharge.

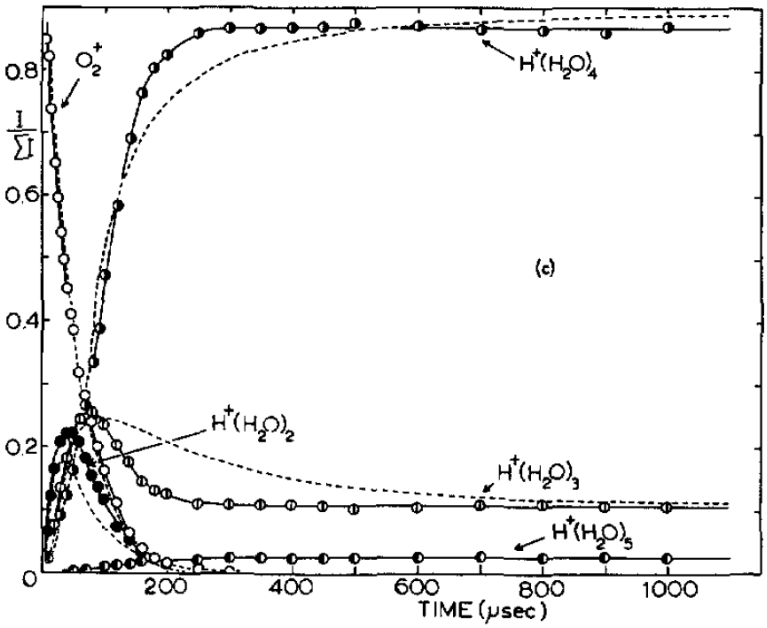

Figure 5.5 Time-dependent relative intensity of ions in oxygen with trace water vapour [65]

Due to the similarity of experimental conditions between nitrogen and oxygen corona discharges, the reactions caused by the ion anode $H^+(H_2O)_n$ are considered the same. Therefore, the hydrogen peroxide produced by the positive ions $H^+(H_2O)_n$ at the interface in oxygen corona discharge should be equal to the amount in nitrogen corona discharge.

5.3.1 H_2O_2 production with different gas flow rates

The gas flow rate can influence the concentration of oxygen and water vapour in the reactor, which may influence the production of reactive species. Hence, the effect of gas flow rate on H_2O_2 production was investigated. In this section, the gas flow rate was set as 0.002, 0.02, 0.2, 0.5 and 1.0 slpm at 760 Torr. The treatment time was 30 minutes.

As shown in Figure 5.6, the minimum H_2O_2 production was obtained at the largest gas flow rate of 1.0 slpm for both water cathode tests and mesh cathode

tests. The H_2O_2 production shows a slight decrease as the gas flow rate increased. However, compared to the velocity of ionic wind (several meters per second), the gas flowing velocity caused by the gas flow rate was negligible. Therefore, the gas flow rate was not supposed to influence the ionic wind generated by the corona discharges.

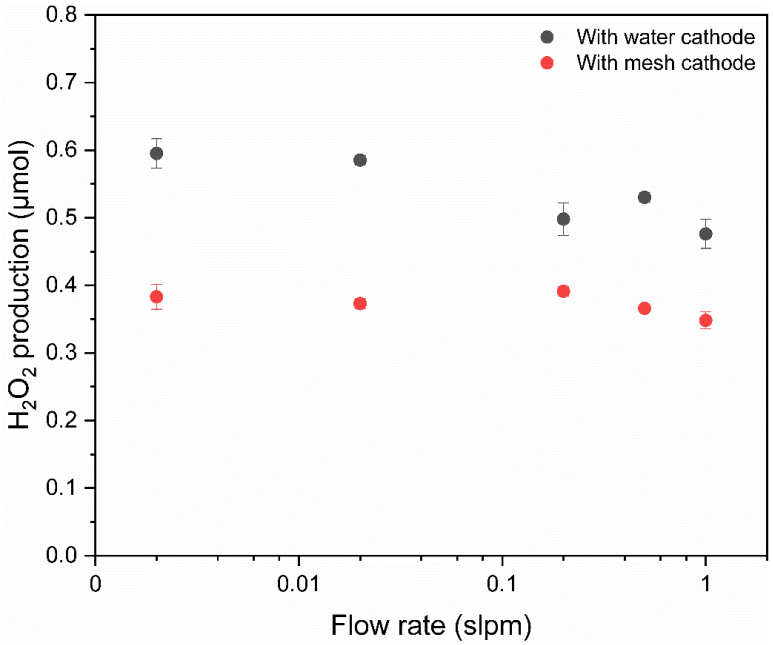

Figure 5.6 H_2O_2 production by oxygen corona discharge in deionized water at 760 Torr with gas flow rate of 0.002, 0.02, 0.2, 0.5 and 1.0 slpm. The treatment time is 30 minutes.

Since the gas flow rates of 0.002 slpm and 0.02 slpm were out of range for the ozone analyser, the ozone concentration in the off gas was only measured at gas flow rate of 0.2, 0.5 and 1.0 slpm. In both water cathode tests and mesh cathode tests, the ozone concentration decreased as the gas flow rate increased, reaching approximately 30 ppm at 1.0 slpm. The ozone concentration in both water and mesh cathode tests was similar at the gas flow rates of 0.5 slpm and 1.0 slpm

but has a clear difference at the flow rate of 0.2 slpm, with a higher ozone concentration in mesh cathode test. This phenomenon can be explained by the difference of the relative humidity in water cathode tests and mesh cathode tests. At the same gas flow rate, water cathode resulted in higher relative humidity than mesh cathode due to that the joule heating can increase the water vaporization rate. However, when the gas flow rate is high, the relative humidity was dominated by the gas flow rate, instead of the difference of cathode types. When the gas flow rate was low, the difference of relative humidity between water and mesh cathode tests became significant. In mesh cathode tests, lower relative humidity resulted in higher O_3 production [200], as well as the O_3 concentration.

As shown in Figure 5.7, the O_3 concentration was in the order of 10^1-10^2 ppm, which indicates that the concentration of ozone in water was low, in the order of 0.1-1 μmol at the experimental conditions. In gas phase, ozone can react with OH or H to produce HO_2, which can contribute to the H_2O_2 production in water. However, in this case, ozone concentration has little effect on hydrogen peroxide production in water by comparing Figure 5.6 and Figure 5.7.

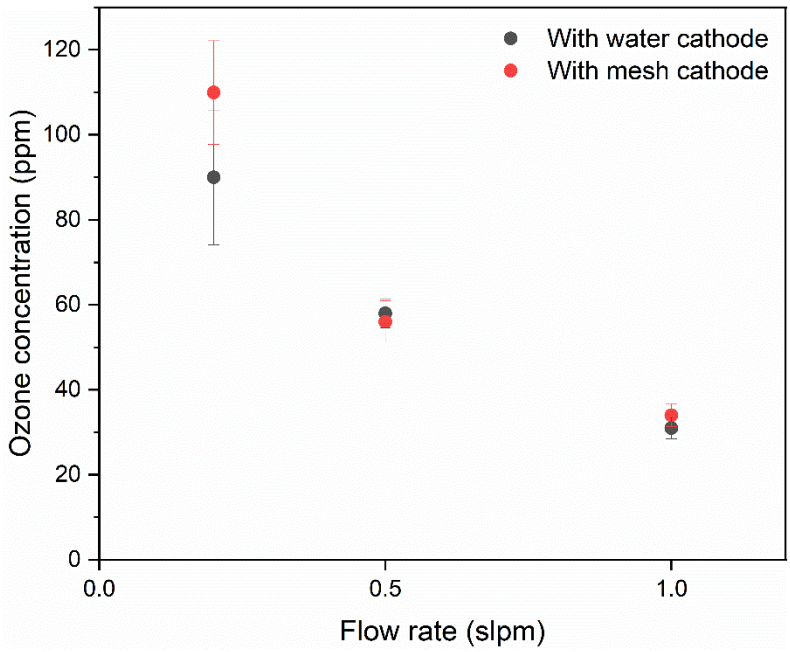

Figure 5.7 Ozone concentration in off gas for oxygen corona discharge at 760 Torr. The treatment time is 30 minutes and the gas flow rate is 0.2, 0.5 and 1.0 slpm.

5.3.2 H_2O_2 production with different gas pressures

Figure 5.8 illustrates the H_2O_2 production at gas pressures of 760, 500, 300 and 200 Torr. The gas flow rate was 0.2 slpm and the treatment time was 30 minutes. In water cathode tests, the H_2O_2 production slightly increased from 0.50 to 0.56 µmol as the gas pressure dropped from 760 to 200 Torr. In mesh cathode tests, the H_2O_2 production varied between 0.30 and 0.39 µmol and the H_2O_2 production was always lower than that in water cathode tests for the same gas pressure.

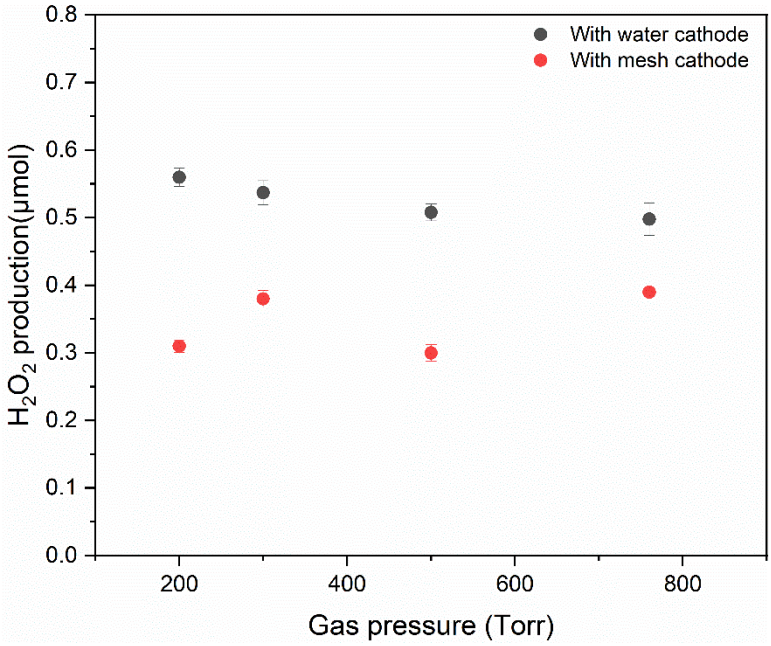

Figure 5.8 H_2O_2 production in deionized water by oxygen corona discharge with gas pressures of 200, 300, 500, and 760 Torr. The treatment time is 30 minutes and the gas flow rate is 0.2 slpm.

As aforementioned, the hydrogen peroxide production by positive ions in oxygen corona discharge is equal to that in nitrogen corona discharges. Hence, the hydrogen peroxide produced by reactive neutral species in oxygen corona discharges can be calculated by subtracting the amount produced by positive ions from the total hydrogen peroxide production in water cathode tests. The figures are listed in Table 5.1.

Table 5.1 H_2O_2 production by positive ions and reactive neutral species in oxygen corona discharge at different gas pressures. The treatment time is 30 minutes and the gas flow rate is 0.2 slpm.

H_2O_2 (μmol)	200 Torr	300 Torr	500 Torr	760 Torr
Ions	0.135	0.100	0.086	0.075
Reactive neutral species	0.425	0.437	0.422	0.423

As can be seen from Table 5.1, reactive neutral species contributed over 76% of H_2O_2 production in oxygen corona discharges. The gas pressure change did not show an influence on the H_2O_2 production by the reactive neutral species in oxygen corona discharges, which is similar to that in nitrogen corona discharges.

In oxygen corona discharges, the difference between water cathode tests and mesh cathode tests is larger than the contribution of ions, which indicates that the attenuation effect of mesh on reactive neutral species is significant.

The oxygen atom is considered the main deactivated neutral species at the mesh. It has been reported that the oxygen atom can recombine at the surface of stainless-steel mesh [184, 185], as:

$$2O_g \xrightarrow{\text{wall}} O_{2(g)} \qquad \text{(R 5.1)}$$

Although the nitrogen atom can recombine at the stainless-steel surface, the recombination rate is lower than that of oxygen atom. The surface recombination coefficient of N and O radicals in pure N_2 and O_2 plasma was estimated to be 0.07 and 0.17 respectively, on a stainless-steel wall of a inductively coupled plasma reactor at a gas pressure of 10-30 mTorr and temperature of 330 K [186].

To keep the d.c. current constant at 30 μA, the applied voltage was adjusted at different gas pressures. As Figure 5.8 shows, as the gas pressure decreased, the hydrogen peroxide production increased, while the discharge voltage decreased. Therefore, the energy yield of H_2O_2 increased as gas pressure decreased as shown in Figure 5.9.

Similar to the nitrogen corona discharge, when the pressure increased from 200 to 760 Torr in oxygen corona discharge, the input power increased by approximately 2 times. however, H_2O_2 production by reactive neutral species did not increase significantly.

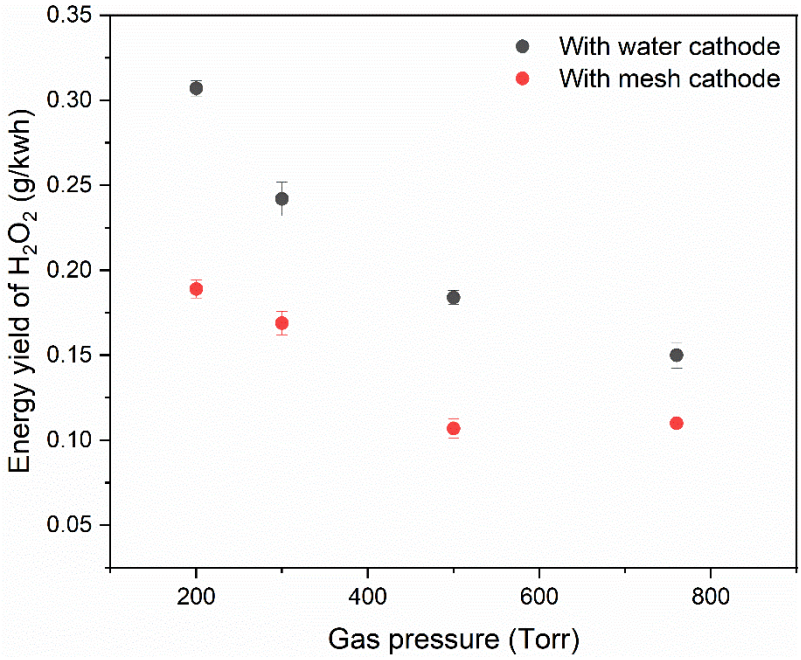

Figure 5.9 Energy yield of H_2O_2 production for oxygen corona discharge in deionized water at gas pressure of 200, 300, 400, 500 and 760 Torr. The treatment time is 30 minutes and the gas flow rate is 0.2 slpm.

5.3.3 H_2O_2 production with OH scavengers in water

To investigate how the hydrogen peroxide was produced in water under oxygen corona discharge and whether it is was from OH dimerization, the OH scavengers tert-butanol (TB) and dimethyl sulfoxide (DMSO) were applied in the experiment. The tested samples were divided into three groups: deionized water, 0.01 M TB solution and 0.01 M DMSO solution. The sample solutions were treated for 30 minutes at a pressure of 760 Torr and a gas flow rate of 0.2 slpm.

As Figure 5.10 shows, in water cathode tests, 0.89 μmol of H_2O_2 was produced in deionized water. With addition of TB, the H_2O_2 production increased by 48.31%. With addition of DMSO, the H_2O_2 production increased by 13.48%.

In mesh cathode tests, 0.69 μmol of H_2O_2 production was produced in deionized water. With addition of TB, the H_2O_2 production increased by 46.38 %. With addition of DMSO, H_2O_2 production has a slight increase, around 8.70%.

As can be seen in Figure 5.10, the addition of TB significantly increased H_2O_2 production by both ions and reactive neutral species. In mesh cathode tests, the increase of H_2O_2 production by the addition of DMSO was negligible. Neither TB or DMSO reduced H_2O_2 production in water for the water and mesh cathode tests, implying that the H_2O_2 production was not mainly from OH dimerization.

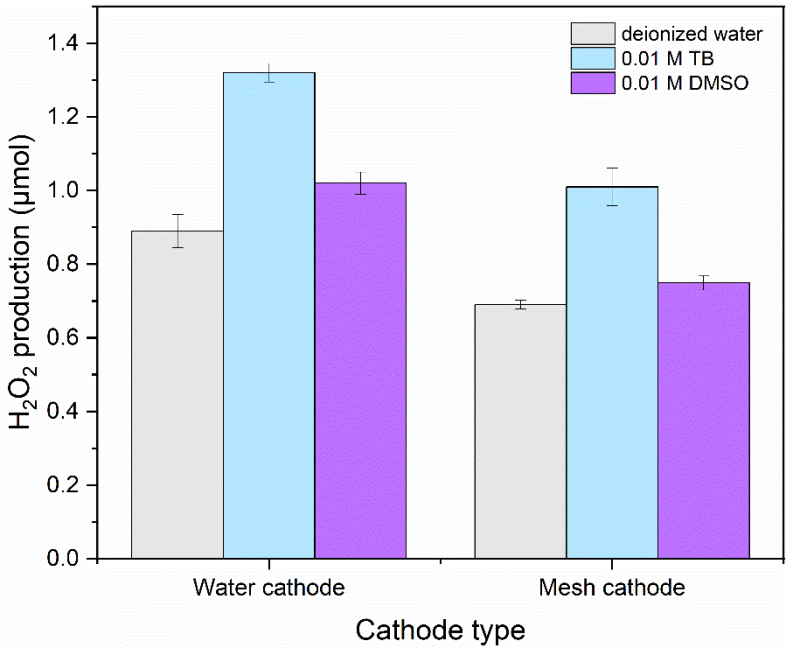

Figure 5.10 H_2O_2 production by oxygen corona discharge at 760 Torr in deionized water, 0.01 M TB solution and 0.01 M DMSO solution. The treatment time is 30 minutes and the gas flow rate is 0.2 slpm.

5.3.4 pH and conductivity of treated deionized water

The conductivity and pH of the treated deionized water were measured for providing more information on interface reactions. 5mL deionized water was treated for 60 minutes with a gas flow rate of 0.2 slpm at 760 Torr. After treatment, the conductivity of deionized water increased in both water and mesh cathode tests, but not as much as those observed in the nitrogen corona discharge. Table 5.2 shows the change of conductivity and pH in water cathode tests is larger than that in mesh cathode tests, implying that positive ions played an important role on the change of pH and conductivity in water. Porter et al. also reported that the discharge in oxygen over water can cause the decrease of pH and increase of conductivity in water [201]. In their experiments, small

amount of nitrate was found in the water after discharge in oxygen. Hence, the pH and conductivity change can be caused by the traces of residual air in the reactor.

Table 5.2 pH and conductivity change of deionized water after 60-minute treatment by nitrogen and oxygen corona discharge at 760 Torr. The gas flow rate is 0.2 slpm.

Cathode type	pH and Conductivity (μS/cm)			
	$pH_{nitrogen}$	pH_{oxygen}	$Cond_{nitrogen}$	$Cond_{oxygen}$
Water cathode	4.38	5.14	38.0	26.2
Mesh cathode	4.60	5.40	41.3	16.9

5.3.5 Off gas analysis

As in the nitrogen corona discharge investigation, a gas-washing bottle was employed to explore if there was reactive neutral species present in off gas, as Figure 3.7 shows. Three configurations using mesh cathode were tested, with the mesh-water distance setting to 5.3 mm, 33.3 mm, and the PTFE barrier to water distance of 33.3 mm, as shown in Figure 4.9. A volume of 20 mL deionized water was filled in the gas-washing bottle. The gas flow rate was 0.5 slpm and the gas pressure was 760 Torr.

H_2O_2 production after 60 minutes of treatment is shown in Table 5.3. The H_2O_2 production in the gas-washing bottle was lower than 0.1 μmol for all three configurations. In the tests without the PTFE barrier, the H_2O_2 production in the gas-washing bottle was much lower than that produced in the reactor. In the test with the PTFE barrier, the H_2O_2 production in the reactor decreased significantly, even lower than that produced in the gas-washing bottle. These results suggested that reactive neutral species producing H_2O_2 have lifetime

shorter than 1.4 seconds, as calculated in Section 4.3.6. These results also proved that ozone did not produce H_2O_2 in water. In the tests with the PTFE barrier, the reactive neutral species could not reach water surface directly. Most of the reactive species were carried by off gas to the gas-washing bottle. Therefore, the H_2O_2 production in the gas-washing bottle was higher than that in the reactor when applying the PTFE barrier.

Table 5.3 H_2O_2 production in reactor and in gas-washing bottle by oxygen corona discharge at 760 Torr with mesh cathode in three different configurations (cf. Figure 4.9). The treatment time is 60 minutes and the gas flow rate is 0.5 slpm.

Mesh configuration	Mesh-water distance (mm)	H_2O_2 production in reactor (μmol)	H_2O_2 production in gas-washing bottle (μmol)
No PTFE barrier	5.3	0.662	0.073
	33.3	0.354	0.047
With PTFE barrier	33.3	0.032	0.060

The water pH and conductivity in the gas-washing bottle were also measured after 60 minutes of treatment using a gas flow rate of 0.2 slpm and gas pressure of 760 Torr. The change in conductivity and pH are listed in Table 5.4. Under the same condition (the same gas pressure, gas flow rate and discharge time), the water pH and conductivity change in oxygen corona discharge was smaller than that in nitrogen corona discharge. For the corona discharge in nitrogen, nitrate and nitrite production in water dominated the change of pH and conductivity.

Table 5.4 pH and conductivity change of water in reactor and in gas-washing bottle by oxygen corona discharge at 760 Torr. The treatment time is 60 minutes and the gas flow rate is 0.2 slpm (needle to water/mesh cathode distance is 10 mm; mesh-water distance is 5.3 mm).

Cathode type	Water in reactor		Water in gas-washing bottle	
	pH	Conductivity (μS/cm)	pH	Conductivity (μS/cm)
Mesh	5.40	16.87	5.80	2.06
Water	5.14	26.16	5.76	1.01

5.4 The influence of mesh on the ionic wind

Compared to corona discharge in nitrogen, the reactive neutral species in oxygen corona discharge contributed more H_2O_2 production, around 88.5%, as shown in Table 5.5. The mesh can influence the ionic wind via two pathways. Firstly, the mesh can filter the positive ions, only allow reactive neutral species reach water. Secondly, as discussed in Section 5.3.2, oxygen atoms can be deactivated at the mesh by recombining to oxygen molecules. Thirdly, the mesh can attenuate the ionic wind, result in fewer reactive neutral species reaching the water surface. Analysis of the influences of mesh can help in verifying the discussion in Section 5.3.2.

Table 5.5 H_2O_2 production in deionized water by drift ions and reactive neutral species following 30-minute treatment by nitrogen and oxygen corona discharge at 760 torr. The gas flow rate is 0.2 slpm.

H_2O_2 (μmol)	Nitrogen	Oxygen
Ions	0.057	0.057
Neutral species	0.068	0.441
Total	0.125	0.498

5.4.1 The influence of mesh openings

Similar to the investigation in nitrogen corona discharge, a comparative study using the mesh with a 2 mm opening (mesh A) and the mesh with a 10 mm opening (mesh B) was undertaken at a gas pressure of 760 Torr and a gas flow rate of 0.2 slpm. The H_2O_2 production after 30 minutes of treatment using the two mesh types is shown in Table 5.6.

Table 5.6 The hydrogen peroxide production by oxygen corona discharge at 760 Torr with two types of mesh cathodes. The treatment time is 30 minutes and the gas flow rate is 0.2 slpm.

Mesh type	Opening	Wire width	Thickness	Open area percent	H_2O_2 production (μmol)
A	2 mm	0.3 mm	0.6 mm	59.2%	0.391
B	10 mm	2 mm	3 mm	69.4%	0.281

The H_2O_2 production using mesh B (10 mm opening) was lower than that using mesh A (2 mm opening). Larger opening had a lower hydrogen peroxide production. However, the discharge voltage with 10 mm opening mesh was 8.32

kV, higher than the 8.01 kV when using 2 mm opening mesh. It is still not clear what caused the difference. The difference in discharge voltage and electrical field distribution may account for the difference in hydrogen peroxide production.

5.4.2 The influence of the mesh-water distance

After passing through the mesh cathode, the ionic wind will lose the driving force from the electric field. The distance from mesh to water surface influences both the travel time and the proportion of the reactive neutral species that could reach the water surface. The H_2O_2 production with a mesh-water distance of 5.3 mm and 33.3 mm was investigated at 760 Torr. The mesh with 2 mm openings was applied in this section. The other parameters are listed in Table 5.7.

Table 5.7 H_2O_2 production by oxygen corona discharge at 760 Torr with different mesh-water distances.

Mesh-water distance (mm)	Mesh configuration	Flow rate (slpm)	Treatment time (mins)	H_2O_2 production (μmol)
5.3	Single layer	0.2	30	0.391
33.3	Single layer	0.2	30	0.263

In Table 5.7, when the mesh-water distance increased from 5.3 mm to 33.3 mm, the H_2O_2 production decreased by 32.7%. On one hand, the larger mesh-water distance would decrease the amount of reactive neutral species reaching water surface, as there is higher chance for reactive neutral species to diffuse away from the water surface. On the other hand, the larger mesh-water distance would also result in a longer travel time for reactive neutral species to reach water surface, and hence, to react with each other and de-excite to less non-reactive species.

5.4.3 Comparison of single-layer and double-layer mesh cathode

Experiments with both a single and a double-layer mesh cathode were tested to explore the effect of mesh on deactivation of reactive neutral species, and further, the effect on the production of H_2O_2 in water. Figure 5.11 (a) and Figure 5.11 (b) show the configurations with a 5.3 mm mesh-water distance. Figure 5.11 (c) and Figure 5.11 (d) show the configurations with a 33.3 mm mesh-water distance. The double layer was configured by two segments of the same mesh (mesh A, 2mm opening) with PTFE spacers to keep 1 mm gap between the two meshes, and both layers were grounded. The H_2O_2 production with single-layer mesh and double-layer mesh is listed in Table 5.8. The H_2O_2 production was significantly reduced as the mesh-water distance was increased from 5.3 mm to 33.3 mm. To ensure there is sufficient H_2O_2 concentration in the treated water, the treatment time was increased to 60 minutes with mesh-water distance of 33.3 mm.

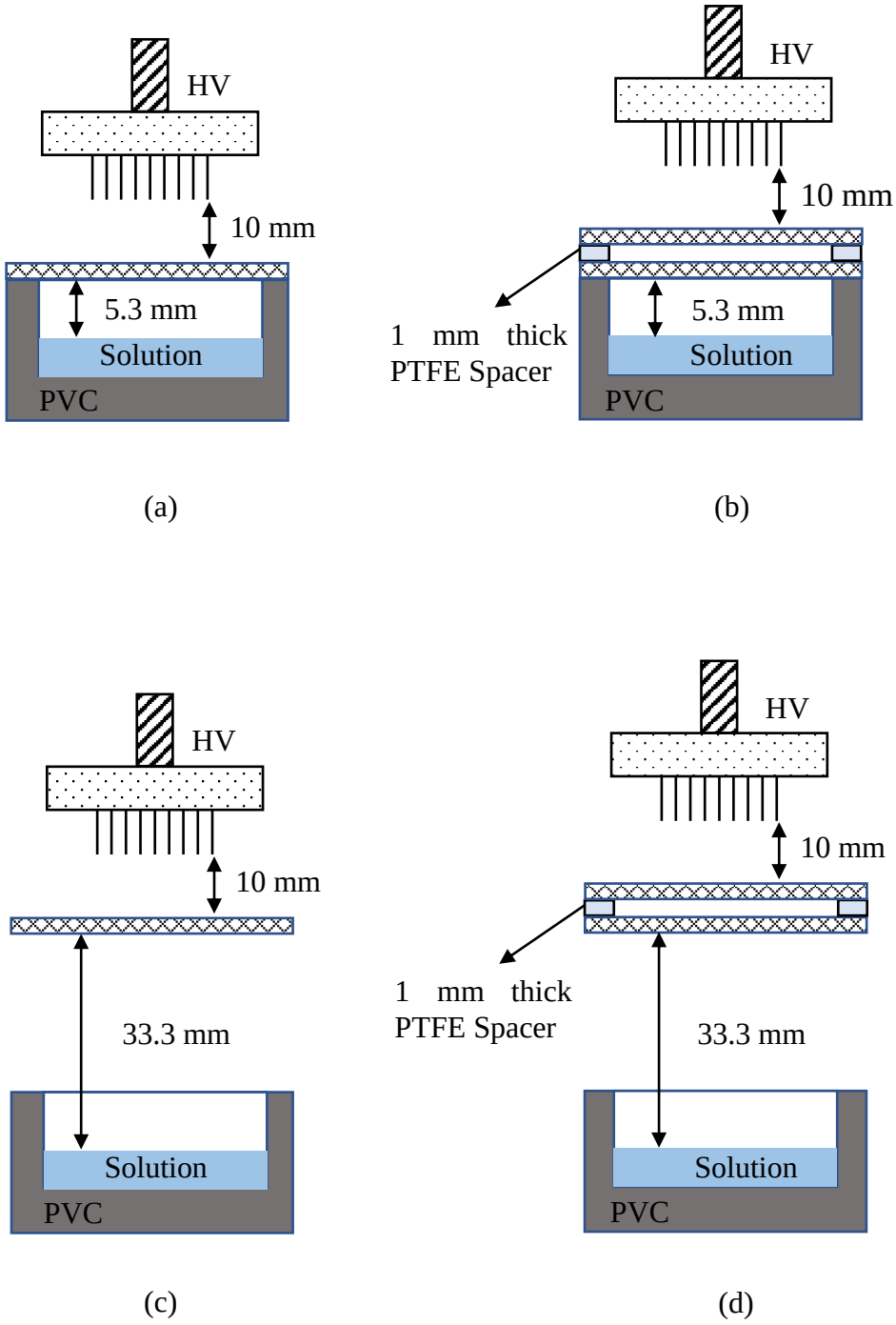

Figure 5.11 Mesh configurations for oxygen corona discharge: (a) single-layer mesh with mesh-water distance of 5.3 mm and (c) 33.3 mm; for (b) double-layer mesh with mesh-water distance of 5.3 mm and (d) 33.3 mm.

Table 5.8 H_2O_2 production by oxygen corona discharge at 760 Torr with single-layer and double-layer mesh cathode.

Mesh-water distance (mm)	Mesh configuration	Flow rate (slpm)	Treatment time (mins)	H_2O_2 production (μmol)
5.3	Single layer	0.2	30	0.391
	Double layer	0.2	30	0.245
33.3	Single layer	0.5	60	0.365
	Double layer	0.5	60	0.206

According to Table 5.8, when the single-layer mesh was replaced by a double-layer mesh, the H_2O_2 production decreased by about 40% for 5.3 and 33.3 mm cases. However, in nitrogen corona discharge, the second layer mesh did not cause any decrease in H_2O_2 production as shown in Table 4.6. The difference in oxygen corona discharge was due to that the oxygen atoms were deactivated at the mesh.

5.4.4 The influence of a PTFE barrier underneath the mesh cathode

In order to see what would happen if the ionic wind was blocked , a PTFE barrier was placed underneath the mesh to prevent the ionic wind from directly passing through the mesh cathode to the water surface. As mentioned previously, the PTFE barrier is a 1-mm thick Polytetrafluoroethylene (PTFE) square plate, with a side length of 60 mm. Figure 5.12 shows the test configuration (a) without the PTFE barrier and (b) with the PTFE barrier.

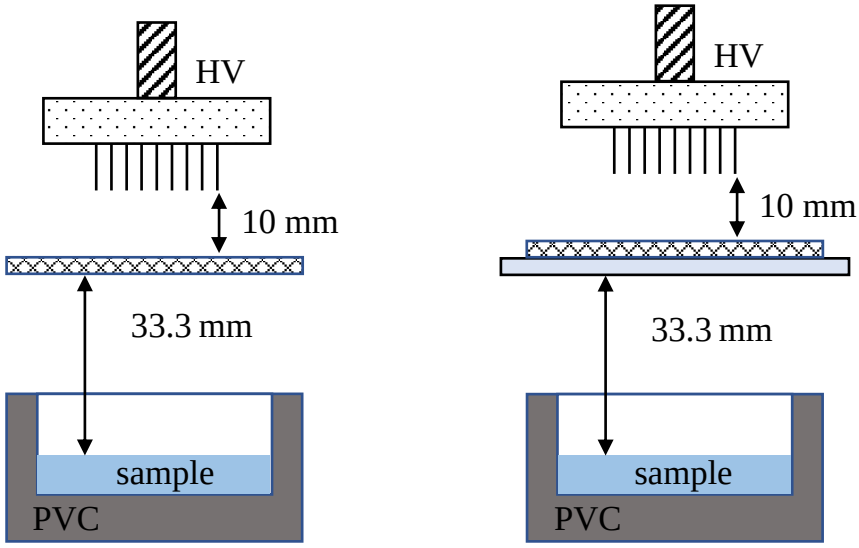

(a) (b)

Figure 5.12 Mesh configurations employed for oxygen corona discharge: (a) without the PTFE barrier; (b) with the PTFE barrier.

With the PTFE barrier underneath the mesh, as shown in Figure 5.12 (b), H_2O_2 production dropped from 0.261 μmol to 0.038 μmol, approximately 85.4% of that in the tests without the PTFE barrier. A gas-washing bottle with 20 mL of deionized H_2O was employed to trap species in the off gas but little H_2O_2 was detected in the bottle. These results imply that the reactive neutral species producing H_2O_2 in the water were consumed rapidly. Therefore, when with the PTFE barrier underneath the mesh, most of reactive neutral species were deactivated before reaching the gas washing bottle. Although the lifetime of $O(^1D)$ has been reported to be 147.1 seconds [172], the real lifetime in this complicated gaseous environment can be much shorter due to the consuming reactions as [187-189]:

$$O + O_2 + O_2 \rightarrow O_3 + O_2 \quad \text{(R 5.2)}$$

$$O + O_3 \rightarrow O_2 + O_2 \quad \text{(R 5.3)}$$

$$O_2^* + O_2 \rightarrow O_3 + O \quad \text{(R 5.4)}$$

$$O + H_2O \rightarrow OH + OH \quad \text{(R 5.5)}$$

$$O + OH \rightarrow O_2 + H \quad \text{(R 5.6)}$$

5.5 Faraday efficiency of H_2O_2 production

5.5.1 Faraday efficiency at different gas pressures

The Faraday efficiency of hydrogen peroxide production by oxygen corona discharge at different gas pressures are listed in Table 5.9. In the mesh cathode test, the Faraday efficiency fluctuate between 0.56 and 0.69 in the gas pressure range of 200-760 Torr. The gas pressure seems to have little influence on the Faraday efficiency of hydrogen peroxide production by oxygen corona discharge.

Table 5.9 Faraday efficiency of H_2O_2 production (H_2O_2/Q) by oxygen corona discharge at different gas pressures. The treatment time is 30 minutes and the gas flow rate is 0.2 slpm.

Cathode type	H_2O_2/Q			
	200 Torr	300 Torr	500 Torr	760 Torr
Water cathode	1.00	0.96	0.91	0.89
Mesh cathode	0.55	0.66	0.56	0.69

However, the results in Table 5.9 only demonstrate the H_2O_2 production in water cathode tests and mesh cathode tests of oxygen corona discharges. Due to the deactivation of oxygen atoms at the mesh, the difference of H_2O_2 production between water cathode tests and mesh cathode tests contains the contribution of filtered ions and deactivated neutral species. As discussed in Section 5.3.2 and

5.3.3, the production of H_2O_2 by ions should be the same in nitrogen and oxygen corona discharges. With known contribution of ions, the H_2O_2 production by ions and reactive neutral species is shown in Table 5.10.

Table 5.10 Faraday efficiency of H_2O_2 production by ions and reactive neutral species in oxygen corona discharge at different gas pressures. The treatment time is 30 minutes and the gas flow rate is 0.2 slpm.

Ionic wind	H_2O_2/Q			
	200 Torr	300 Torr	500 Torr	760 Torr
Ions	0.24	0.17	0.15	0.13
Reactive neutral species	0.76	0.79	0.76	0.76

The production of H_2O_2 by deactivated neutral species ($H_2O_{2_{de}}$) can be calculated as:

$$H_2O_{2_{de}} = H_2O_{2_{wc}} - H_2O_{2_{mc}} - H_2O_{2_{ion}} \quad \text{(Eq. 5.1)}$$

Where $H_2O_{2_{wc}}$ is the production of H_2O_2 in water cathode tests; $H_2O_{2_{mc}}$ is the production of H_2O_2 in mesh cathode tests; $H_2O_{2_{ion}}$ is the production of H_2O_2 by positive ions. Table 5.11 listed the H_2O_2 produced by the deactivated neutral species in mesh cathode tests of oxygen corona discharges.

Table 5.11 Reduction of H_2O_2 production due to the filtered positive ions and deactivated neutral species in mesh cathode tests of oxygen corona discharge at different gas pressures. The treatment time is 30 minutes and the gas flow rate is 0.2 slpm.

Item	H_2O_2/Q			
	200 Torr	300 Torr	500 Torr	760 Torr
Filtered positive ions	0.24	0.17	0.15	0.13
Deactivated neutral species	0.21	0.13	0.20	0.07

It is worthwhile to compare the H_2O_2 production by reactive neutral species in nitrogen and oxygen corona discharge, as listed in Table 5.12.

Table 5.12 Faraday efficiency of H_2O_2 production by reactive neutral species in nitrogen and oxygen corona discharge at different gas pressures.

Gas	H_2O_2/Q				
	100 Torr	200 Torr	300 Torr	500 Torr	760 Torr
Nitrogen	0.15	0.14	0.12	0.11	0.13
Oxygen	-	0.76	0.79	0.76	0.76

These results demonstrate that the Faraday efficiency of hydrogen peroxide production by reactive neutral species are independent of gas pressure in both nitrogen and oxygen corona discharges, and the production in oxygen is approximately 6 times of that in nitrogen. This proves that the reactive neutral species produced in oxygen corona discharge are much more effective to produce hydrogen peroxide at the plasma-water interface. To understand the

neutral reactive species produced in nitrogen corona discharge, the main reactive species in atmospheric-pressure nitrogen plasma jet with 1% water vapour is listed in Table 5.13 [190]:

Table 5.13 Estimated density of main reactive radicals in nitrogen plasma with 1% water. (with an electron temperature of 1 eV and a plasma density of $2\times10^{12}/cm^3$) [190].

Radical	Reaction	Reaction coefficient (cm^3/s)	Steady-state density($molecules/cm^3$)
$N_2(A_3\sum_u^+)$	$N_2 + e \rightarrow N_2(A_3\sum_u^+) + e$	6.4×10^{-12}	2.56×10^{16}
N	$N_2 + e \rightarrow N + N + e$	2.3×10^{-13}	1.9×10^{14}
H	$N_2(A_3\sum_u^+) + H_2O \rightarrow N_2 + H + OH$	5×10^{-14}	1.2×10^{14}
OH	$N_2(A_3\sum_u^+) + H_2O \rightarrow N_2 + H + OH$	5×10^{-14}	2.5×10^{15}
H_2O_2	$OH + OH \rightarrow H_2O_2$	1.78×10^{-11}	2.6×10^{16}
HO_2	$OH + H_2O_2 \rightarrow HO_2 + H_2O$	1.7×10^{-12}	4.3×10^{14}

In nitrogen plasma, excited nitrogen molecules are the dominated radicals, which react with water to produce OH. Then OH can recombine to produce H_2O_2 or react with H_2O_2 to produce HO_2. Hence, in nitrogen corona discharges, as discussed in Section 4.6.2, the main reactive neutral species reaching water are HO_2 and H_2O_2. However, due to the presence of N, NO, NO_2, HNO_2 in nitrogen plasma, the OH can be easily consumed by reacting with these radicals.

In oxygen plasma, the types of OH consumption reactions are less than that in nitrogen plasma. Additionally, oxygen plasma can produce much more singlet oxygen than nitrogen plasma [191]. Figure 5.13 shows the singlet oxygen production after 30-second treatment of water by a plasma jet generated in various gases [191].

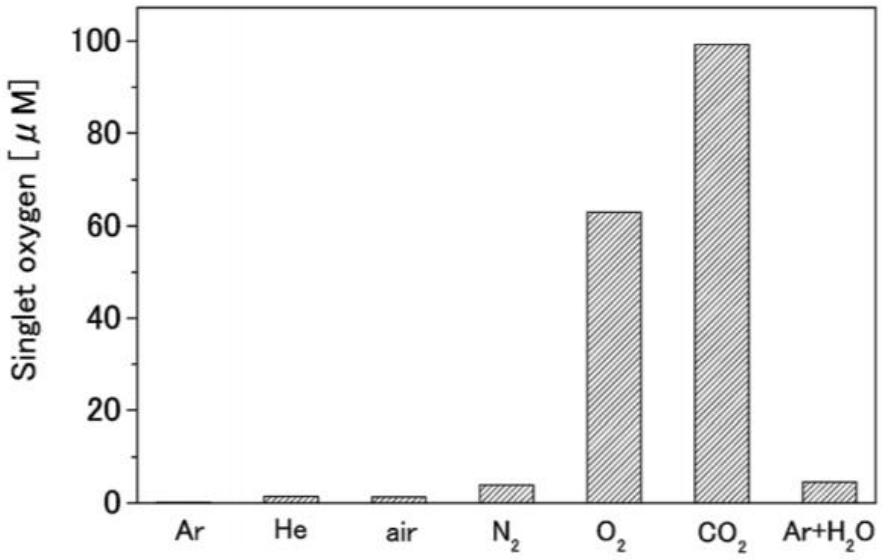

Figure 5.13 Singlet oxygen production by plasma with various gases after 30-second treatment [191].

From Figure 5.13, it can be seen that the singlet oxygen produced in oxygen is around twenty times that produced in nitrogen. Hence, this could explain why H_2O_2 produced by reactive neutral species in oxygen is much more than that in nitrogen.

5.5.2 Faraday efficiency in H_2O, TB and DMSO solutions

The Faraday efficiency of H_2O_2 production increased in both water and mesh cathode tests with addition of TB and DMSO to the deionized water. The results are listed in Table 5.14.

Table 5.14 Faraday efficiency of H_2O_2 production by oxygen corona discharge at 760 Torr in deionized water, 0.01 M TB and 0.01 M DMSO. The treatment time is 30 minutes and the gas flow rate is 0.2 slpm.

Cathode type	H_2O_2/Q		
	Deionized water	0.01 M TB solution	0.01 M DMSO solution
Water cathode	0.89	1.32	1.01
Mesh cathode	0.69	1.01	0.75

By comparing the results listed in Table 5.14 and Table 4.10, it can be found that in mesh cathode tests, the addition of TB resulted in a close increase of H_2O_2 production in oxygen and nitrogen corona discharges, by 46.4% and 43.5% , respectively; while the addition of DMSO resulted a negligible increase of H_2O_2 production in mesh cathode tests for both nitrogen and oxygen corona discharges.

The positive ions reaching water in oxygen corona discharge are the same as those in nitrogen corona discharges. Hence, the formation mechanisms H_2O_2 by positive ions should be the same in nitrogen and oxygen corona discharges. According to Section 4.5.2, with addition of TB or DMSO in water, H_2O_2 production by positive ions was doubled, which should also occur in oxygen corona discharge. Therefore, H_2O_2 production in water cathode tests in Table 5.14 can be specified to the amount produced by positive ions and the amount produced by reactive neutral species. can be specified discharges was listed in Table 5.15.

Table 5.15 Faraday efficiency of H_2O_2 production by positive ions and reactive neutral species for oxygen corona discharge at 760 Torr in water cathode tests in deionized water, 0.01 M TB and 0.01 M DMSO. The gas pressure is 760 Torr and gas flow rate is 0.2 slpm.

Ionic wind	H_2O_2/Q		
	Deionized water	0.01 M TB solution	0.01 M DMSO solution
Ions	0.13	0.26	0.26
Reactive neutral species	0.76	1.06	0.75
Total	0.89	1.32	1.01

In As listed in Table 5.15, with addition of TB in water, the H_2O_2 production by reactive neutral species increased by 39.5%, which is close to the increase of 43.5% in nitrogen corona discharges as listed in Table 4.10. The addition of DMSO did not change the H_2O_2 production by reactive neutral species, which is consistent with the results of nitrogen corona discharge.

5.6 Analysis of interface reactions

5.6.1 Reactions between water and positive ions

The main gas components in the reactor were oxygen and water vapour before the corona discharge. At the room temperature of 20° C, the saturated concentration of water vapour is around 2%. As discussed above, the corona discharge produced O_2^+, then O_2^+ could react with oxygen to produce O_4^+ [65]:

$$O_2^+ + 2O_2 \rightarrow O_4^+ + O_2 \qquad \text{(R 5.7)}$$

O_4^+ can react with water vapour to produce OH [65]:

$$O_4^+ + H_2O \rightarrow O_2^+(H_2O) + O_2 \qquad \text{(R 5.8)}$$

$$O_2^+(H_2O) + H_2O \rightleftarrows O_2^+(H_2O)_2^* \rightarrow H_3O^+ \cdot OH + O_2 \quad \text{(R 5.9)}$$

$$H_3O^+ \cdot OH \rightarrow H_3O^+ + OH \quad \text{(R 5.10)}$$

H_3O^+ can react with water molecules in gas phase to produce clusters:

$$H_3O^+ + H_2O \rightarrow H^+(H_2O)_2 \quad \text{(R 5.11)}$$

$$H^+(H_2O)_2 + H_2O \rightarrow H^+(H_2O)_3 \quad \text{(R 5.12)}$$

…

$$H^+(H_2O)_{n-1} + H_2O \rightarrow H^+(H_2O)_n \quad \text{(R 5.13)}$$

As discussed in Section 5.5, most of the positive ions reaching water surface were thought to be $H^+(H_2O)_n$ clusters. The reactions between $H^+(H_2O)_n$ and water is discussed in Section 4.6.1. The interface reactions caused by the positive ions are presented in Figure 4.13.

5.6.2 Reactions between water and reactive neutral species

The reactive neutral species reaching water surface contributed more than 76% of the H_2O_2 production in oxygen corona discharge at a gas pressure between 200 to 760 Torr. At 760 Torr, this proportion reached 85%. The contribution of reactive neutral species in oxygen corona discharge is much more significant than that in the nitrogen corona discharge. In comparison to water cathode test, the decrease in hydrogen peroxide production in mesh cathode test, could be attributed to two factors. One is the drift positive ions filtered by the mesh; the other is the loss of reactive neutral species at the mesh surface. While in nitrogen corona discharge, the loss of reactive neutral species at the mesh surface was negligible; but in oxygen corona discharge, as shown previously, the loss of reactive neutral species at the mesh surface has a notable influence. However, the positive ions reaching water in nitrogen and oxygen corona discharge were the same. It is believed that the positive drift ions in both nitrogen and oxygen

should have the same contribution to hydrogen peroxide production under the similar conditions.

Up to 110 ppm of ozone was detected in the off gas during discharge at gas flow rate of 0.2 slpm as shown in Figure 5.7. According to the Henry's law, the dissolved ozone is proportional to the partial pressure of ozone in gas phase. With this low concentration (ppm), the dissolved ozone was in the order of μg/L, which is negligible in water. However, the results have shown that the ozone concentration almost has no influence on the hydrogen peroxide production. Similar to nitrogen corona discharge, in oxygen corona discharge, the addition of TB significantly increased the H_2O_2 production by reactive neutral species. The addition of DMSO had limited influence on H_2O_2 production by reactive neutral species.

According to these analyses, HO_2 was produced in corona discharges by the reactions:. When in the deionized water, the self-reaction of HO_2 can produce H_2O_2 as stated in reaction R 5.14 [173, 174].

$$HO_2 + HO_2 \rightarrow H_2O_2 + O_2 \qquad \text{(R 5.14)}$$

From reaction R 5.14, 1 mol of HO_2 can produce 0.5 mol of H_2O_2. With addition of TB in water, 1 mol of HO_2 can produce 1 mol of H_2O_2 by reacting with TB [175]:

$$\text{tert} - C_4H_9OH + HO_2 \rightarrow (CH_3)2C(OH)CH_2 + H_2O_2 \qquad \text{(R 5.15)}$$

Atomic oxygen can be also generated in oxygen corona discharge. Reactions R 5.16 and R 5.17 describe the mechanism of atomic oxygen generation by electron collision [154].

$$e* + O_2 \rightarrow O(^3P) + O(^3P) + e \qquad \text{(R 5.16)}$$

$$e* + O_2 \rightarrow O(^1D) + O(^3P) + e \qquad \text{(R 5.17)}$$

$O(^3P)$ can react with O_2 and form O_3 [154, 177]:

$$O(^3P) + O_2 \rightarrow O_3 \quad \text{(R 5.18)}$$

$O(^1D)$ can react with water vapour and form OH [154, 179-182]:

$$O(^1D) + H_2O \rightarrow OH + OH \quad \text{(R 5.19)}$$

And then the produced OH can recombine to form H_2O_2 at the interface and transported into liquid water:

$$OH + OH \rightarrow H_2O_2 \quad \text{(R 5.20)}$$

the produced OH could react with ozone or hydrogen peroxide to produce HO_2 and transported into liquid water [77, 190]:

$$OH + O_3 \rightarrow HO_2 + O_2 \quad \text{(R 5.21)}$$

$$OH + H_2O_2 \rightarrow HO_2 + H_2O \quad \text{(R 5.22)}$$

The reaction pathways of oxygen atoms in phenol solutions have been reported, as shown in Figure 5.14. Oxygen atoms can form oxygen molecules, ozone or react with phenol [203]. Hence, in this case, the oxygen atoms entering the liquid water were believed to conduct the similar reactions, forming oxygen molecules, ozone or oxidize TB or DMSO. The dissolved oxygen atoms do not produce H_2O_2 in liquid water directly.

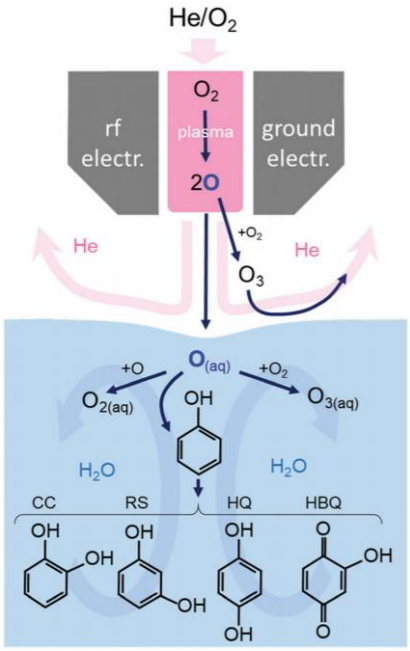

Figure 5.14 The gas-phase and aqueous reaction pathways of oxygen atoms produced by plasma in He/0.6%O_2 gas mixture. The broad arrows in the background indicate the gas and liquid movement [203].

According to the above discussion, the interface reactions caused by reactive neutral species generated by oxygen corona discharge are demonstrated in Figure 5.15.

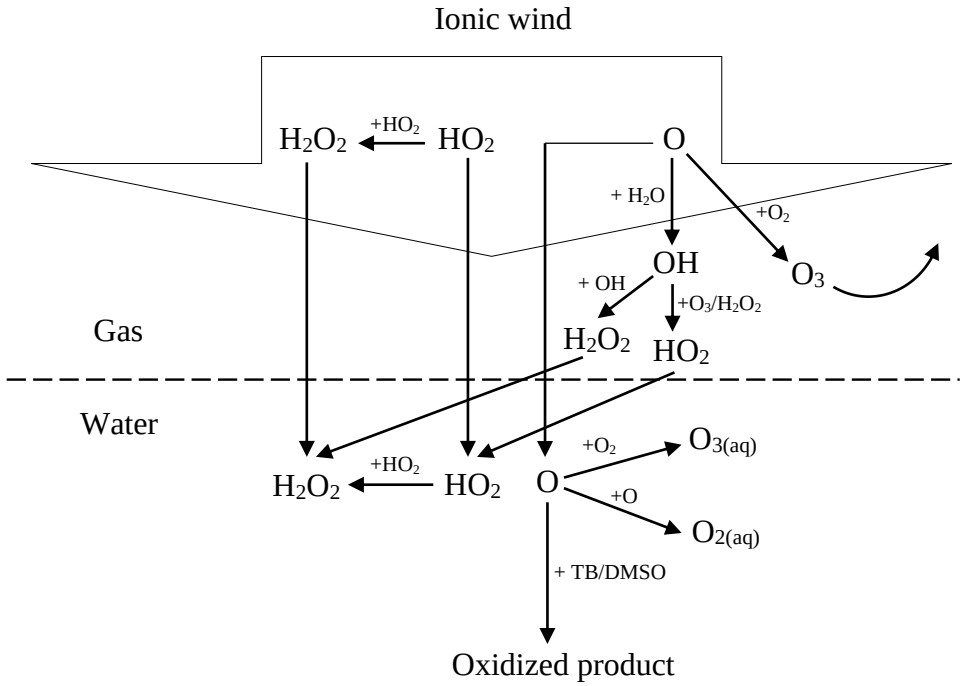

Figure 5.15 Interface reactions caused by reactive neutral species for oxygen corona discharge.

As Figure 5.15 shows, three types of reactive neutral species are produced in gas phase: H_2O_2, HO_2 and O. H_2O_2 can be transported into aqueous phase directly. HO_2 react mutually in gas phase or aqueous phase to produce H_2O_2. Some of oxygen atoms (O) react with oxygen molecules (O_2) to form ozone (O_3); and some of oxygen atoms (O) can react with water vapour to produce OH, which would produce H_2O_2 by dimerization or HO_2 by reacting with O_3 and H_2O_2.

The results in this chapter have shown that the discharge power has little effect on H_2O_2 production by reactive neutral species. A good example is that the discharge power was doubled as gas pressure increased from 200 to 760 Torr, while the H_2O_2 production by reactive neutral species did not increase. This is due to that most of the increased discharge power was dissipated in drift region in the plasma. The increase of gas pressure resulted in an increase of gas density

in drift region, thereby increasing the resistance to ion motion. However, the power applied in discharge region which produced reactive neutral species was not increased in this process. Hence the production of reactive neutral species was not increased.

5.7 Conclusions

This chapter discussed the interface reactions between water and the ionic wind in oxygen corona discharge. It has been found that both positive ions and reactive neutral species produced H_2O_2 in water, and the contribution of reactive neutral species is over 76% in the gas pressure range of 200 to 760 Torr. Compared to the nitrogen corona discharge, the oxygen corona discharge has higher Faraday efficiency of hydrogen peroxide production, with a maximum value of 1.0 obtained with a water cathode at 200 Torr. The energy efficiency of hydrogen peroxide production increased as the gas pressure decreased, with the maximum energy efficiency of 0.260 g/kWh, obtained at the lowest gas pressure tested (200 Torr) in water cathode tests.

The positive ions reaching water surface, $H^+(H_2O)_n$, in oxygen corona discharge, are the same as those in nitrogen corona discharge, thereby the reaction mechanisms between positive ions and water are also the same. The reactive neutral species including O, O_3, HO_2 and H_2O_2 were produced by oxygen corona discharge. However, due to the presence of multiple reactive species, the lifetime of the reactive neutral species, including oxygen atom, is estimated less than 1.4 seconds.

The production of H_2O_2 by reactive neutral species in water was from three pathways: 1) The H_2O_2 produced in the gas was transported into water; 2) The HO_2 produced in the gas was transported into water and self-react to produce H_2O_2 in water; 3) Oxygen atoms produce H_2O_2 and HO_2 at interface by reacting with water vapour, and then they were transported into water.

The mesh can significantly reduce the amount of oxygen atom reaching water due to their recombination on the metal surface, thereby reducing the production of hydrogen peroxide in water.

The findings in this work provide three suggestions for improving the water treatment technology. Firstly, energy consumption in the discharge gap is key to the overall efficiency of water treatment. Secondly, metal surfaces can cause significant consumption of reactive neutral species, which thereby should be avoided as much as possible. Thirdly, the presence of oxygen can increase the production of reactive neutral species, which in turn could improve the water treatment capability of plasma.

6. Interface Reactions between Water and Positive Glow Discharge in N_2, O_2 and He

6.1 Introduction

6.1.1 Motivation

Chapter 4 and Chapter 5 have discussed the interface reactions between water and the ionic wind generated by positive corona discharge. The positive ions generated by corona discharge have low kinetic energy of 0.01-0.1 eV [147], and only potential energy works in the interface reactions. The positive ions at the interface act as an ion anode in nitrogen corona discharge, on which the adsorbed form of hydroxyl radicals and oxygen atoms are formed. These adsorbed agents can form H_2O_2 in deionized water, or react with TB or DMSO in the solution.

This Chapter introduces d.c. glow discharges generated in nitrogen, oxygen and helium, to investigate the reaction mechanism between water and positive ions with kinetic energy. The higher kinetic energy of positive ions (greater than 100 eV [148]) in glow discharges has two potential effects on the interface reactions: One is that the kinetic energy can directly dissociate or ionize water molecules [74, 75]; the other is the kinetic energy may affect the reaction mechanisms between the ion anode and water cathode [42]. It has been suggested in the literature that, different from corona discharges, the hydrogen peroxide produced in water by d.c. glow discharge was mainly from the dimerization of OH [171]. In d.c. glow discharge generated in contact with water, in addition to positive ions, reactive neutral species are also produced in two main regions: one is the plasma region where H, OH and O derived from water vapor via the plasma chemical mechanism; and the other is the plasma-liquid interfacial region where H and OH derived from liquid water via radiolytic mechanism

[42].

6.1.2 Objectives

In this Chapter, d.c. glow discharge was generated between single-needle anode and water cathode in nitrogen (N_2), oxygen (O_2) and helium (He). By comparing the results of corona discharges and d.c. glow discharges, the effect of kinetic energy in interface reactions, especially in the charge-transfer process, is investigated. The investigation of the reactions between water and d.c. glow discharge includes:

i) The voltage and current characteristics of d.c. glow discharge in N_2, O_2 and He with water cathode.
ii) The formation mechanisms of H_2O_2 in the interface reactions between d.c. glow discharge and water cathode.
iii) The effect of gas flow rate, gas pressure and OH scavenger (TB and DMSO) on H_2O_2 production.
iv) The change of pH and conductivity of water caused by d.c. glow discharge.
v) The effect of kinetic energy on the interface reactions of ion anode and water cathode.

The results of these investigation will contribute to the understanding of OH and H_2O_2 production mechanisms at interface of plasma and water. Analysis of the results in corona discharge and glow discharge will determine the roles of energetic ions and low energy ions in interface process. These findings will be beneficial to improve the efficiency of water treatment by plasma.

6.2 Discharge characteristics

The experimental setup has been introduced in Chapter 3. To acquire a stable and uniform glow discharge in each type of gas, it was necessary to adjust the needle tip to water distance. In nitrogen and helium, the distance from needle tip to water surface was set to 2 mm. In oxygen discharge, the needle-water distance was set 8 mm, due to the observation that the glow discharge in oxygen in contact with water became unstable at a shorter needle-water distance. The discharge current and the sample treatment time is as shown in Table 6.1. The treatment time was selected to ensure that the concentration of H_2O_2 produced was high enough for accurate measurement.

Table 6.1 d.c. glow discharge current and treatment time in nitrogen, oxygen and helium.

Gas	Needle-water Distance	Discharge Current	Treatment Time
Nitrogen	2 mm	3 mA	4 minutes
Oxygen	8 mm	2 mA	5 minutes
Helium	2 mm	3 mA	4 minutes

6.2.1 Observation of discharge

Figure 6.1 shows the images of d.c. glow discharge in nitrogen, oxygen and helium. In nitrogen discharge, the discharge was stable and quiet.

In nitrogen, the major wavelengths are 600-900 nm, caused by the first positive band system; and 300-420 nm, caused by the second positive band system: these wavelengths present as red and violet respectively so that the mixture gives the pink colour [87].

The oxygen d.c. glow discharge in contact with deionized water was unstable at the first tens of seconds. The discharge channel appeared to be branched. The water surface was disturbed, and small drops of water was sputtered to the reactor wall. The voltage and current waveforms exhibited small fluctuations. As the discharge continued after tens of seconds, the discharge became stable, which was due to the conductivity increase of the water.

The d.c. glow discharge in helium was stable and quiet. The discharge channel broadens at the water surface. This phenomenon indicates a lower current density in cathode glow region. The positive column in helium discharge was uniform and bright.

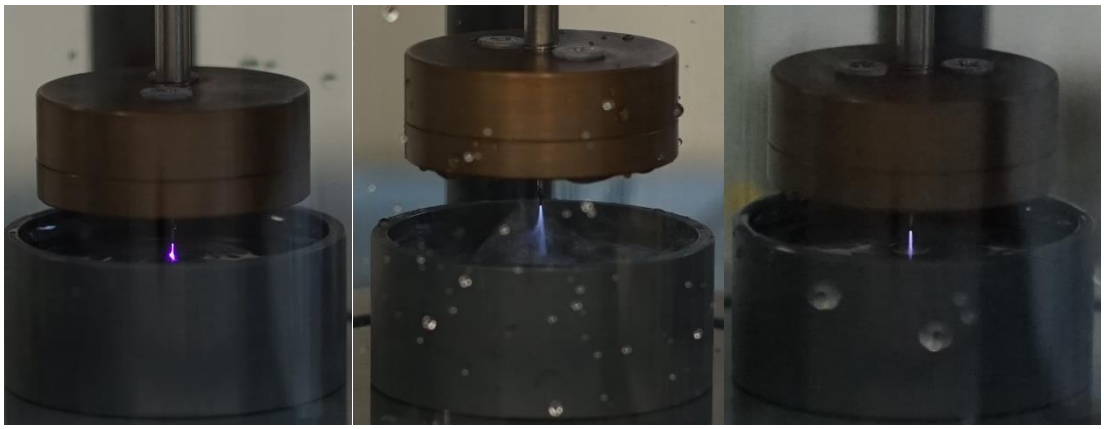

(a) (b) (c)

Figure 6.1 Images of positive DC glow discharge in (a) N_2 (3 mA, 2 mm gap), (b) O_2 (2 mA, 8 mm gap) and (c) He (3 mA, 2 mm) at 760 Torr with gas flow rate of 0.2 slpm.

The water vaporization was observed in the reactor in all three gases. The glow discharge in contact with water and the joule heating by water resistance accelerated the water vaporization. The saturated concentration of water vapour at room temperature of 20 ℃ is about 2.3% [160]. Hence the discharges were actually generated in the mixture with water vapour.

6.2.2 Voltage and current characteristics

For nitrogen and helium discharges, the current and voltage waveforms were smooth and flat. For oxygen discharge, the current and voltage are erratic with slight ripples, which might be caused by the water surface disturbance. The discharge current was also measured using a 50 Ω coaxial cable, and the oscilloscope with 50 Ω input impedance, but no impulse current was detected. At atmospheric pressure and gas flow rate of 0.5 slpm, the discharge voltages are as recorded in Table 6.2. The power (P) and injected energy (E_{in}) was calculated as:

$$P = V \times I \quad \text{(Eq. 6.1)}$$

$$E_{in} = V \times I \times t \quad \text{(Eq. 6.2)}$$

V is the discharge voltage; I is the discharge current; t is the treatment time.

Table 6.2 Electric characteristics of glow discharges in nitrogen, oxygen and helium.

Gas type	Discharge voltage (kV)	Power (W)	Injected energy (kWh)
N_2	1.45	4.35	2.90×10^{-4}
O_2	5.62	11.24	9.37×10^{-4}
He	1.37	4.11	2.74×10^{-4}

As Table 6.2 shows, the discharge voltage, power and the injected energy of helium and nitrogen discharge are close, but much lower than that of the oxygen discharge due to an 8 mm needle-water distance in oxygen. The electrical charge injected into the water cathode during the treatment process was 0.72 C in nitrogen and helium, and 0.6 C in oxygen.

6.3 Interface reactions between plasma and water cathode

6.3.1 The effect of gas flow rate

The gas flow rate can influence the concentration of water vapour in the reactor, which might influence the discharge. The effect of gas flow rate on discharge voltage, H_2O_2 production, pH and conductivity change was investigated. The gas (N_2, O_2 or He) was injected into the sealed reactor at a gas flow rate of 0.2, 0.5, 1, 2 and 5 slpm respectively. The pressure in the reactor was kept at 760 Torr.

6.3.1.1 The effect of gas flow rate on discharge voltage

Figure 6.2 shows the discharge voltage at different gas flow rates for all three gases. The discharge voltage consists of the voltage between the needle tip and water and the partial voltage across the water.

In nitrogen discharge, the voltage remained at 1.45 kV when the gas flow rate increased from 0.2 to 0.5 slpm. For flow rates from 0.5 to 5.0 slpm, the discharge voltage presented a slight increase, from 1.45 kV to 1.65 kV.

In helium discharge, the discharge voltage increased from 1.28 kV to 1.51 kV when the gas flow rate rose from 0.2 to 1.0 slpm. After 1.0 slpm, the discharge voltage only slightly increased from 1.51 kV to 1.66 kV.

In oxygen discharge, the discharge voltage had a slight decrease as gas flow rate increased from 0.2 to 2.0 slpm. When the gas flow rate increased from 2.0 to 5.0 slpm, the discharge voltage jumped from 5.34 kV to 6.52 kV.

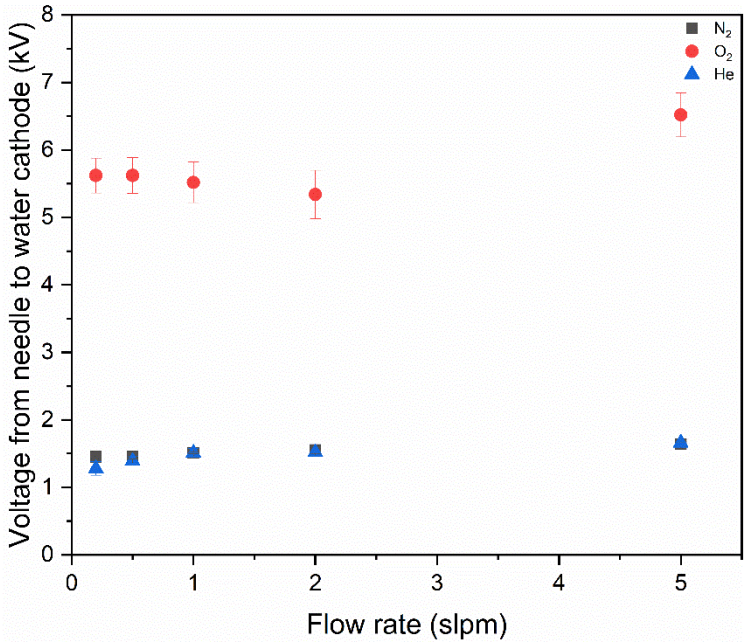

Figure 6.2 Glow discharge voltage from needle to water cathode in N_2, O_2 and He at 760 Torr with gas flow rate of 0.2, 0.5, 1.0, 2.0 and 5.0 slpm.

As shown in Figure 6.2, the discharge voltages in nitrogen and helium are subequal, which are much lower than the discharge voltage in oxygen. The main cause for this difference is the needle-water distance, which is much larger in oxygen discharge. Additionally, since the oxygen is electronegative gas, the affinity of electrons to oxygen molecules reduces the electron density, and further, reduced the plasma conductivity, which resulted in higher discharge voltage [199].

However, there is no obvious trend between the discharge voltage and gas flow rate. Although the discharge voltage in oxygen rose suddenly when gas flow rate increased from 2.0 to 5.2 slpm. The reason for this rise is still unclear. In nitrogen and helium discharge, the discharge voltages of the three repeated experiments were consistent and the standard deviation is negligible. The standard deviation of the discharge voltage in oxygen is much bigger in comparison.

6.3.1.2 The effect of gas flow rate on H_2O_2 production

Figure 6.3 shows the Faraday efficiency of H_2O_2 production with gas flow rates of 0.2, 0.5, 1.0, 2.0 and 5.0 slpm at gas pressure of 760 Torr. The Faraday efficiency was calculated using the method introduced in Section 4.6. It represents the ratio of the number of hydrogen peroxide molecules produced in water to the number of positive ions injected into the water cathode.

In nitrogen discharge, as the gas flow rate increased, the Faraday efficiency of H_2O_2 production increased and always remain larger than 1 at the whole range of tested gas flow rate. The highest Faraday efficiency of H_2O_2 production of the three gases was 1.28, obtained in nitrogen discharge at gas flow rate of 5.0 slpm.

In helium discharge the highest Faraday efficiency of H_2O_2 production shows a slightly decreasing trend as the gas flow rate increased. In the whole range of tested gas flow rates, the Faraday efficiency of H_2O_2 production by helium discharge is greater than 1.0, which is similar to that in nitrogen discharge.

The Faraday efficiency in oxygen discharge was significantly lower than those in nitrogen and helium discharge, remaining lower than 1.0 for tje tested gas flow rates. The lowest Faraday efficiency of H_2O_2 production of the three gases is 0.87, obtained in oxygen discharge at 2.0 slpm.

Refer to the results in Figure 6.2 and Figure 6.3, when the gas flow rate increased from 2.0 to 5.0 slpm in oxygen, there was a significant increase in both the discharge voltage (increased by 22%) and the Faraday efficiency of H_2O_2 production (increased by 13%). The synchronous ascent also demonstrated there is a strong correlation between discharge voltage and

Faraday efficiency of H_2O_2 production.

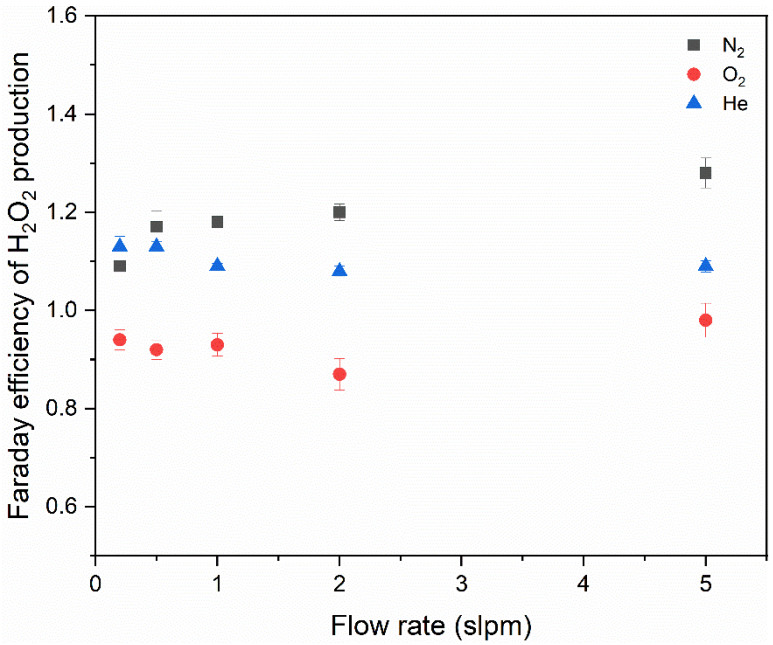

Figure 6.3 Faraday efficiency of H_2O_2 production by glow discharge in N_2, O_2 and He at 760 Torr with gas flow rate of 0.2, 0.5, 1.0, 2.0 and 5.0 slpm.

Figure 6.4 shows the H_2O_2 production in nitrogen, oxygen and helium discharge with gas flow rate of 0.2, 0.5, 1.0, 2.0 and 5.0 slpm. The energy yield of H_2O_2 in nitrogen presented an increase from 0.960 to 0.994 g/kWh as gas flow rate increased from 0.2 to 0.5 slpm. Then the energy yield shows a slight increasing trend as gas flow rate continues to rise. The maximum energy yield of 1.119 g/kWh of three gases was acquired in nitrogen at gas flow rate of 5.0 slpm.

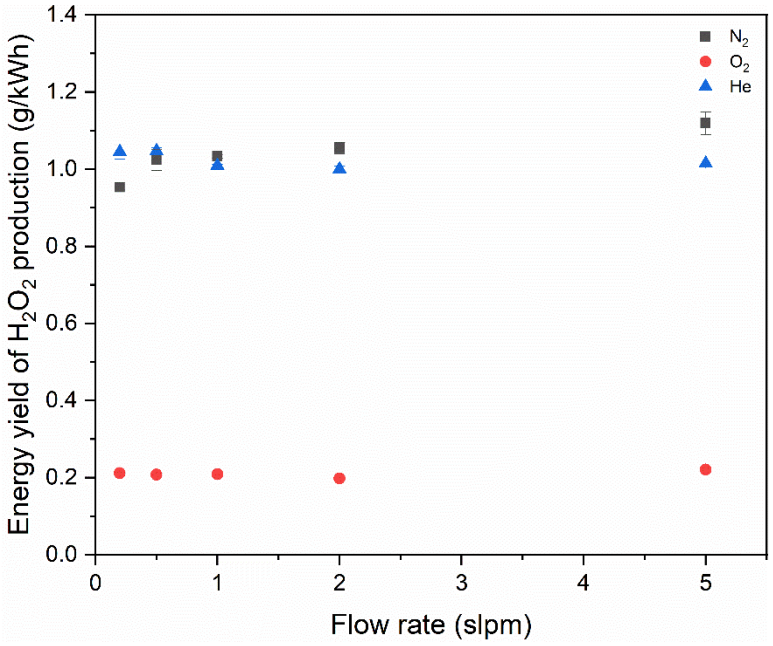

Figure 6.4 Energy yield of H_2O_2 production by glow discharge in N_2, O_2 and He at 760 Torr with gas flow rate of 0.2, 0.5, 1.0, 2.0 and 5.0 slpm.

In oxygen, the energy yield of H_2O_2 production was approximately equal to one-fifth of that in nitrogen and helium. This large difference was mainly caused by the discharge voltage, which in oxygen was around 5 times of that in nitrogen and helium. However, the Faraday efficiency was not increased by the high discharge voltage. Most of the energy was dissipated in the discharge gap in oxygen.

6.3.1.3 The effect of gas flow rate on pH and conductivity of treated deionized water

The gas flow rate influences the concentration of water vapour in the reactor, which can affect the discharge characteristics and the chemical reactions in gas phase and at the plasma-water interface change. By investigating the effect of gas flow rate on water pH and conductivity, it would provide more information on the plasma-water interface reactions.

Figure 6.5 shows the pH value of the treated deionized water at gas flow rate of 0.2, 0.5, 1.0, 2.0 and 5.0 slpm. In nitrogen discharge, the deionized water presented a significant decrease in pH value after treatment, around 3.6 at all gas flow rates. There is a significant decrease of pH in nitrogen, which is due to the HNO_x produced in water by the discharge [157, 158].

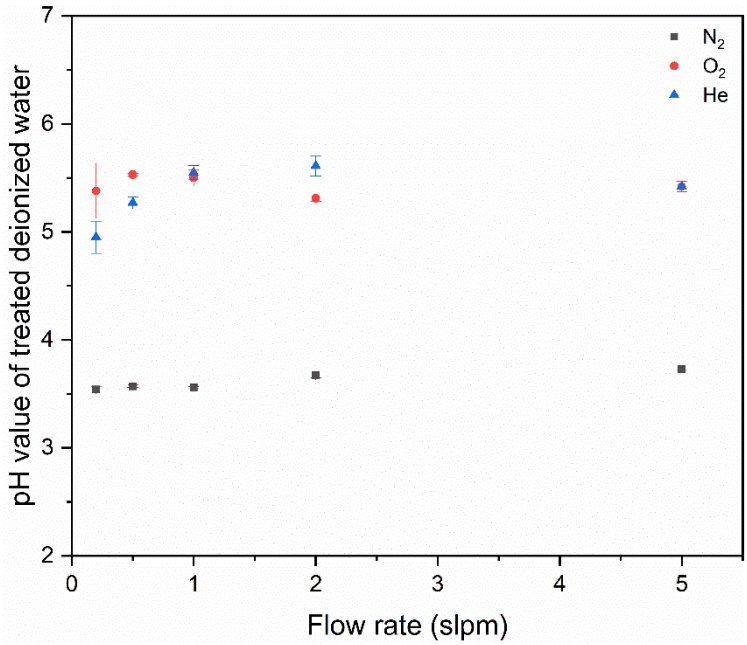

Figure 6.5 pH of deionized water after treatment by glow discharge in N_2, O_2 and He at 760 Torr with gas flow rate of 0.2, 0.5, 1.0, 2.0 and 5.0 slpm.

In oxygen discharge, as gas flow rate increased from 0.2 to 5.0 slpm, the pH value of treated deionized water varies from 5.31 to 5.53. There is no obvious trend between water pH and the gas flow rate in oxygen.

In helium discharge, the lowest pH value of treated deionized water was 4.95, obtained at a gas flow rate of 0.2 slpm. As gas flow rate increased from 0.2 to 1.0 slpm, the pH value of treated water slightly increased from 4.95 to 5.55.

Overall, the interaction between glow discharge and water caused decrease of pH in water from the initial value around 6.4. In nitrogen, the decrease of pH

was mainly caused by the production of HNO_x in water. In oxygen and helium, the slight decrease of water pH was still unclear.

Figure 6.6 shows the conductivity of the treated deionized water at gas flow rate of 0.2, 0.5, 1.0, 2.0 and 5.0 slpm.

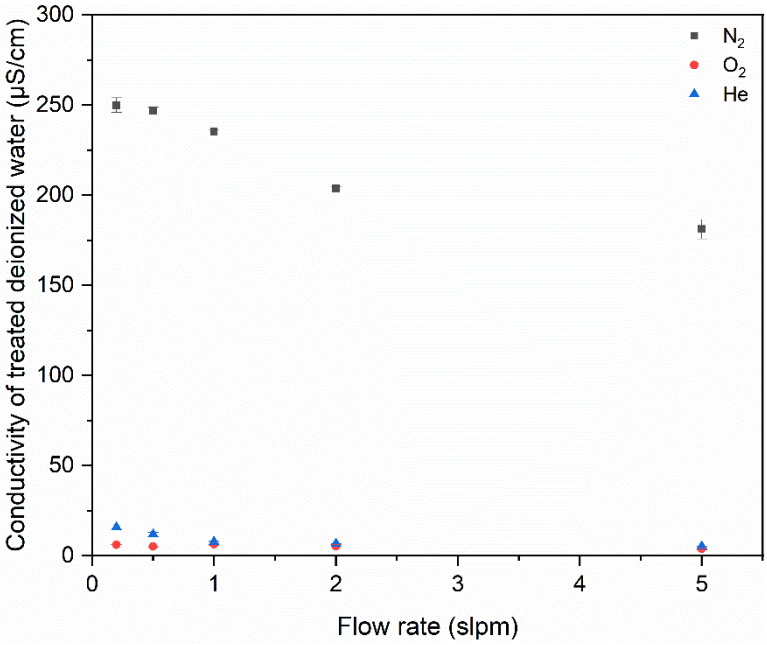

Figure 6.6 Conductivity of deionized water after treatment by glow discharge in N_2, O_2 and He at 760 Torr with gas flow rate of 0.2, 0.5, 1.0, 2.0 and 5.0 slpm.

The water conductivity in nitrogen glow discharge, presenting a downward trend as gas flow rate increased, is much higher than that for oxygen and helium glow discharge. The conductivity decreased from 250.0 to 181.2 μS/cm as the gas flow rate increased from 0.2 to 5.0 slpm. This suggested that with higher gas flow rate, less NO_x was produced. This result corresponds to the result in Figure 6.5, in which the pH increased as the gas flow rate increased.

The increase of water conductivity in oxygen and helium glow discharge was much smaller than that in nitrogen glow discharge. The conductivity is averaged around 5 μS/cm in oxygen. The water conductivity in helium glow discharge

slightly decreased from 15.8 to 5.3 μS/cm as gas flow rate increased from 0.2 to 5.0 slpm. This result corresponds to the results of pH in Figure 6.5 and Faraday efficiency of H_2O_2 production in Figure 6.3.

6.3.1.4 Off gas analysis

The off gas was put into the gas-washing bottle with 20 mL of deionized water. No H_2O_2 was detected in the gas-washing bottle after glow discharges in all three gases. In the oxygen and helium glow discharges, the pH and conductivity of the water in the gas-washing bottle showed no significant change. In nitrogen glow discharges, the pH of the water in gas-washing bottle decreased: Figure 6.7 shows the pH change of the water in gas-washing bottle with gas flow rate of 0.2, 0.5, 1.0, 2.0 and 5.0 slpm. As the gas flow rate increased from 0.2 to 5.0 slpm, the pH of the treated water in gas-washing bottle decreased from 5.31 to 4.64.

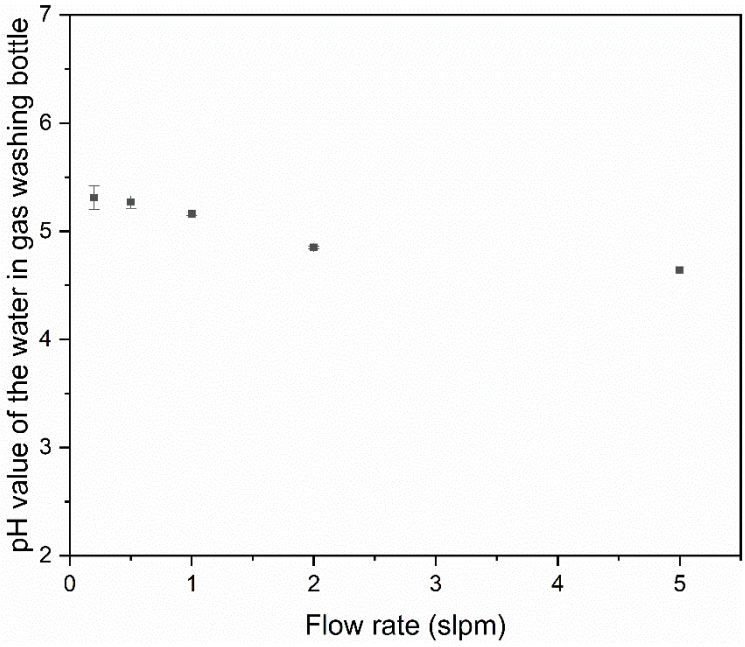

Figure 6.7 pH of the water in gas-washing bottle after glow discharge in N_2 at 760 Torr with gas flow rate of 0.2, 0.5, 1.0, 2.0 and 5.0 slpm.

In nitrogen discharge, the conductivity of the water in the gas-washing bottle increased from 3.84 to 18.09 μS/cm as gas flow rate increased from 0.2 to 5.0 slpm, as shown in Figure 6.8. The increase of water conductivity was a result of the increasing amount of NO_x injected into the gas washing bottle at higher gas flow rate.

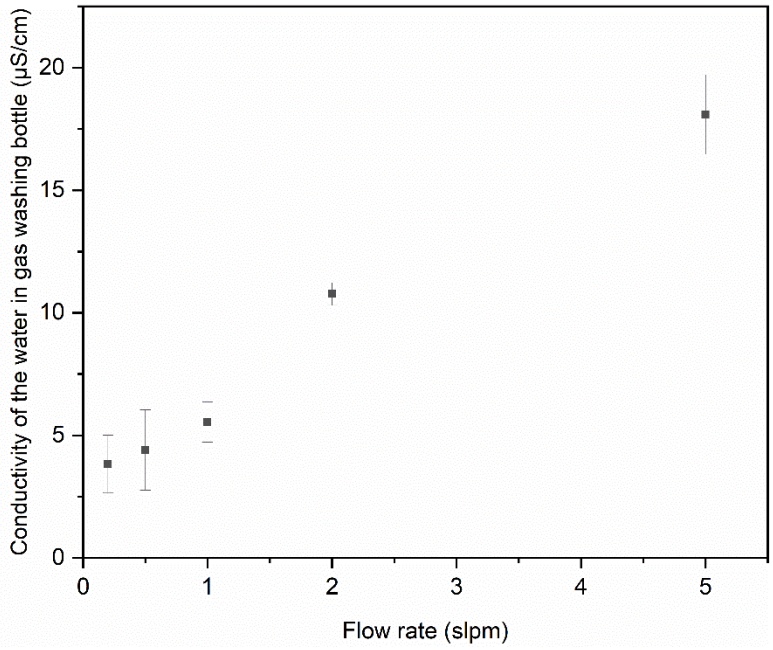

Figure 6.8 Conductivity of the water in gas-washing bottle after glow discharge in N_2 at 760 Torr with gas flow rate of 0.2, 0.5, 1.0, 2.0 and 5.0 slpm.

6.3.2 The effect of gas pressure

The gas pressure can influence the gas density and the rate of water evaporation in the reactor. When the gas pressure decreased, the water vaporization was promoted and the proportion of water vapor in the reactor increased, which can influence the discharge characteristics. As gas pressure decreased, the mean free path would increase, which resulted in an increase in their kinetic energy. In the discussion of nitrogen corona discharge in Chapter 4, it has been proved that at lower gas pressure, the H_2O_2 production by positive ions increased. This

suggested that the change of kinetic energy could influence the interface reactions. This section investigated the discharge characteristics, hydrogen peroxide production and water pH and conductivity as gas pressure decreased from 760 to 100 Torr. The experimental setup for this section is the same as that in Section 6.2. The discharge current was kept the same as introduced in Section 6.3.1, which is: 3 mA for nitrogen and helium glow discharge and 2 mA for oxygen glow discharge. The gas flow rate was 0.5 slpm for all experiments in this section.

6.3.2.1 The effect of gas pressure on discharge voltage

As Figure 6.9 shows, the discharge voltages in three gases show an upward trend as gas pressure increased. The increase of discharge voltage in oxygen is more distinct than that in nitrogen and helium. Oxygen is an electronegative gas, the affinity of electrons to oxygen molecules significantly reduces electron density in oxygen plasma and require higher discharge voltage to produce sufficient electrons [192]. As gas pressure decreased, the density of oxygen molecules decreased, which reduced the effect of electron attachment, therefore, easier to sustain the plasma discharge. There are studies reporting that the addition of oxygen in argon could significantly increase the discharge voltage to maintain the equal discharge current [192, 193].

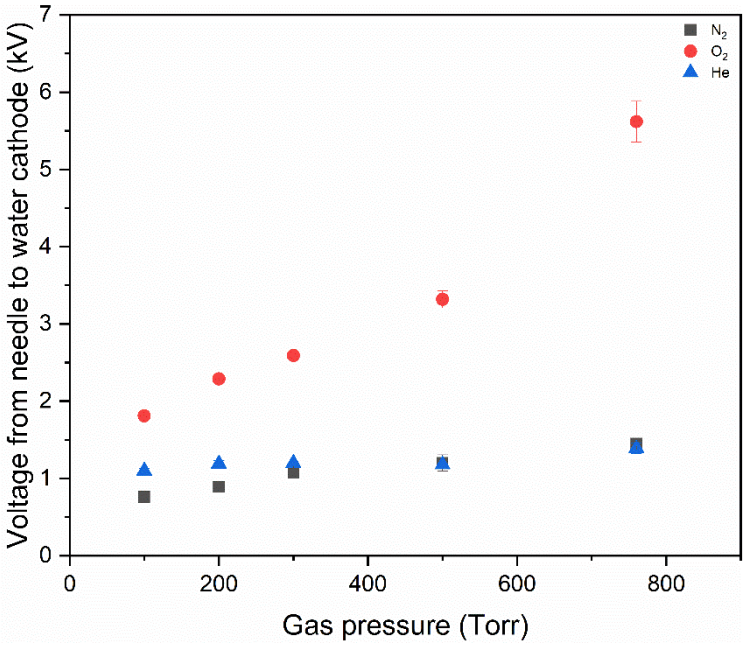

Figure 6.9 Glow discharge voltage from needle to water cathode in N_2, O_2 and He at gas pressure of 100, 200, 300, 500 and 760 Torr. The gas flow rate is 0.5 slpm.

6.3.2.2 The effect of gas pressure on H_2O_2 production

Figure 6.10 shows the Faraday efficiency of H_2O_2 production for all three gases at gas pressure of 100, 200, 300, 500, and 760 Torr and gas flow rate of 0.5 slpm.

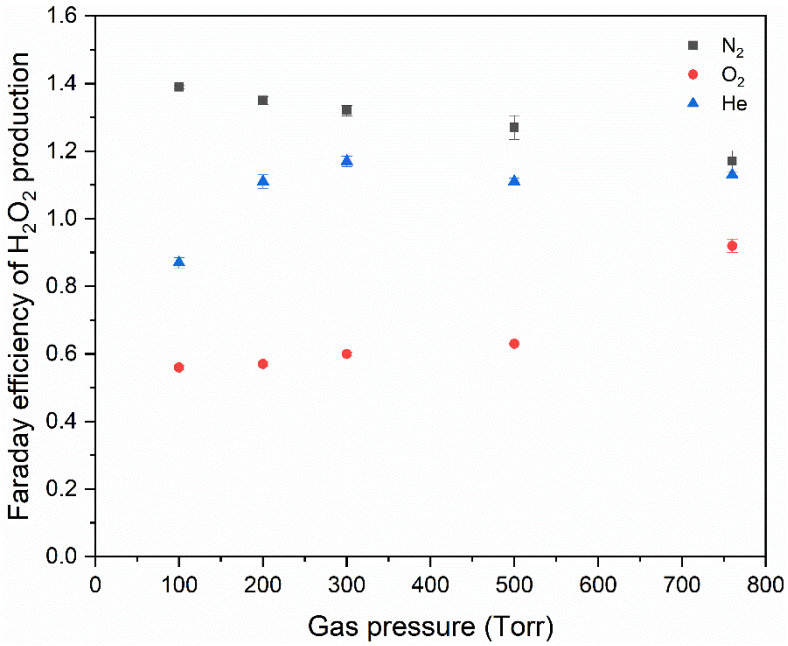

Figure 6.10 Faraday efficiency of H_2O_2 production by glow discharge in N_2, O_2 and He at gas pressure of 100, 200, 300, 500 and 760 Torr. The gas flow rate is 0.5 slpm.

The highest Faraday efficiency of H_2O_2 production was obtained in nitrogen glow discharge at 100 Torr, with 1 mol of positive ions producing 1.39 mol of hydrogen peroxide molecules. This ratio is much higher than the value predicted by Faraday's law. The plasma induced electrochemical process of hydrogen peroxide production has also been reported previously able to exceed 100% current efficiency by Faraday's law. Hickling investigated contact glow discharge electrolysis, and found that the hydrogen peroxide produced in the electrolyte can reach 1.8 times of the predicted by Faraday's law at 760 torr; the hydrogen peroxide formation was thought due to the positive ions accelerated through the cathode fall entering the liquid and dissociating water molecules [194].

The kinetic energy of positive ions bombarding the water surface contributed to hydrogen peroxide production. Water molecules can be sputtered to the gas

phase after impinged by the energised ions [195]. Additionally, kinetic ions bombard the water surface to excite, ionize or dissociate the water molecules, and produce protons and hydroxyl radicals [36, 196].

As the gas pressure increased, the width of discharge channel and the reduced electrical field decreased. As the gas pressure increased from 100 to 760 Torr, the discharge voltage increased by 97% in nitrogen, 210% in oxygen and 26% in helium. With the discharge gap unchanged, the average reduced electrical field decreased as the gas pressure increased. As gas pressure increased, the Faraday efficiency in N_2 glow discharge decreased gradually. The minimum Faraday efficiency of 1.17 in nitrogen glow discharge was recorded at 760 Torr.

The Faraday efficiency of H_2O_2 production in oxygen glow discharge was the lowest of the three gases in all gas pressure range. Contrary to the results in nitrogen, the Faraday efficiency increased in oxygen as the gas pressure increased. However, the reason for this result is still unclear.

The Faraday efficiency in helium was averaged around 1.14. At gas pressure range from 200 to 760 Torr, the Faraday efficiency fluctuates around 1.14.

On one hand, the gas pressure affects the reduced electrical field, which resulted in a change of kinetic energy of positive ions reaching water surface when gas pressure changes. On the other hand, the lower gas pressure would expand the discharge channel and increase the gas-liquid contacting area. These factors could all play roles in the plasma-water interface reactions.

Figure 6.11 shows the energy yield of hydrogen peroxide production in the three gases. The highest energy yield was obtained in nitrogen, recorded as 2.33 g/kWh at 100 Torr, and, the energy yield decreased rapidly as gas pressure increased.

The energy yield in oxygen is the lowest among three gases. As the gas pressure

increased from 100 to 760 Torr, the energy yield decreased slowly from 0.39 to 0.21 g/kWh.

In helium, the gas pressure did not significantly affect energy yield of H_2O_2 production: energy yield of H_2O_2 production was between 1.0 and 1.24 g/kWh.

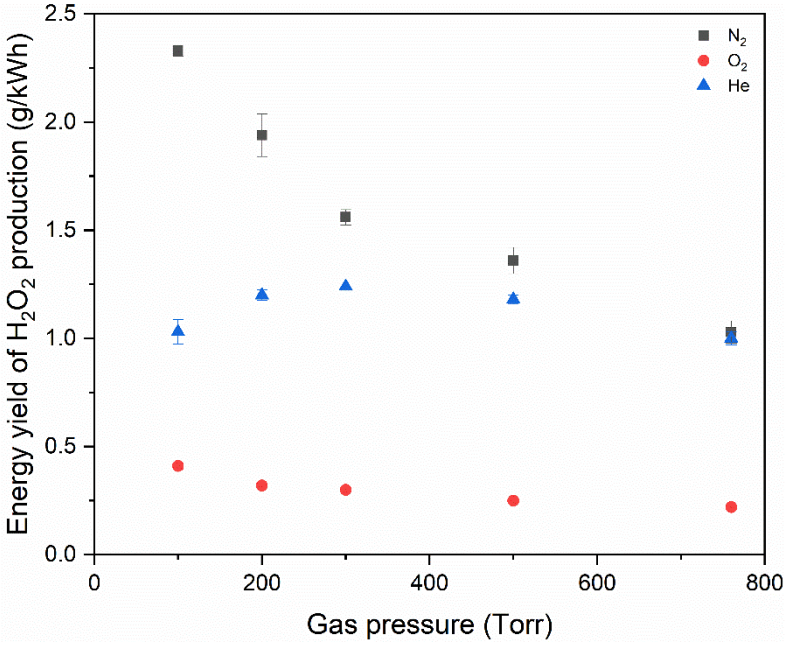

Figure 6.11 Energy yield of H_2O_2 production by glow discharge in N_2, O_2 and He at gas pressure of 100, 200, 300, 500 and 760 Torr. The gas flow rate is 0.5 slpm.

The energy yield of H_2O_2 production can be expressed as:

$$EY_{H_2O_2} = \frac{FE_{H_2O_2} \times Num_{ion} \times M_{H_2O_2}}{V_D \times I_D \times t} \quad \text{(Eq. 6.3)}$$

where

$EY_{H_2O_2}$ is the energy yield of H_2O_2 production;

$FE_{H_2O_2}$ is the Faraday efficiency of H_2O_2 production;

Num_{ion} is the total number of positive ions injected into water cathode;

$M_{H_2O_2}$ is the molar mass of hydrogen peroxide;

V_D is the discharge voltage;

I_D is the discharge current;

t is the treatment time.

Num_{ion} can be expressed by the discharge current and treatment time, as:

$$Num_{ion} = (I_D \times t)/q_e \quad \text{(Eq. 6.4)}$$

Where q_e is the elementary charge, equals to 1.6×10^{-19} C

Put Eq. 6.4 into Eq. 6.3:

$$EY_{H_2O_2} = \frac{FE_{H_2O_2}\times[(I_D\times t)/q_e]\times M_{H_2O_2}}{V_D\times I_D\times t} = \frac{FE_{H_2O_2}\times M_{H_2O_2}}{V_D\times q_e} \quad \text{(Eq. 6.5)}$$

Since $M_{H_2O_2}$ and q_e are constants, the $EY_{H_2O_2}$ is determined by Faraday efficiency ($FE_{H_2O_2}$) and discharge voltage (V_D).

Comparing Figure 6.9 and Figure 6.10, nitrogen glow discharge has the lowest discharge voltage and the highest Faraday efficiency, which resulted in the highest energy yield of H_2O_2 production; oxygen glow discharge has the highest discharge voltage but the lowest Faraday efficiency, which resulted in the lowest energy yield.

6.3.2.3 The effect of gas pressure on pH and conductivity of treated deionized water

For further investigation of the effect of the gas pressure on interface reactions, the pH and conductivity of treated water was analysed.

Figure 6.12 shows the pH value of treated water at gas pressure of 100, 200, 300, 400, 500 and 760 Torr. Glow discharge in nitrogen can produce nitrite and nitrate in water as introduced in Section 2.3.2, which significantly decreased pH value of water. The glow discharges in oxygen and helium only reduced the pH value of water slightly. The gas pressure had no significant influence on the pH value of treated water.

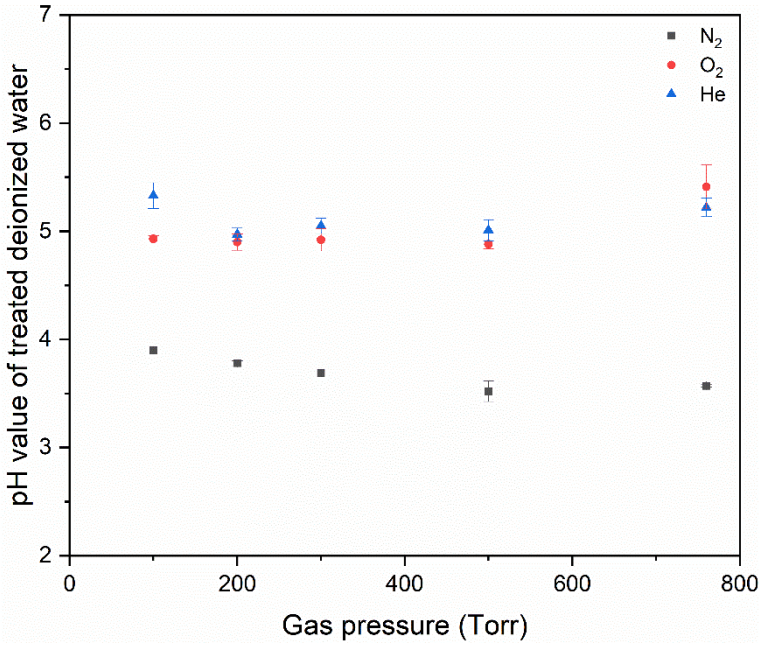

Figure 6.12 pH value of deionized water after treatment by glow discharge in N_2, O_2 and He at gas pressure of 100, 200, 300, 500 and 760 Torr. The gas flow rate is 0.5 slpm.

Figure 6.13 shows the conductivity of treated water after treatment with all gases at gas pressure of 100, 200, 300, 500 and 760 Torr. The water conductivity increased to 10-25 μS/cm after treatment by glow discharge in helium and oxygen. Glow discharge in nitrogen increased water conductivity significantly as gas pressure increased from 100 to 760 Torr, i.e. from 128 to 247 μS/cm.

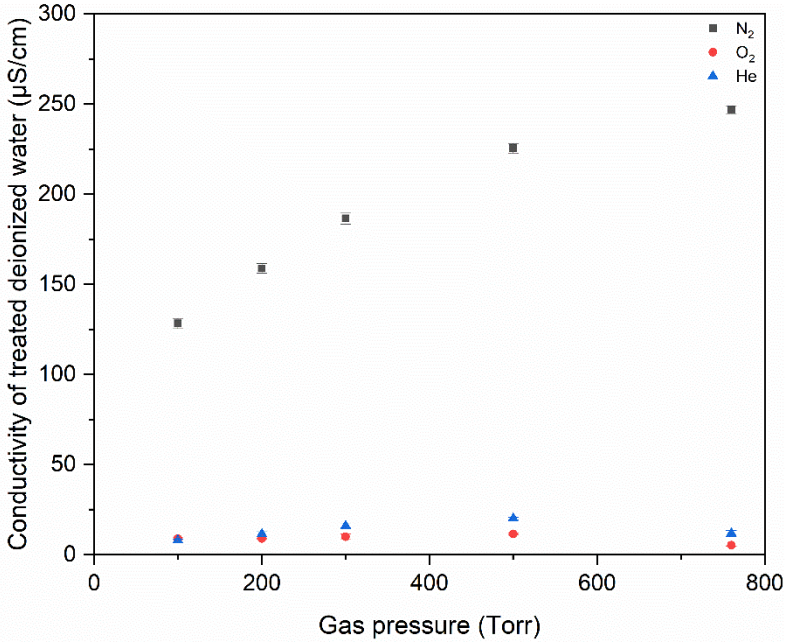

Figure 6.13 Conductivity of deionized water after treatment by glow discharge in N_2, O_2 and He at gas pressure of 100, 200, 300, 500 and 760 Torr. The gas flow rate is 0.5 slpm.

According to the results, the gas pressure has rare effects on the pH and conductivity of water in oxygen and helium. In nitrogen, as gas pressure increased from 100 to 760 Torr, the conductivity of water increased by around 2 times; meanwhile, the pH value decreased from 3.90 to 3.57, which implies the concentration of H^+ increased by around 2 times as well. These two data demonstrated that the change of pH and conductivity in nitrogen was caused by the same elements, which are nitrite and nitrate [158]. This mechanism was similar to that in corona discharge as introduced in Section 4.3.5. Compared the

results shown in Figure 6.9, Figure 6.12 and Figure 6.13, it suggested the higher gas pressure would promote the HNO_x production but suppress the H_2O_2 production.

6.3.3 The effect of Tert-butanol

To investigate the formation pathway of H_2O_2 in water, tert-butanol, an OH scavenger, was added to deionized water. The discharge time and discharge current were kept the same as given in Table 6.1. Two concentrations of TB solutions were applied: 0.01 M and 0.1 M. The treated TB solution volume was 10 mL. In this section, all the experiments were conducted at 760 Torr and gas flow rate of 1.0 slpm.

6.3.3.1 The effect of TB on discharge voltage

Figure 6.14 shows the discharge voltages for three gases with the three sample solutions. In oxygen, the addition of TB significantly reduced the discharge voltage. In nitrogen, the discharge voltage with 0.1 M TB solution was increased dramatically. In helium, the addition of TB caused a slight decrease of the discharge voltage.

In oxygen, the addition of TB significantly decreased the discharge voltage. However, the discharge voltage with 0.1 M TB is moderately lower than that with 0.01 M TB. This change does not completely coincide with the change in conductivity shown in Figure 6.16.

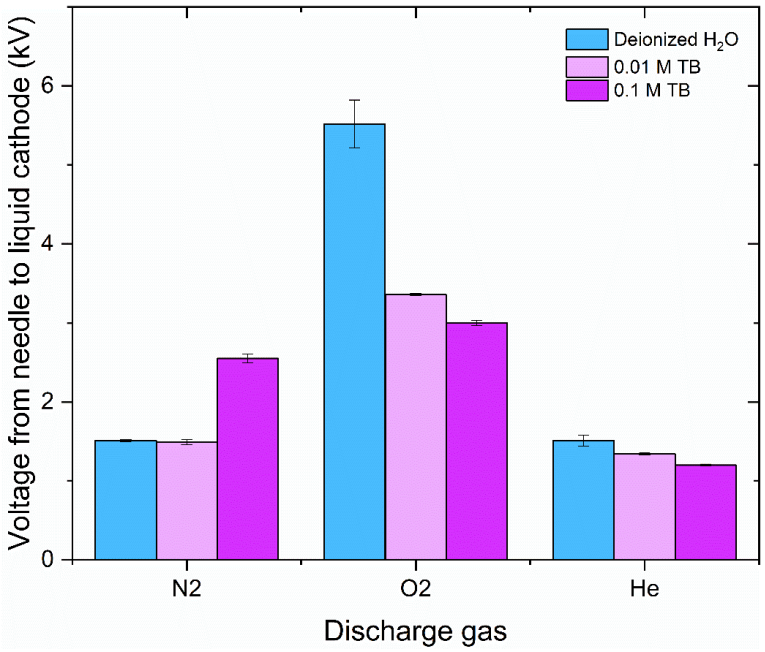

Figure 6.14 Glow discharge voltage from needle to liquid cathode in deionized water, 0.01 M and 0.1 M TB solution. The gas flow rate is 1.0 slpm.

6.3.3.2 The pathway of H_2O_2 production in TB solutions

As Figure 6.15 shows, in nitrogen and helium glow discharge, the addition of TB reduced the Faraday efficiency of H_2O_2 production. TB can rapidly react with OH and prevent OH from dimerising into H_2O_2. This is particularly evident with 0.1 M TB solution, where the Faraday efficiency decreased to 0.12 in nitrogen and 0.16 in helium.

In contrast to the results obtained in nitrogen and helium, in oxygen, the Faraday efficiency of H_2O_2 production increased with addition of TB. In 0.1 M TB solution, the Faraday efficiency of H_2O_2 production was 1.61. These results indicate that the TB participated in either the gas phase or aqueous reactions to produce more H_2O_2.

There is rare research reporting the increase of hydrogen peroxide production by plasma with the addition of TB in water. However, the promotion of electrochemical production of H_2O_2 by organic electron donors (e.g. bisphenol) has been reported [197]. In this case, due to the speciality of ion anode at the interface in oxygen discharge, TB as the organic electron donors, can be adsorbed on the ion anode and preventing the decomposition of H_2O_2 in oxygen; meanwhile, TB can scavenge OH and reduce its oxidation of H_2O_2. By these two pathways, the TB promoting the accumulation of H_2O_2 in oxygen discharge.

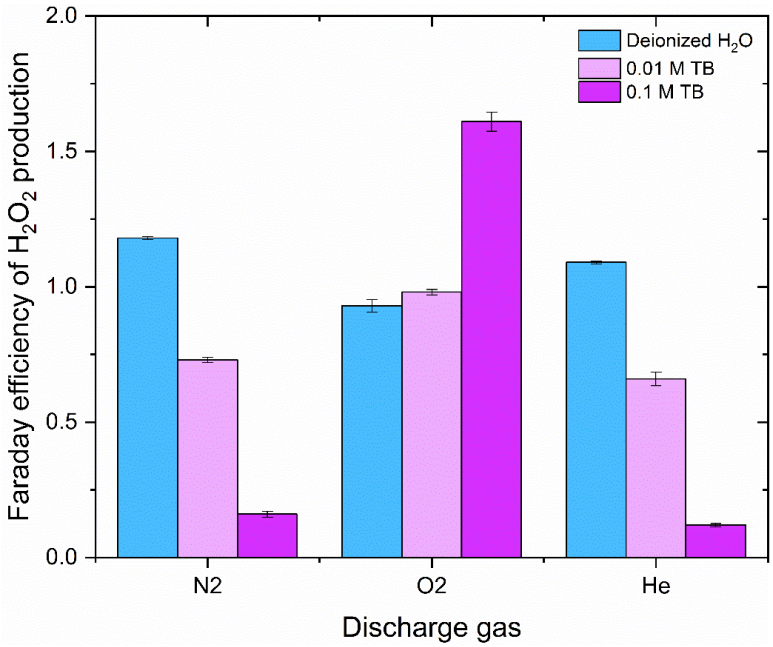

Figure 6.15 Faraday efficiency of H_2O_2 production at 760 Torr in deionized water, 0.01 M and 0.1 M TB solution. The gas flow rate is 1.0 slpm.

6.3.3.3 The effect of TB on pH and conductivity of treated solution

The original pH of the deionized water, 0.01 M and 0.1 M TB solution are 6.40, 5.87 and 5.84 respectively. Figure 6.16 shows the pH change of three treated

solutions.

In oxygen and helium discharge, the pH of TB solution is lower than that of deionized water after treatment. Differently, in nitrogen discharge, the pH of 0.1 M TB solution became much higher than that of the deionized water and 0.01 M TB.

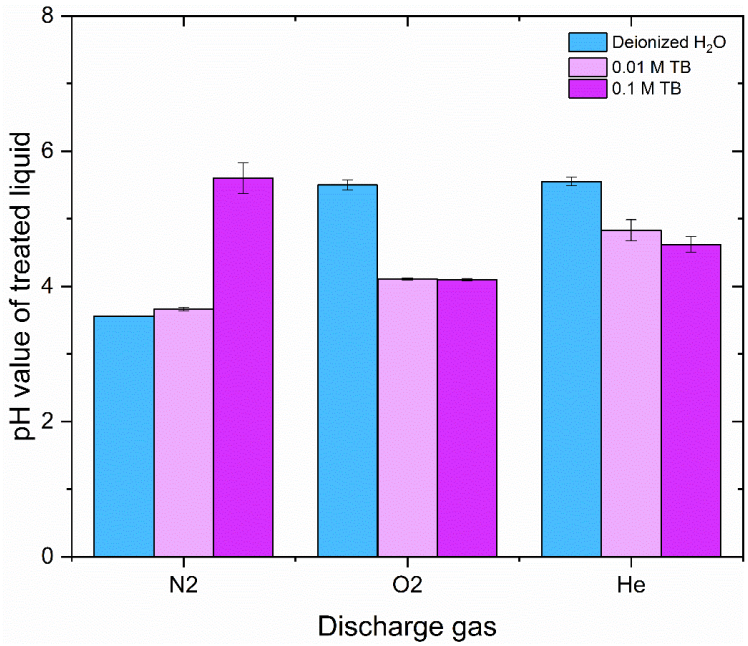

Figure 6.16 pH of deionized water, 0.01 M and 0.1 M TB solution after treatment at 760 Torr. The gas flow rate is 1.0 slpm.

The original conductivity of the deionized water, 0.01 M and 0.1 M TB solution are 0.7, 1.0 and 1.0 μS/cm respectively. Figure 6.17 shows the conductivity of the deionized water, 0.01 M TB solution and 0.1 M TB solution after the treatment. In oxygen and helium glow discharges, TB solutions had a higher conductivity than deionized water. But in nitrogen glow discharge, 0.1 M TB solution has a much lower conductivity compared with the deionized water and 0.01 M TB solution. The significant reduction of conductivity corresponds to the pH and the discharge voltage in 0.1 M TB solution after nitrogen glow discharge.

Comparing Figure 6.14, Figure 6.16 and Figure 6.17, after treatment by glow discharge in nitrogen, 0.1 M TB solution has lower conductivity, higher pH and higher discharge voltage. This suggested that the presence of TB reduced the production of nitrites and nitrates in the solution.

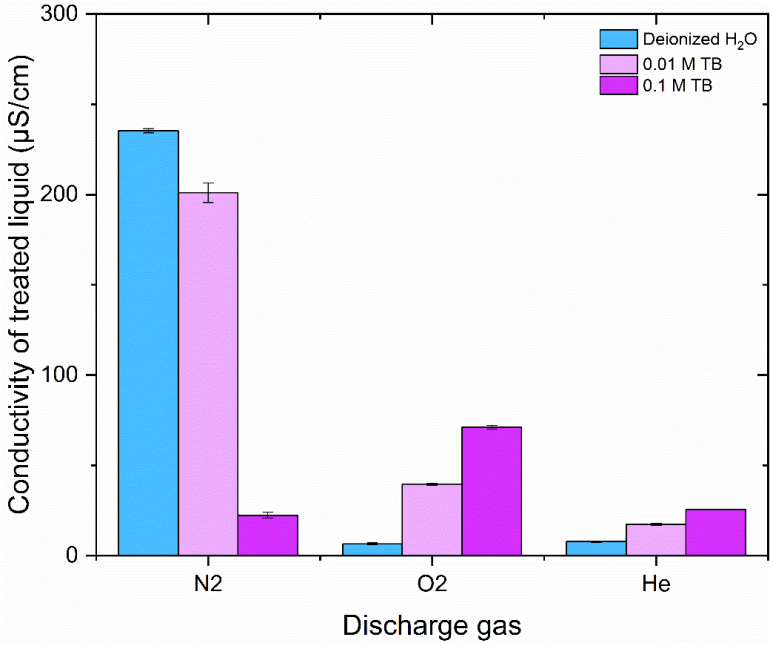

Figure 6.17 Conductivity of deionized water and TB solutions after treatment by glow discharge in N_2, O_2 and He at 760 Torr. The gas flow rate is 1.0 slpm.

6.3.4 The effect of DMSO

In nitrogen and oxygen corona discharge introduced in Chapter 4 and 5, the addition of TB in the sample solution increased the H_2O_2 production in the solution but the addition of DMSO didn't.

6.3.4.1 The effect of DMSO on discharge voltage

Figure 6.18 shows the discharge voltage using deionized water, 0.01 M DMSO solution and 0.1 M DMSO solution. The addition of DMSO in the sample

solution led to the reduction of discharge voltage in all three gases, especially in oxygen and helium. However, different to the addition of TB in the solution, the voltage reduction for 0.01 M and 0.1 M DMSO solutions are very similar.

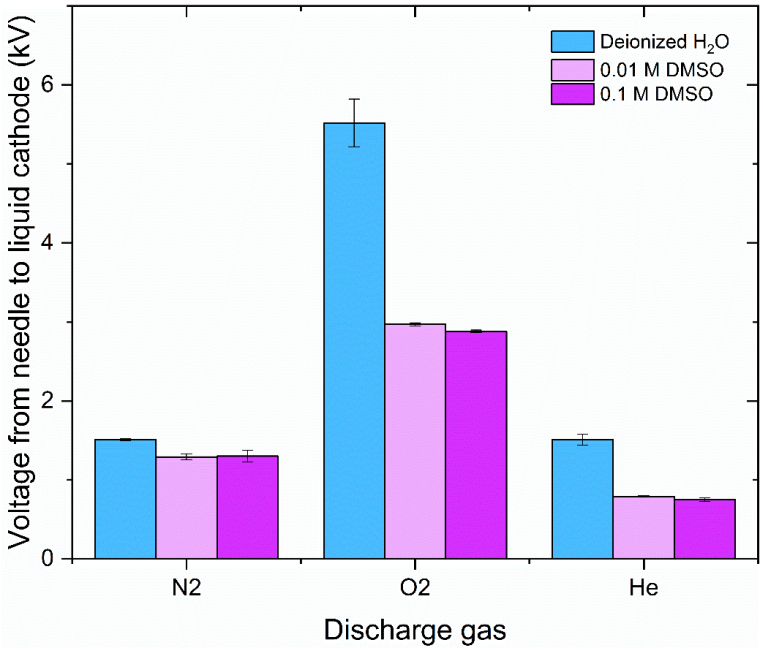

Figure 6.18 Glow discharge voltage from needle to liquid cathode in N_2, O_2 and He with deionized water, 0.01 M and 0.1 M DMSO solution at 760 Torr. The gas flow rate is 1.0 slpm.

6.3.4.2 The effect of DMSO on H_2O_2 production

After treatment by nitrogen glow discharge, as Figure 6.18 shows, the Faraday efficiency of H_2O_2 production was reduced with addition of DMSO. The Faraday efficiency was much lower than that in deionized water, especially in 0.1 M DMSO solution. Concentration of DMSO has a dramatic effect on Faraday efficiency in nitrogen discharge.

The situation regarding Faraday efficiency of H_2O_2 production by oxygen glow discharge is less clearly defined. In deionized water the value was lower than

that in 0.01 M DMSO solution but higher than that in 0.1 M DMSO solution. This is different from the data presented for TB solutions. In TB solutions, the Faraday efficiency of H_2O_2 production increased with higher TB concentration. These results further prove that, in oxygen glow discharge, the interface reactions did not produce OH leading to the production of H_2O_2.

In helium glow discharge, the Faraday efficiency of H_2O_2 production was reduced by around 70% with the addition of DMSO in the water. Variation in the concentration of DMSO did not cause significant change in Faraday efficiency of H_2O_2 production.

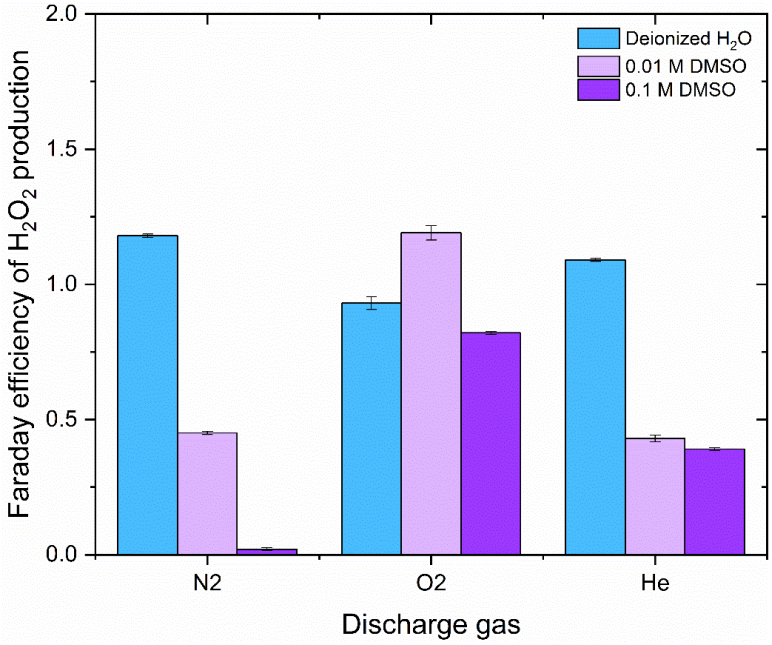

Figure 6.19 Faraday efficiency of H_2O_2 production by glow discharge in N_2, O_2 and He in deionized water, 0.01 M DMSO solution and 0.1 M DMSO solution at 760 Torr. The gas flow rate is 1.0 slpm.

6.3.4.3 The effect of DMSO on solution pH and conductivity

The original pH of 0.01 M DMSO solution and 0.1 M DMSO solution was 6.06 and 6.09; the original conductivity of 0.01 M DMSO solution and 0.1 M DMSO solution was 1.1 and 0.9 μS/cm.

As Figure 6.20 shows, in nitrogen glow discharge, the addition of DMSO only slightly decreased the solution pH after treatment. In oxygen and helium glow discharge, the pH in DMSO solutions was much lower than that of the deionized water after treatment. These results prove that there were acidic substances produced, especially with the addition of DMSO.

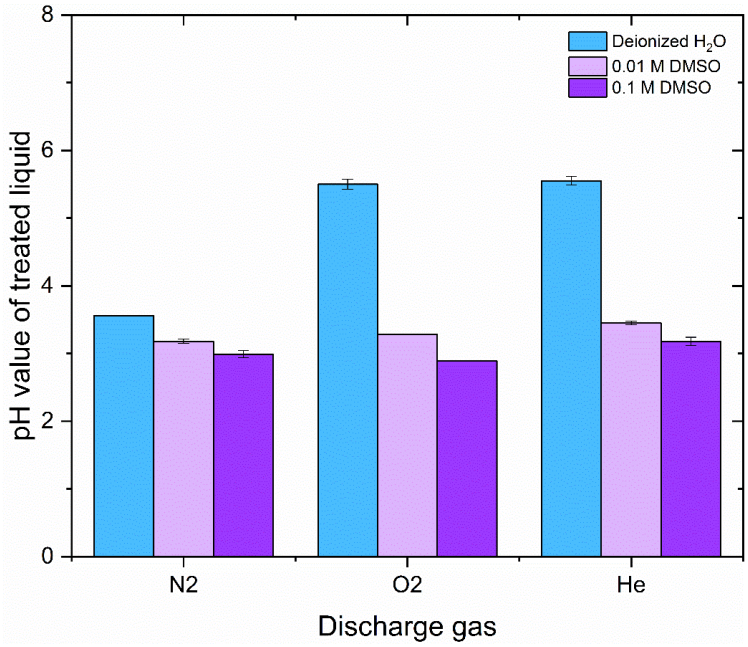

Figure 6.20 pH of deionized water, 0.01 M and 0.1 M DMSO solution after treatment by glow discharge in N2, O2 and He at 760 Torr. The gas flow rate is 1.0 slpm.

Figure 6.21 shows the solution conductivity after treatment. The addition of DMSO increased solution conductivity significantly in all three gases. The

highest conductivity reached 1083 µS/cm, acquired in 0.1 M DMSO solution in oxygen discharge. These results suggested that the DMSO took part in the reactions in the solution and produced conductive electrolyte.

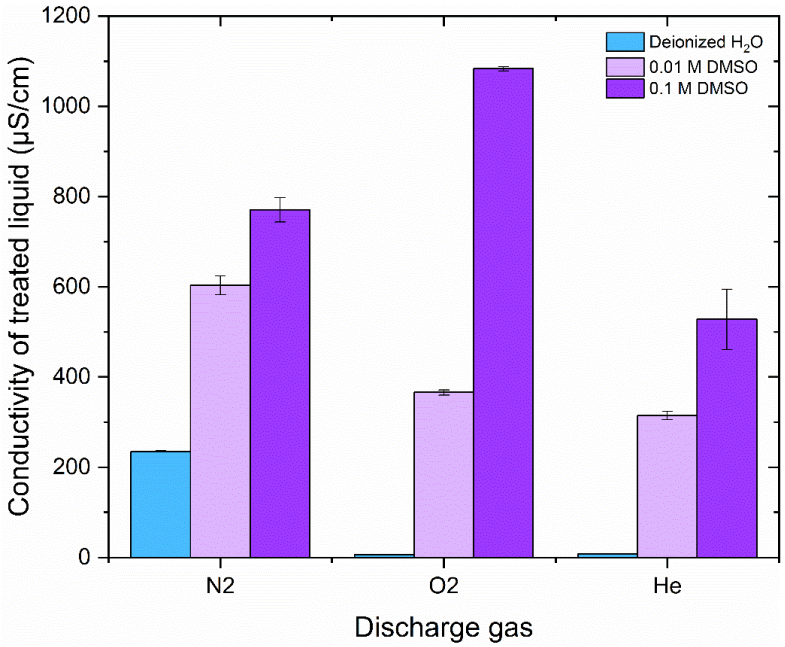

Figure 6.21 Conductivity of deionized water, 0.01 M and 0.1 M DMSO solution after treatment by glow discharge in N_2, O_2 and He at 760 Torr. The gas flow rate is 1.0 slpm.

6.4 Discussions

The glow discharge generated in nitrogen, oxygen and helium with a water cathode has been proved to produce H_2O_2 in water. In corona discharges, the kinetic energy of positive ions reaching water is only 0.01-0.1 eV [147]; while in glow discharges, the average kinetic energy of positive ions entering the water can be greater than 100 eV [117]. The large kinetic energy resulted in higher Faraday efficiency of H_2O_2 production. It has been proved that the positive ions accelerated by cathode fall can dissociate water molecules to produce hydrogen peroxide, even exceeding the 100% current efficiency

predicted by Faraday's law [194].

It has been suggested that in glow discharge with liquid cathode, the water molecules can be transported to the plasma by three pathways: 1) sputtered by the fast positive ions; 2) carried by hydrated negative ions which pulled out by electrical field and 3) evaporated by plasma and Joule heating. After entering the plasma, water molecules can react with plasma species to produce OH [198].

However, according to the analysis in Chapter 4 and Chapter 5, the positive ions accumulated on water surface may act as ion anode, on which the water molecules lose electron and produce H_2O_2 through the electrochemical process. Similarly, this kind of interface process also occurs in glow discharges. Differently, the positive ions reaching water may not be $H^+(H_2O)_n$. One significant evidence is that the addition of TB or DMSO has different effects on hydrogen peroxide production in different gases: in nitrogen and helium glow discharge, the H_2O_2 production was decreased but in oxygen, the H_2O_2 production was increased. If the positive ions are all the same, such as $H^+(H_2O)_n$, this difference cannot be explained. In oxygen, the ion anode is different from that in nitrogen or helium, the organic substance TB and DMSO can participate in the ion-anode process and promoted the production of H_2O_2.

The energy yield of H_2O_2 can be calculated as:

$$EY_{H_2O_2} = \frac{H_2O_2 \text{ Production}}{EY_{plasma} + EY_{interface} + EY_{liquid}} \quad \text{(Eq. 6.6)}$$

where $Energy_{plasma}$ is the energy dissipated in plasma in gas phase; $Energy_{interface}$ is the energy dissipated at plasma-water interface and $Energy_{liquid}$ is the energy dissipated in liquid. Similar to corona discharges, most of the energy is dissipated in plasma for sustaining the discharges.

In summary, the Faraday efficiency of H_2O_2 production by glow discharges are

higher than those in corona discharges, up to 1.39, obtained in nitrogen. The high Faraday efficiency was attributed to the contribution of kinetic energy. The electrochemical process at the interface may also produce H_2O_2. The energy yield of H_2O_2 in glow discharges is higher than that in corona discharge, due to the higher Faraday efficiency and lower discharge voltage. However, most of the energy is consumed in the plasma channel as well as small amount of energy is consumed by the joule heating of water resistance. Producing one positive ion still needs to consume hundreds of electron volts; and approximately, one positive ion can only produce one H_2O_2 molecule. This is the main limitation for increasing the energy yield of H_2O_2.

6.5 Conclusions

The order of Faraday efficiency of H_2O_2 production by glow discharge in three gases was: nitrogen > helium > oxygen. The highest Faraday efficiency of H_2O_2 production in deionized water were: 1.39 in nitrogen glow discharge, 0.92 in oxygen glow discharge and 1.17 in helium glow discharge.

The highest energy yield of H_2O_2 production were 2.33 g/kWh in nitrogen glow discharge, 0.41 g/kWh in oxygen glow discharge and 1.24 g/kWh in helium glow discharge. At lower gas pressure, the Faraday efficiency of H_2O_2 production by nitrogen glow discharge was higher: the highest value of 1.39 for nitrogen glow discharge was obtained at 100 Torr. The Faraday efficiency of H_2O_2 production by oxygen and helium glow discharge reached their lowest value at 100 Torr, which is 0.56 and 0.87 respectively.

Only nitrogen glow discharge significantly decreased the pH of deionized water. The lowest pH was 3.54, obtained at 760 Torr. The nitrogen glow discharge can increase the solution conductivity significantly, reaching the highest conductivity, 250.0 μS/cm, at 760 Torr. The increase of solution conductivity was due to the transportation of NO_x into the solution and forming nitrate and

nitrate.

As gas pressure decreased from 760 to 100 Torr, the discharge voltage in oxygen glow discharge decreased significantly, from 5.62 to 1.81 kV. In nitrogen and helium glow discharge, the discharge voltage showed only a slight decrease as gas pressure decreased.

The addition of TB and DMSO significantly reduced the H_2O_2 production in nitrogen and helium glow discharge, but not in oxygen glow discharge, indicating that OH was the precursor of the H_2O_2 in nitrogen and helium glow discharge. While in oxygen glow discharge, the production of H_2O_2 was not from the dimerization of OH.

7. Conclusions and Future Work

7.1 Conclusions

This research aimed to investigate the interface reactions between positive plasma and water, and explore the formation mechanisms of OH and H_2O_2 in water. The three main achievements were:

1. The effects of low energy positive ions and reactive neutral species produced by corona discharge in N_2 and O_2 on interface reactions have been determined.

2. The difference of interface reactions caused by low energy and energetic positive ions has been identified.

3. The mechanism about why the energy yield of OH and H_2O_2 by plasma-water reactions is limited have been analysed.

The three achievements provide further information about the reaction mechanism between water cathodes and positive plasma based upon the current knowledge of interface process. This information identifies why it is difficult to achieve significant improvements in the energy yield of OH and H_2O_2 by plasma-water reactions. The core reason is: no matter how the reactor geometry is designed, it needs to consume at least hundreds of eV to transport one positive ion to water cathode which then produces around one OH molecule in the water. Most of the energy is dissipated in the gas discharge, not in the production of OH at the water-plasma interface. Due to the short lifetime of OH, the OH produced in gas phase would be consumed by self-quenching or other species. Hence, only the OH produced at the interface can be transported into water. Based on these findings in this research, two proposed research directions for improving the energy yield of OH are to:

1. Reduce the energy consumption of producing and transporting positive ions
2. Multiply the OH production proportion by positive ions at the interface.

The arc discharge can deliver the positive ions from anode to cathode while only consuming tens of eV, which may significantly increase the energy efficiency of OH production in water by positive ions.

Another novelty of this research is the design of the reactor for corona discharges. A nine-needle electrode was biased at high voltage to generate corona discharge, which produced positive ions drifting to the water. With this reactor configuration, a d.c. cathode current was obtained, which allowed a uniform ionic wind blowing to the water surface. The mesh cathode can filter the positive ions, allowing only reactive neutral species to reach the water surface. This design allowed the separation of the effects of positive ions and reactive neutral species on the mechanisms of OH and H_2O_2 formation.

By analysing the results from corona discharges and glow discharges, the interface reaction mechanisms between plasma and water are explored. The important findings in the research can be summarized as:

1. The drift positive ions generated by corona discharge in nitrogen and oxygen react with water to produce hydrogen peroxide, not hydroxyl radicals.

2. The reaction mechanisms between positive ions and water cathode are the same in nitrogen and oxygen corona discharge. The positive ions reaching water cathode are $H^+(H_2O)_n$, which can produce H_2O_2 in deionized water or react with organics in the solution.

3. The Faraday efficiency of hydrogen peroxide production by positive ions in corona discharge increased as gas pressure decreased. At 100 Torr, 1 mol of positive ions can produce 0.29 mol of hydrogen peroxide.

4. In corona discharges, the reactive neutral species consisting of H_2O_2 and HO_2, were transported from gas phase to water, contributed to hydrogen peroxide production in water.

5. In oxygen corona discharge, oxygen atoms (O) react with water vapour at interface, producing more H_2O_2 and HO_2. The reactive neutral species contributed more than 76% hydrogen peroxide production in oxygen corona discharge.

6. The reactive neutral species in corona discharges would deactivate within several seconds.

7. Hydrogen peroxide produced by positive glow discharge in nitrogen and helium is mainly from dimerization of OH, but not in oxygen glow discharge.

8. The Faraday efficiency of hydrogen peroxide production in glow discharge is much higher than that in corona discharge. The maximum Faraday efficiency was 1.39 in nitrogen, 0.92 in oxygen and 1.17 in helium.

9. Both corona discharge and glow discharge in nitrogen can significantly decrease pH and increase the conductivity of water. The change in pH and conductivity is mainly caused by nitrate and nitrite, which were due to the NO_x transported from gas phase to water.

In nitrogen corona discharge, both positive ions and reactive neutral species contributed to hydrogen peroxide production. In nitrogen corona discharge at 760 Torr, 1 mol of positive ions can produce 0.13 mol of hydrogen peroxide,

which is equal to the contribution of reactive neutral species. As gas pressure decreased, hydrogen peroxide production increased significantly, at 100 Torr, 1 mol of positive ions can produce 0.29 mol of hydrogen peroxide, over twice the production. The increase was found to be due to the increased amount of hydrogen peroxide produced by positive ions. Hydrogen peroxide production by reactive neutral species did not show a significant change as gas pressure decreased. The highest energy yield of hydrogen peroxide production by nitrogen corona discharge was 0.178 g/kWh, obtained at 100 Torr. The addition of OH scavengers TB and DMSO in water did not reduce hydrogen peroxide production by nitrogen corona discharge, which proves that the production of H_2O_2 was not from OH dimerization, for both the positive ions and the reactive neutral species. The production of H_2O_2 by reactive neutral species in nitrogen corona discharge was from two pathways: 1) the H_2O_2 produced in gas phase was transported into water; 2) the HO_2 produced in gas phase was transported into water and self-react to produce H_2O_2 in water.

, In nitrogen corona discharge, the pH of water decreased and the conductivity of water increased, mainly caused by the formation of nitrate and nitrite, proved that the NO_x was carried to the water by the ionic wind.

The analysis suggested the positive ions reaching water surface were $H^+(H_2O)_n$, which deposited at the interface, acting as an ion anode. Adsorbed hydroxyl radicals $H^+(H_2O)_n(\cdot OH)$ and active oxygen $H^+(H_2O)_n(\cdot O)$, formed on the ion anode, which can synergistically act when either TB or DMSO was added to water, producing twice as much hydrogen peroxide as that in deionized water.

In oxygen corona discharge, the positive ions reaching water surface are the same as those in nitrogen corona discharge, which are $H^+(H_2O)_n$, thereby the reaction mechanisms between positive ions and water, as well as the amount of H_2O_2 produced by the positive ions, are thought the same. The reactive neutral species generated by oxygen corona discharge also produced H_2O_2 in water, and

they contribute more than 76% of the total H_2O_2 production within the tested gas pressure range of 200 to 760 Torr. The production of H_2O_2 in water by reactive neutral species generated by oxygen corona discharge was mainly from three pathways: 1) the H_2O_2 produced in gas phase was transported into water; 2) the HO_2 produced in gas phase was transported into water and self-react to produce H_2O_2 in water; 3) H_2O_2 and HO_2 produced by oxygen atoms (O) reacting with water vapour at interface, and then they were transported into water. The oxygen atoms (O) can recombine on the mesh surface, thereby the production of hydrogen peroxide by oxygen atoms was reduced by the mesh. However, due to the presence of multiple reactive species, the lifetime of the reactive neutral species, including oxygen atom, is estimated less than 1.4 seconds.

Compared to the nitrogen corona discharge, the oxygen corona discharge has higher Faraday efficiency and energy yield of hydrogen peroxide production. The highest value was obtained at 200 Torr, with a Faraday efficiency of 1.0 and an energy yield of 0.260 g/kWh. In oxygen corona discharge, the OH scavenger, TB and DMSO, did not reduce the hydrogen peroxide production, proved that H_2O_2 was not from the dimerization of OH.

Corona discharge in oxygen resulted in a slight decrease in pH and a slight increase in conductivity of water. Both positive ions and reactive neutral species contributed to the change of water pH and conductivity.

The glow discharge produced positive ions with high kinetic energy, resulted in higher Faraday efficiency of H_2O_2 production, compared to the corona discharges. In glow discharge, the order of Faraday efficiency of H_2O_2 production in the three gases was: nitrogen > helium > oxygen. The highest Faraday efficiency of H_2O_2 production in deionized water were: 1.39 in nitrogen glow discharge, 0.92 in oxygen glow discharge and 1.17 in helium glow discharge. Compared to corona discharges, glow discharge led to higher energy

yield of H_2O_2 production due to the higher Faraday efficiency and lower discharge voltage. The highest energy yield of H_2O_2 production were 2.33 g/kWh in nitrogen glow discharge, 0.41 g/kWh in oxygen glow discharge and 1.24 g/kWh in helium glow discharge. The kinetic energy of the positive ions reaching water contributed to the production of H_2O_2.

Among the three gases, only nitrogen glow discharge significantly decreased the pH and increased the conductivity of water. The obtained lowest pH was 3.54, and the obtained highest conductivity was 250.0 μS/cm, obtained at 760 Torr. The change of water pH and conductivity was due to the transportation of NO_x into the solution, which formed nitrate and nitrate.

The addition of TB and DMSO significantly reduced the H_2O_2 production in nitrogen and helium glow discharge, but not in oxygen glow discharge, indicating that OH was the precursor of the H_2O_2 in nitrogen and helium glow discharge. While in oxygen glow discharge, the production of H_2O_2 did not come from the dimerization of OH.

7.2 Future work

For further investigation of the interface reactions between plasma and water, there are several suggestions.

Firstly, the presence of more chemical components in aqueous phase should be tested for. In this research, only H_2O_2 production and HNO_x were measured in aqueous phase. Although the discharges in helium and oxygen do not introduce other chemical elements in water, the production of HO_2 should be measured as well in future to understand the aqueous reaction process. The chemical components in the treated TB and DMSO solutions should be clarified and measured. The technique of high-performance liquid chromatography and isotopic labelling can be employed to analyse the treated TB and DMSO

solutions. This information will identify and quantify the products produced by reactive neutral species and drift positive ions in the solution, and further determine the interface reaction mechanisms.

Secondly, the gas composition in the reactor should be analysed by optical emission spectroscopy. The components such as ions, atoms, molecules and radicals in the gas can be identified and quantified. This can help determine the ions and reactive neutral species in the gas phase, which will help in analysing the gas phase reactions and interface reactions. In addition to H_2O_2, the positive ions can produce H_2 and O_2 in the interface reactions. Quantifying the production of H_2 and O_2 would help in determining the electrochemical process at ion anode and water cathode.

Thirdly, the glow discharges can be analysed by optical emission spectroscopy. The production of H_2 and O_2 should be quantified, which can help determine the interface reactions caused by kinetic positive ions.

Finally the effect of arc discharge with water cathode should be investigated. According to this research, 1 mol of positive ions generated by glow discharge can produced up to 1.39 mol of hydrogen peroxide molecules. If the discharge voltage can be reduced to tens of volts, the energy yield of OH would be promoted significantly. Therefore, an arc discharge with low discharge voltage can possibly increase the OH production.

8. Published Paper

Zhang, Z., Wilson, M. P., MacGregor, S. J., Timoshkin, I. V., Given, M. J., Wang, T., 2020. Interface reactions between water and ionic wind generated by d.c. corona discharge in nitrogen., Plasma Sources Sci. Technol., 29, 095022

9. Appendix

Table 9.1 Specifications of Alicat mass flow controllers.

Model	Range	Resolution	Accuracy
ALICAT (MCS Series)	0-10 slpm	0.01slpm	±0.8% of reading or ±0.2% of Full scale
ALICAT (MC Series)	0-5 slpm	0.001 slpm	
ALICAT (MC Series)	0-500 sccm	0.1 sccm	

Table 9.2 Alicat pressure controller specifications.

Model	Range	Resolution	Accuracy
ALICAT (PC Series)	0-760 Torr absolute	1 Torr	±0.25%

Table 9.3 Ozone analyser specifications.

Model	Range	Resolution	Accuracy
BMT 964	0-10000 ppm	1 ppm	0.4% of measurement + 0.1% of scale

Table 9.4 Glassman d.c. power supply specifications.

Model	Polarity	Output voltage	Output current	Max stored energy	Voltage accuracy
EJ20R30	Positive	0-20 kV	0-30 mA	19 Joule	0.5% of setting + 0.2% of rated

Table 9.5 "Tektronix P6015A" HV probe specifications.

Maximum input voltage	d.c. Attenuation	Input resistance	Input capacitance	Rise time	Bandwidth
20 kV d.c. & 40 kV pulse	1000:1	100 MΩ	3 pF	4 ns	75 MHz

Table 9.6 Specifications of coaxial cable RG405.

Probe model	Input resistance	Input capacitance	Maximum operating voltage	Maximum operating frequency
Coaxial cable RG405	50 ±1.5Ω	95.1 pF/m	1500Vrms	20 GHz

Table 9.7 Specifications of Teledyne LeCroy PP008 probe.

Probe model	d.c. Attenuation	Input resistance	Input capacitance	Maximum operating voltage
Teledyne LeCroy PP008	10:1	10 MΩ	9.5pF	$400V_{pp}$ or $300V_{rms}$

Table 9.8 Teledyne LeCroy Waverunner 610Zi Specifications.

Analog Bandwidth @ 1 MΩ (-3 dB)	500 MHz
Analog Bandwidth @ 50 Ω (-3 dB)	1 GHz (≥ 2 mV/div)
Rise Time (10–90%, 50 Ω)	375 ps (typical)
Input Impedance	50 Ω ±2% or 1 MΩ || 17pF, 10 MΩ || 9.5 pF with supplied Probe
Input Coupling	1 MΩ: AC, DC, GND; 50 Ω: DC, GND
Maximum Input Voltage	50 Ω: 5 Vrms ±10 V peak 1 MΩ: 400 V max. (DC + peak AC < 10 kHz)
Single-Shot Sample Rate/Ch	10 GS/s on 4 Ch 20 GS/s on 2 Ch
Time/Division Range	20 ps/div - 1.6 ks/div with standard memory

Table 9.9 Specifications of employed Gilson pipettes.

Model	Part Number	Volume	Systematic error	Random error
P200	F123601	200 µL	± 1.60 µL	≤ 0.30 µL
P1000	F123602	1000 µL	± 8.0 µL	≤ 1.5 µL
P5000	F123603	5000 µL	± 30 µL	≤ 8 µL

Table 9.10 Characteristics of water from Milli-Q Integral 15 Water Purification System.

Resistivity	18.2 MΩ.cm@25°C
TOC	< 5 ppb
Particulates (> 0.22 Pm)	< 1 Particulates/mL
Bacteria	< 1 cfu/mL
Pyrogens	< 0.001 Eu/mL
RNases	< 0.01 ng/mL
DNases	< 4 pg/µL
Flow Rate	0.05 - 2 L/min

Table 9.11 Specifications of Thermo scientific evolution UV-Visible 201.

Accuracy (Photometric)	0.5: ±0.0004; 1: ±0.006; 2: ±0.010;
Beam Geometry	Double beam
Detector Type	Dual Silicon Photodiodes
Lamp	Xenon Flash Lamp
Noise	0A: <0.00015A 1A: <0.00025A 2A: <0.00080A
Repeatability	±0.0002A
Wavelength Range	190 to 1100 nm
Wavelength Accuracy	±0.8nm (full range)
Min. Data Interval	1 nm

Table 9.12 pH meter specifications.

Operating temperature (ambient)	Range	Accuracy	Resolution
5-45 ℃	-2 to 16	±0.002 pH	0.01

Table 9.13 Conductivity meter specifications.

Operating temperature (ambient)	Range	Accuracy	Resolution
5-45 ℃	0.001 µS/cm to 3000 mS/cm	0.5% of reading ±1 digit > 3 µS; 0.5% of reading ±0.01 µS ≤ 3 µS	0.001 µS minimum, auto ranging up to 4 significant digits

10. Reference

1. Glaze, W., Kang, J. W., Chapin, D. H., 1987. The Chemistry of Water Treatment Processes Involving Ozone, Hydrogen Peroxide and Ultraviolet Radiation. Ozone-Sci. Eng., 9, 335-352
2. Misra, N. N., 2015. The contribution of non-thermal and advanced oxidation technologies towards dissipation of pesticide residues. Trends Food Sci. Technol., 45, 229-244
3. Foster, J. E., 2017. Plasma-based water purification: Challenges and prospects for the future. Phys. Plasmas, 24, 055501
4. Bruggeman, P. J. et al., 2016. Plasma–liquid interactions: a review and roadmap. Plasma Sources Sci. Technol. 25, 053002
5. Oturan, M. A., Aaron, J. J., 2014. Advanced oxidation processes in water/wastewater treatment: Principles and applications. A review. Crit. Rev. Environ. Sci. Technol., 44 , 2577-2641
6. Buxton, G. V., Greenstock, C. L., Helman, W. P., Ross, A. B., 1988. Critical Review of rate constants for reactions of hydrated electrons, hydrogen atoms and hydroxyl radicals ($\cdot OH/\cdot O^-$) in Aqueous Solution. J. Phys. Chem. Ref. Data, 17, 513-886
7. Andreozzi, R., 1999. Advanced Oxidation Processes (AOP) for Water Purification and Recovery. Catalysis Today. 53 (1), 51-59
8. Suty, H. , De Traversay, C., Cost, M., 2004. Applications of advanced oxidation processes: Present and future. Water Sci. Technol., 49, 227-233
9. Wang, J., 2012. Advanced Oxidation Processes for Wastewater Treatment: Formation of Hydroxyl Radical and Application. Critical Reviews in Environ. Sci. and Technol., 42 (3), 251-325
10. Chong, M. N., Sharma, A. K., Burn, S., Saint, C. P., 2012. Feasibility study on the application of advanced oxidation technologies for decentralised wastewater treatment. J. Clean. Prod., 35, 230-238

11. Munter, R., 2001. Advanced Oxidation Processes-Current Status and Prospects. Proc. Estonian Acad. Sci. Chem. 50 (2), 59-80
12. Miklos, D.B., Remy, C., Jekel, M., Linden, K.G., Drewes, J.E., Hubner, U., 2018. Evaluation of advanced oxidation processes for water and wastewater treatment – A critical review. Water Res., 139, 118-131
13. Bruggeman, P., Leys, C., 2009. Non-thermal plasmas in and in contact with liquids. J. Phys. D: Appl. Phys. 42, 053001
14. Korobeinikov, S., Melekhov, A. V., Besov, A. S., 2002. Breakdown initiation in water with the aid of bubbles. High Temp., 40, 652-659
15. Naidis, G. V., 2014. Production of active species in cold helium—air plasma jets., Plasma Source Sci. Technol., 23, 065014
16. Akishev, Y., Aponin, G., Grushin, M., Karalnik, V., Petryakov, A., Trushkin, N, 2008. Self-running low-frequency pulsed regime of DC electric discharge in gas bubble immersed in a liquid., J. Optoelectr. Adv. Maert., 10, 1917-1921
17. Xiong, Q. , Yang, Z., Bruggeman, P. J., 2015. Absolute OH density measurements in an atmospheric pressure dc glow discharge in air with water electrode by broadband UV absorption spectroscopy., J. Phys. D: Appl. Phys. 48, 424008
18. Burlica, R., Shih, K. Y., Locke, B. R., 2010. Formation of H_2 and H_2O_2 in a Water-Spray Gliding Arc Nonthermal Plasma Reactor., Ind. Eng. Chem. Res., 49, 6342-6349
19. Tachibana, K., Takekata, Y., Mizumoto, Y., Motomura, H., Jinno, M., 2011. Analysis of a pulsed discharge within single bubbles in water under synchronized conditions., Plasma Source Sci. Technol., 20, 034005
20. Bruggeman, P., Verreycken, T., Gonzalez, M. A., Walsh, J. L., Kong, M. G., Leys, C., Schram, D., 2010. Optical emission spectroscopy as a diagnostic for plasmas in liquids: opportunities and pitfalls., J. Phys. D: Appl. Phys., 43, 124005

21. Miichi, T., Hayashi, N., Ihara, S., Satoh, S., Yamabe, C., 2002. Generation of Radicals using Discharge inside Bubbles in Water for Water Treatment., Ozone: Sci. Eng., 24, 471-477
22. Sano, N., Kawashima, T., Fujikawa, J., Fujimoto, T., Kitai, T., Kanki, T., 2002. Decomposition of Organic Compounds in Water by Direct Contact of Gas Corona Discharge: Influence of Discharge Conditions. Ind. Eng. Chem. Res. 41, 5906-5911
23. Magureanu, M., Bradu, C., Piroi, D., Mandache, N. B., Parvulescu, V., 2013. Pulsed Corona Discharge for Degradation of Methylene Blue in Water., Plasma Chem. Plasma P., 33, 51-64
24. Hoeben, W. F. L. M., van Veldhuizen, E. M., Rutgers, W. R., Kroesen, G. M. W., 1999. Gas-Phase Corona Discharges for Oxidation of Phenol in an Aqueous Solution. J. Phys. D: Appl. Phys. 32, L133-L137
25. Malik, M.A., Ghaffar, A., Malik, S.A., 2001. Water purification by electrical discharges. Plasma Sources Sci. Technol., 10, 82-91
26. Kirkpatrick, M.J., Locke, B.R., 2005. Hydrogen, Oxygen, and Hydrogen Peroxide Formation in Aqueous Phase Pulsed Corona Electrical Discharge. Ind. Eng. Chem. Res., 44, 4243-4248
27. Akiyama, H., 2000. Streamer Discharges in Liquids and their Applications. IEEE Trans. Dielectr. Electr. Insul., 7, 646-653
28. Sun, B., Sato, M., Clements, J. M., 1997. Optical study of active species produced by a pulsed streamer corona discharge in water. J. Electrostat. 39, 189-202
29. Grymonpré, D. R., Sharma, A. K., Finney, W. C., Locke, B. R., 2001. The role of Fenton's reaction in aqueous phase pulsed streamer corona reactors., Chem. Eng. J., 82, 189-207
30. Mizuno, T., Akimoto, T., Azumi, K., Ohmori, T., Aoki, Y., Takahashi, A., 2005. Hydrogen evolution by plasma electrolysis in aqueous solution. Jpn. J. Appl. Phys., 44, 396-401

31. Yan, Z., Chen, L., Wang, H., 2009. Hydrogen generation by glow discharge plasma electrolysis of methanol solutions., Int. J. Hydrog. Energy, 34, 48-55
32. Bullock, A.T., Gavin, D.L., Ingram, M.D., 1980. Electron spin resonance detection of spin-trapped radicals formed during the glow-discharge electrolysis of aqueous solutions., J. Chem. Soc. Faraday. Trans, 76, 648-653
33. Liu, Y., Sun, B., Wang, L., Wang, D., 2012. Characteristics of Light Emission and Radicals Formed by Contact Glow Discharge Electrolysis of an Aqueous Solution., Plasma. Chem. Plasma. P., 32, 359-368
34. Mezei, P., Cserfalvi, T., 2007. Electrolyte Cathode Atmospheric Glow Discharges for Direct Solution Analysis., Appl. Spectrosc. Rev., 42, 573-604
35. Lu, X., Laroussi, M., 2005. Atmospheric Pressure Glow Discharge in Air Using a Water Electrode., IEEE. Trans. Plasma Sci., 33, 272-273
36. Cserfalvi, T., Mezei, P., 1996. Operating mechanism of the electrolyte cathode atmospheric glow discharge., Fresenius. J. Anal. Chem., 355, 813-819
37. Hart, E. J., Anbar, M., 1970. The hydrated electron, p 63. Wiley, New York
38. Verreycken, T., Schram, D. C., Leys, C., Bruggeman, P., 2010. Spectroscopic study of an atmospheric pressure dc glow discharge with a water electrode in atomic and molecular gases., Plasma. Sources. Sci. Technol., 19, 045004
39. Malik, M. A., 2010. Water Purification by Plasmas: Which Reactors are Most Energy Efficient? Plasma. Chem. Plasma. Process., 30, 21-31
40. Sugama, C., Tochikubo, F., Uchida, S., 2006. Glow Discharge Formation over Water Surface at Saturated Water Vapor Pressure and Its Application to Wastewater Treatment. Jpn. J. Appl. Phys., 45, 8858

41. Gao, J., Yu, J., Lu, Q., Yang, W., Li, Y., Pu, L., 2004. Plasma degradation of 1-naphthylamine by glow discharge electrolysis. Pakistan. J. Biol. Sci., 7, 1715-1720
42. Gupta, S. K. S., 2015. Contact glow discharge electrolysis: its origin, plasma diagnostics and non-faradaic chemical effects. Plasma Sources Sci. Technol., 24, 063001
43. Meichsner, J., 2012. Nonthermal Plasma Chemistry and Physics. Boca Raton: CRC Press
44. Fridman, A., Nester, S., Kennedy, L. A., Saveliev, A., Yardimci, O. M., 1998. Gliding arc gas discharge. Prog. Energy Combust. Sci., 25, 211-231
45. Burlica, R., Kirkpatrick, M. J., Locke, B. R., 2006. Formation of reactive species in gliding arc discharges with liquid water. J Electrostat., 64, 35-43
46. Du, C. M., Shi, T. H., Sun, Y. W., Zhuang, X. F., 2007. Decolorization of Acid Orange 7 solution by gas–liquid gliding arc discharge plasma. J. Hazard. Mater., 154, 1192-1197
47. Patrick Vanraes, Anton Y. Nikiforov and Christophe Leys (April 20th 2016). Electrical Discharge in Water Treatment Technology for Micropollutant Decomposition, Plasma Science and Technology - Progress in Physical States and Chemical Reactions, Tetsu Mieno, IntechOpen, DOI: 10.5772/61830. Available from: https://www.intechopen.com/books/plasma-science-and-technology-progress-in-physical-states-and-chemical-reactions/electrical-discharge-in-water-treatment-technology-for-micropollutant-decomposition
48. Burlica, R., Locke, B. R., 2008. Pulsed Plasma Gliding-Arc Discharges with Water Spray. IEEE Trans. Ind. Appl., 44, 482-489
49. Xu, X., 2001. Dielectric barrier discharge properties and applications., Thin Solid Films, 390, 237-242
50. Laurita, R., Barbieri, D., Gherardi, M., Colombo, V., Lukes, P., 2015.

Chemical analysis of reactive species and antimicrobial activity of water treated by nanosecond pulsed DBD air plasma., Clin. Plasma. Med., 3, 53-61

51. Huang, F., Li, C., Wang H., Ya, Z., 2010. Analysis of the degradation mechanism of methylene blue by atmospheric pressure dielectric barrier discharge plasma., Chem. Eng. J., 250-256
52. Zhang, Y., Zhou, M., Hao, X., Lei, L., 2007. Degradation mechanisms of 4-chlorophenol in a novel gas–liquid hybrid discharge reactor by pulsed high voltage system with oxygen or nitrogen bubbling., Chemosphere, 67, 702-711
53. Locke, B. R., Shih, K. Y., 2011. Review of the methods to form hydrogen peroxide in electrical discharge plasma with liquid water., Plasma Sources Sci. Technol., 20, 034006
54. Parvulescu, V. I., Magureanu, M., Lukes, P., 2012. Plasma Chemistry and Catalysis in Gases and Liquids. Boschstr, Weinheim: Wiley-VCH Verlag & Co. KGaA
55. Rumbach, P., Go, D. B., 2017. Perspectives on Plasmas in Contact with Liquids for Chemical Processing and Materials Synthesis. Top Catal., 60, 799-811
56. Good, A., Durden, D. A., Kebarle, P., 1970. Ion–Molecule Reactions in Pure Nitrogen and Nitrogen Containing Traces of Water at Total Pressures 0.5–4 Torr. Kinetics of Clustering Reactions Forming $H^+(H_2O)_n$. J. Chem. Phys., 52, 212-221
57. Herron, J. T., Green, D. S., 2001. Chemical Kinetics Database and Predictive Schemes for Nonthermal Humid Air Plasma Chemistry. Part II. Neutral Species Reactions., Plasma Chem. Plasma Process., 21, 459-81
58. Lukes, P., Dolezalova, E., Sisrova, I., Clupek, M., 2014. Aqueous-phase chemistry and bactericidal effects from an air discharge plasma in contact with water: evidence for the formation of peroxynitrite through a pseudo-

second-order post-discharge reaction of H_2O_2 and HNO_2., Plasma Sources Sci. Technol., 23, 015019

59. Oehmigen, K., Winter, J., Hahnel, M., Wilke, C., Brandenburg, R., Weltmann, K. D., von Woedtke, T., 2011. Estimation of Possible Mechanisms of Escherichia coli Inactivation by Plasma Treated Sodium Chloride Solution., Plasma. Process. Polym., 8, 904-913
60. Brisset, J. L., Hnatiuc, E., 2012. Peroxynitrite: A Re-examination of the Chemical Properties of Non-thermal Discharges Burning in Air Over Aqueous Solutions., Plasma. Chem. Plasma. Process. 32, 655-674
61. Frein, D., Schildknecht, S, Bachschmid, M., Ullrich, V., 2005. Redox regulation: a new challenge for pharmacology., Biochem. Pharmacol., 70, 1-13
62. Pacher, P., Beckman, J. S., Liaudet, L., 2007. Nitric oxide and peroxynitrite in health and disease., Physiol. Rev., 87, 315-424
63. Goldstein, S., Lind, J., Merenyi, G., 2005. Chemistry of Peroxynitrites as Compared to Peroxynitrates., Chem. Rev., 105, 2457-2470
64. Lias, S. G., NIST Chemistry WebBook, NIST Standard Reference Database Number 69, National Institute of Standards and Technology, Gaithersburg (MD), http://webbook.nist.gov (accessed on Oct. 14, 2019)
65. Good, A., Durden, D. A., Kebarle, P., 1970. Mechanism and Rate Constants of Ion–Molecule Reactions Leading to Formation of $H^+(H_2O)_n$ in Moist Oxygen and Air. J. Chem. Phys., 52, 222-229
66. Staehelin, J., Hoigne, J., 1982. Decomposition of ozone in water: rate of initiation by hydroxide ions and hydrogen peroxide., Environ. Sci. Technol., 16, 676–681
67. Hoigne, J., Bader, H., Haag, W. R., Staehelin, J., 1985. Rate constants of reactions of ozone with organic and inorganic compounds in water—III. Inorganic compounds and radicals. Water. Res., 19, 993-1004
68. Lindinger, W., 1973. Reaction-Rate Constants in Steady-State Hollow-

Cathode Discharges: Ar + H_2O Reactions., Phys. Rev. A, 7, 328-333

69. Lee, C., Lieberman, M. A., 1995. Global model of Ar, O_2, Cl_2, and Ar/O_2 high-density plasma discharges., J. Vac. Sci. Technol. A, 13, 368-380
70. Ikezoe, Y., Matsuoka, S., Takebe, M., Viggiano, A., 2007. Gas Phase Ion–Molecule Reaction Rate Constants Through 1986 (Ion Reaction Research Group Society of Japan)
71. Ricard, A., Decomps, Ph., Massines, F., 1999. Kinetics of radiative species in helium pulsed discharge at atmospheric pressure., Surface Coat. Technol., 112, 1-4
72. Sanders, R. A., Muschlitz Jr, E. E., 1977. Chemiionization and secondary ion reactions in H_2O and D_2O., Int. J. Mass Spectrosc. Ion Phys., 23, 99-108
73. Miller, T. J., Farquhar, P. R. A., Willacy, K., 1997. The UMIST Database for Astrochemistry 1995. Astron. Astrophys. Suppl. Ser. 121, 139-185
74. Itikawa, Y., Mason, N., 2005. Cross Sections for Electron Collisions with Water Molecules., J. Phys. Chem. Ref. Data, 34, 1–22
75. Gao, J., Wang, X., Hu, Z., Deng, H., Hou, J., Lu, X., Kang, J., 2003. Plasma degradation of dyes in water with contact glow discharge electrolysis., Water Res., 37, 267-272
76. Hickling, A., News, G. R., 1961. Glow-discharge electrolysis. Part V. The contact glow-discharge electrolysis of liquid ammonia., J. Chem. Soc., 5186-5191
77. Gorbanev, Y., O'Connell, D., Chechik, V., 2016. Non-Thermal Plasma in Contact with Water: The Origin of Species., Chem. Eur. J., 22, 3496-3505
78. Latimer, W.M., 1952. Oxidation Potentials (2nd ed.), Prentice-Hall, New York, United States
79. Bruggeman, P., Schram, D. C., 2010. On OH production in water containing atmospheric pressure plasmas. Plasma Sources Sci. Technol.,

19, 045025

80. Spyrou, N., Held, B., Peyrous, R., Manassis, Ch., Pignolet, P., 1992. Gas temperature in a secondary streamer discharge: an approach to the electric wind., J. Phys. D: Appl. Phys., 25, 211-216
81. Liu, N., Celestin, S., Bourdon, A., Pasko, V. P., 2007. Application of photoionization models based on radiative transfer and the Helmholtz equations to studies of streamers in weak electric fields., Appl. Phys. Lett., 91, 211501
82. van der Mullen, J. J. A. M., van de Sande, M. J., de Vries, N., Broks, B., Iordanova, E., Gamero, A., Torres, J., Sola, A., 2007. Single-shot Thomson scattering on argon plasmas created by the Microwave Plasma Torch; evidence for a new plasma class., Spectrochim. Acta B, 62, 1135-1146
83. Fridman, A., 2008. Plasma Chemistry. Cambridge: Cambridge University Press
84. Balcon, N., Aanesland, A., Boswell, R., 2007. Pulsed RF discharges, glow and filamentary mode at atmospheric pressure in argon., Plasma Sources Sci. Technol., 16, 217-225
85. Dong, L., Qi, Y., Zhao, Z., Li, Y., 2008. Electron density of an individual microdischarge channel in patterns in a dielectric barrier discharge at atmospheric pressure., Plasma Sources Sci. Technol., 17, 015015
86. Zhu, X. M., Pu, Y. K., Balcon, N., Boswell, R., 2009. Measurement of the electron density in atmospheric-pressure low-temperature argon discharges by line-ratio method of optical emission spectroscopy. J. Phys. D: Appl. Phys., 42, 142003
87. Staack, D., Farouk, B., Gutsol, A., Fridman, A., 2008. DC Normal Glow Discharges in Atmospheric Pressure Atomic and Molecular Gases. Plasma. Sources. Sci. Technol. 17, 025013
88. Buuron, A. J. M., Otorbaev, D. K., van der Sanden, M. C. M., Schram, D.

C., 1994. Absorption spectroscopy on the argon first excited state in an expanding thermal arc plasma., Phys. Rev. E, 50, 1383-1393

89. Dilecce, G., Ambrico, P. F., Simek, M., De Benedictis, S., 2012. OH density measurement by time-resolved broad band absorption spectroscopy in an Ar–H2O dielectric barrier discharge., J. Phys. D: Appl. Phys., 45, 125203
90. Nakagawa, Y., Ono, R., Oda, T., 2011. Density and temperature measurement of OH radicals in atmospheric-pressure pulsed corona discharge in humid air., J. Appl. Phys., 110, 073304
91. Ouaras, K., Magne, L., Pasquiers, S., Tardiveau, P., Jeanney, P., Bournonville, B., 2018. OH density measured by PLIF in a nanosecond atmospheric pressure diffuse discharge in humid air under steep high voltage pulses., Plasma Sources Sci. Technol. 27, 045002
92. Du, Y., Nayak, G., Oinuma, G., Ding, Y., Peng, Z., Bruggeman, P. J., 2017. Emission considering self-absorption of OH to simultaneously obtain the OH density and gas temperature: validation, non-equilibrium effects and limitations., Plasma Sources Sci. Technol., 26, 095007
93. Liu, Z. W., Yang, X. F., Zhu, A. M., Zhao, G. L., Xu, Y., 2008. Determination of the OH radical in atmospheric pressure dielectric barrier discharge plasmas using near infrared cavity ring-down spectroscopy., Eur. Phys. J. D, 48, 365-373
94. Fuh, C. A., Clark, S. M., Wu, W., Wang, C., 2016. Electronic ground state OH(X) radical in a low-temperature atmospheric pressure plasma jet., J. Appl. Phys., 120, 163303
95. Chen, Z., Liu, D., Chen, C., Xu, D., Liu, Z., Xia, W., Rong, M., Kong, M. G., 2.18. Analysis of the production mechanism of H_2O_2 in water treated by helium DC plasma jets., J. Phys. D: Appl. Phys., 51, 325201
96. Hsieh, K. C., Wang, H., Locke, B. R., 2016. Analysis of Electrical Discharge Plasma in a Gas-Liquid Flow Reactor Using Optical Emission

Spectroscopy and the Formation of Hydrogen Peroxide., Plasma Process. Polym., 13, 908-917

97. Benstaali, B., Boubert, P., Cheron, B. G., Addou, A., Brisset, J. L., 2002. Density and Rotational Temperature Measurements of the OH° and NO° Radicals Produced by a Gliding Arc in Humid Air. Plasma Chem. Plasma Proc., 22, 553-571
98. Ono, R., Oda, T., 2001. OH radical measurement in a pulsed arc discharge plasma observed by a LIF method., IEEE Trans. Ind. Appl., 37, 709-714
99. Srivastava, N., Wang, C., Dibble, T. S., 2009. A study of OH radicals in an atmospheric AC discharge plasma using near infrared diode laser cavity ringdown spectroscopy combined with optical emission spectroscopy., Eur. Phys. J. D, 54, 77-86
100. Machala, Z., Janda, M., Hensel, K., Jedlovsky, I., Lestinska, L., Foltin, V., Martisovits, V., Morova, M., 2007. Emission Spectroscopy of Atmospheric Pressure Plasmas for Bio-medical and Environmental Applications. J. Molec. Spectrosc., 243,194-201
101. Hibert, C., Gaurand, I., Mortret, O., Pouvesle, J. M., 1999. [OH(X)] measurements by resonant absorption spectroscopy in a pulsed dielectric barrier discharge., J. Appl. Phys., 85, 7070-7075
102. Ono, R., Oda, T., 2003. Dynamics of ozone and OH radicals generated by pulsed corona discharge in humid-air flow reactor measured by laser spectroscopy., J. Appl. Phys. 93, 5876-5882
103. Bruggeman, P., Liu, J., Degroote, J., Kong, M. G., Vierendeels, J., Leys, C., 2008. Dc excited glow discharges in atmospheric pressure air in pin-to-water electrode systems., J. Phys. D: Appl. Phys., 41, 215201
104. Bruggeman, P., Ribezl, E., Maslani, A., Degroote, J., Malesevic, A., Rego, R., Vierendeels, J., Leys, C., 2008. Characteristics of atmospheric pressure air discharges with a liquid cathode and a metal anode. Plasma Sources Sci. Technol., 17, 025012

105. Wang, C., Srivastava, N., Dibble, T. S., 2010. Observation and quantification of OH radicals in the far downstream part of an atmospheric microwave plasma jet using cavity ringdown spectroscopy., Appl. Phys. Lett., 95, 051501
106. Wang, C., Srivastava, N., Scherrer, S., Jang, P. R., Dibble, T. S., Duan, Y., 2009. Optical diagnostics of a low power-low gas flow rates atmospheric-pressure argon plasma created by a microwave plasma torch., Plasma Sources Sci. Technol., 18, 025030
107. Kanazawa, S., Furuki, T., Nakaji, T., Akamine, S., Ichiki, R., 2012. Measurement of OH Radicals in Aqueous Solution Produced by Atmospheric-pressure LF Plasma Jet., Int. J. Environ. Sci. Technol., 6, 166-171
108. Kanazawa, S., Kawano, H., Watanabe, S., Furuki, T., Akamine, S., Ichiki, R., Ohkubo, T., Kocik, M., Mizeraczyk, J., 2011. Observation of OH radicals produced by pulsed discharges on the surface of a liquid., Plasma Sources Sci. Technol., 20, 034010
109. Sahni, M., Locke, B. R., 2006. Quantification of Hydroxyl Radicals Produced in Aqueous Phase Pulsed Electrical Discharge Reactors., Ind. Eng. Chem. Res., 45, 5819-5825
110. Hsieh, K. C., Wandell, R. J., Bresch, S., Locke, B. R., 2017. Analysis of hydroxyl radical formation in a gas-liquid electrical discharge plasma reactor utilizing liquid and gaseous radical scavengers., Plasma Processes Polym., 14, 1600171
111. Yang, Y., Cho, Y. I., Fridman, A., 2012. Plasma Discharge in Liquid: Water Treatment and Applications. Boca Raton, Florida: CRC Press
112. Knochel, P., Molander, G. A., 2014. Comprehensive Organic Synthesis. 2nd ed. Oxford: NEWNES
113. Drougui, P., Elmaleh, S., Rumeau, M., Bernard, C., Rambaud, A., 2000. Hydrogen peroxide production by water electrolysis: Application to

disinfection., J. Appl. Electrochem., 31, 877-882

114. Maehara, T., Nishiyama, K., Onishi, S., Mukasa, S., Toyota, H., Kuramoto, M., Nomura, S., Kawashima, A., 2010. Degradation of methylene blue by radio frequency plasmas in water under ultraviolet irradiation., J. Hazard. Mater., 174, 473-476
115. Shih, K. Y., Locke, B. R., 2010. Chemical and Physical Characteristics of Pulsed Electrical Discharge Within Gas Bubbles in Aqueous Solutions., Plasma Chem. Plasma Process., 30, 1-20
116. Jin, X., Wang, X., Zhang, H., Ren, H., 2013. Study on the Onset of DC Diaphragm Glow Discharge. Electrochimica. Acta., 87, 336-340
117. Sengupta, S. K., Singh, R., and Srivastava, A. K., 1998. A study on non-faradaic yields of anodic contact glow discharge electrolysis using cerous ion as the OH• scavenger: An estimate of the primary yield of OH• radicals., J. Indian Chem., 37A, 558-560
118. Yamabe, C., Takeshita, F., Miichi, T., Hayashi, N., Ihara, S., 2005. Water Treatment Using Discharge on the Surface of a Bubble in Water., Plasma Process. Polym., 2, 246-251
119. Wang, H. J., Li, J., Quan, X., Wu, Y., Li, G. F., Wang, F. Z., 2007. Formation of hydrogen peroxide and degradation of phenol in synergistic system of pulsed corona discharge combined with TiO2 photocatalysis., J. Hazardous Mater., 141, 336–343
120. Wang, H. J., Li, H., Quan, M., 2006. Decoloration of azo dye by a multi-needle-to-plate high-voltage pulsed corona discharge system in water. J. Electrost., 64, 416–421
121. Aristova, N. A., Piskarev, I. M., Ivanovskii, A. V., Selemir, V. D., Spirov, G. M., Shlepkin, S. I., 2004. Initiation of chemical reactions with an electric discharge in a solid dielectric-gas-liquid system., Russ. J. Phys. Chem., 78, 1144-1148
122. Velikonja, J., Bergougnou, M. A., Castle, G. S. P., Cairns, W. L., Inculet,

I. I., 2001. Co-generation of ozone and hydrogen peroxide by dielectric barrier AC discharge in humid oxygen., Ozone Sci. Eng., 23, 467-478

123. Hickling, A., 1971. Electrochemical processes in glow discharge at the gas-solution interface. Boston: Springer
124. Jin, X., Zhang, H., Wang, X., Zhou, M. 2012. An Improved Multi-anode Contact Glow Discharge Electrolysis Reactor for Dye Discoloration. Electrochimica. Acta., 59, 474-478
125. Nemcova´, L., Nikiforov, A., Leys, C., Krcma, F., 2011. Chemical Efficiency of H_2O_2 Production and Decomposition of Organic Compounds Under Action of DC Underwater Discharge in Gas Bubbles. IEEE. Trans. Plasma. Sci., 39, 865-870
126. Lukes, P., Appleton, A. T., Locke, B. R., 2004. Hydrogen Peroxide and Ozone Formation in Hybrid Gas–Liquid Electrical Discharge Reactors., IEEE Trans. Ind. Appl., 40, 60-67
127. Koprivanac, N., Kusic, H., Vujevic, D., Peternel, I., Locke, B. R., 2005. Influence of iron on degradation of organic dyes in corona., J. Hazard Mater., B117, 113-119
128. Markovic, M., Jovic, M., Stankovic, D., Kovacevic, V., Roglic, G., Gojgic-Cvijovic, G., Manojlovic, D., 2015. Application of non-thermal plasma reactor and Fenton reaction for degradation of ibuprofen., Sci. Total Environ., 505, 1148-1155
129. Pillai, K. C., Kwon, T. O., Moon, I. S., 2009. Degradation of Wastewater from Terephthalic Acid Manufacturing Process by Ozonation Catalyzed with Fe^{2+}, H_2O_2 and UV light: Direct Versus Indirect Ozonation Reactions., J. Appl. Catal. B: Environ., 91, 319-328
130. Parsa, J. B., Negahdar, S. H., 2012. Treatment of Wastewater Containing Acid Blue 92 Dye by Advanced Ozone-based Oxidation Methods., Sep. Purif. Technol. 98, 315-320
131. Sharma, S., Buddhdev, J., Patel, M., Ruparelia, J. P., 2013. Studies on

Degradation of Reactive Red 135 Dye in Wastewater using Ozone., Procedia Eng. 51, 451-455

132. Trushkin, A. N., Grushin, M. E., Kochetov, I. V., Trushkin, N. I., Akishev, Yu. S., 2012. Decomposition of Toluene in a SteadyState Atmospheric Pressure Glow Discharge., Plasma Phys. Rep., 39, 167-182
133. Ono, R., Oda, T., 2007. Optical Diagnosis of Pulsed Streamer Discharge under Atmospheric Pressure., I. J. PEST. 1, 123-129
134. Baulch, D. L., Bowman, C. T., Cobos, C. J., Cox, R. A., Just, Th., Kerr, J. A., Pilling, M. J., Stocker, D., Troe, J., Tsang, W., Walker, R. W., Warnatz, J., 2005. Evaluated Kinetic Data for Combustion Modeling: Supplement II., J. Phys. Chem. Ref. Data, 34, 757-1397
135. Malik, M. A., Rehman, U. U., Ghaffar, A., Ahmed, K., 2002. Synergistic effect of pulsed corona discharges and ozonation on decolourization of methylene blue in water., Plasma Sources Sci. Technol., 11, 236-240
136. Machala, Z., Tarabova, B., Hensel, K., Spetlikova, E., Sikurova, L., Lukes, P. 2013. Formation of ROS and RNS in Water Electro-Sprayed through Transient Spark Discharge in Air and their Bactericidal Effects. Plasma. Process. Polym., 10, 649-659
137. Sunka, P., Babicky, V., Clupek, M., Lukes, P., Simek, M., Schmidt, J., Cernak, M., 1999., Generation of chemically active species by electrical discharges in water., Plasma Sources Sci. Technol., 8, 258-265
138. Joshi, A. A., Locke, B. R., Arce, P., Finney, W., C., 1995. Formation of hydroxyl radicals, hydrogen peroxide and aqueous electrons by pulsed streamer corona discharge in aqueous solution., J. Hazard. Mater., 41, 3-30
139. Anpilov, A. M., Barkhudarov, E. M., Bark, Y. B., Zadiraka, Y. V., Christofi, M., Kozlov, Y. N., Kossyi, I. A., Kop'ev, V. A., Silakov, V. P., Taktakishvili, M. I., Temchin, S. M., 2001. Electric discharge in water as a source of UV radiation, ozone and hydrogen peroxide. J. Phys. D:

Appl. Phys., 34, 993-999

140. Lukes, P., Clupek, M., Babicky, V., Janda, V., Sunka, P., 2005. Generation of ozone by pulsed corona discharge over water surface in hybrid gas–liquid electrical discharge reactor., J. Phys. D: Appl. Phys., 38, 409-416
141. Eliasson, B., Kogelschatz, U., 1991. Modeling and Applications of Silent Discharge Plasmas. IEEE Trans. Plasma Sci., 19, 309-23
142. Mok, Y. S., Ham, S. W., 1998. Conversion of NO to NO_2 in air by a pulsed corona discharge process., Chem. Eng. Sci., 53, 1667-1678
143. Chang, J. S., Lawless, P. A., Yamamoto, T., 1991. Corona Discharge Processes., IEEE Trans. Plasma Sci., 19, 1152-1166
144. Mukkavilli, S., Lee, C. K., Varghese, K., Tavlarides, L. L., 1988. Modeling of the electrostatic corona discharge reactor., IEEE Trans. Plasma Sci., 16, 652-660
145. Manning, T. J., 2000. Production Of Ozone in an Electrical Discharge Using Inert Gases as Catalysts., Ozone Sci. Eng., 22, 53-64
146. Manning, T. J., Hedden, J., 2001. Gas Mixtures and Ozone Production in an Electrical Discharge., Ozone Sci. Eng., 23, 95-103
147. Chen, J., Davidson, J. H., 2003. Model of the negative DC corona plasma: Comparison to the positive DC corona plasma. Plasma Chem. Plasma Process. 23, 83-102
148. Sellers, R. M., 1980. Spectrophotometric determination of hydrogen peroxide using potassium titanium (IV) oxalate. Analyst ,105, 950-954
149. Abou-Ghazala, A., Katsuki, S., Schoenbach, K. H., Dobbs, F. C., Moreira, K. R., 2002. Bacterial Decontamination of Water by Means of Pulsed-Corona Discharges. IEEE Trans. Plasma Sci. 30, 1449-1453
150. Van Heesch, E. J. M., Pemen, A. J. M., Huijbrechts, P. A. H. J., van der Laan, P. C. T., Ptasinski, K. J., Zanstra, G. J., de Jong, P., 2000. A Fast Pulsed Power Source Applied to Treatment of Conducting Liquids and Air. IEEE Trans. Plasma Sci. 28, 137-143

151. Shin, W. T., Yiacoumi, S., Tsouris, C., Dai, S., 2000. A Pulseless Corona-Discharge Process for the Oxidation of Organic Compounds in Water. Ind. Eng. Chem. Res., 39, 4408-4414
152. Shimizu, T., Iwafuchi, Y., Morfill, G. E., Sato, T., 2011. Formation of thermal flow fields and chemical transport in air and water by atmospheric plasma. New. J. Phys., 13:053025
153. 6.4 Ke, Z., Huang, Q., Zhang, H., Yu, Z. 2011. Reduction and Removal of Aqueous Cr(VI) by Glow Discharge Plasma at the Gas–Solution Interface. Environ. Sci. Technol., 45, 7841–7847
154. Magureanu, M., Piroi, D., Gherendi, F., Mandache, N.B., Parvulescu, V., 2008. Decomposition of Methylene Blue in Water by Corona Discharges. Plasma. Chem. Plasma. Process., 28, 677-688
155. ILO International Chemical Safety Cards (ICSC). Available at: http://www.ilo.org/dyn/icsc/showcard.display?p_version=2&p_card_id=0114 (Accessed: 26 November 2019).
156. ILO International Chemical Safety Cards (ICSC). Available at: http://www.ilo.org/dyn/icsc/showcard.display?p_version=2&p_card_id=0459 (Accessed: 26 November 2019).
157. Cadorin, B. M., et al., 2015. Treatment of methyl orange by nitrogen non-thermal plasma in a corona reactor: The role of reactive nitrogen species. J. Hazard. Mater. 300, 754-764
158. Takahashi, K., Satoh, K., Itoh, H., Kawaguchi, H., Timoshkin, I., Given, M., MacGregor, S., 2016. Production characteristics of reactive oxygen/nitrogen species in water using atmospheric pressure discharge plasmas. Jpn. J. Appl. Phys., 55, 15030
159. Zhang, Y., Liu, L., Chen, Y., Ouyang, J., 2015. Characteristics of ionic wind in needle-to-ring corona discharge. J. Electrostat., 74, 15-20
160. Engineering ToolBox, (2004). Water - Saturation Pressure. [online] Available at: https://www.engineeringtoolbox.com/water-vapor-

saturation-pressure-d_599.html [27 DEC. 2018].

161. Davies, R. A., Hickling, A., 1952. Glow-discharge Electrolysis. Part I. The Anodic Formation of Hydrogen Peroxide in Inert Electrolytes. J. Chem. Soc., 0, 3595-3602
162. Liang, W.J., Lin, T. H., 1994. The Characteristics of Ionic Wind and Its Effect on Electrostatic Precipitators. Aerosol. Sci. Technol., 20, 330-344
163. Wilson, J., Perkins, H. D., Thompson, W. K., 2009. An Investigation of Ionic Wind Propulsion. NASA Report, NASA/TM 2009-215822
164. Marselli, B., Garcia-Gomez, J., Michaud, P.-A., Rodrigo, M. A., Comninellis, Ch., 2003. Electrogeneration of Hydroxyl Radicals on Boron-Doped Diamond Electrodes. J. Electrochem. Soc., 150, D79-D83
165. Comninellis, C., 1994. Electrocatalysis in the Electrochemical Conversion/Combustion of Organic Pollutants for Waste Water Treatment. Electrochem. Acta, 39,1857-1862
166. Martı´nez-Huitle, C. A., Ferro, S. 2006. Electrochemical oxidation of organic pollutants for the wastewater treatment: direct and indirect processes. Chem. Soc. Rev., 35(12), 1324-1340
167. Zhao, Y., Wang, T., Wilson, M.P., MacGregor, S.J., Timoshkin, I.V., Ren, Q.C., 2016. Hydroxyl radicals and hydrogen peroxide formation at nonthermal plasma-water interface. IEEE T. Plasma Sci., 44, 2084-2091
168. Wang, W., Wang, S., Liu, F., Zheng, W., Wang, D., 2006. Optical study of OH radical in a wire-plate pulsed corona discharge. Spectrochimica. Acta., Part A, 63, 477-482
169. Zheng, S., Zhang, L., Liu, Y., Wang, W., Wang, X., 2008. Modeling of the production of OH and O radicals in a positive pulsed corona discharge plasma. Vacuum. 83, 238-243
170. Lichten, W., 1957. Lifetime Measurements of Metastable States in Molecular Nitrogen. J. Chem. Phys. 26, 306-313
171. Davies, R. A., Hickling, A., 1952. Glow-discharge Electrolysis. Part I. The

Anodic Formation of Hydrogen Peroxide in Inert Electrolytes. J. Chem. Soc., 0, 3595-3602

172. Lieberman, L.A., Lichtenberg, A.J., 2005. Principles of Plasma Discharges and Materials Processing. 2nd ed. Hoboken, New Jersey: John Wiley & Sons, Inc.
173. Christensen, H., Sehested, K., 1988. HO_2 and O_2^- Radicals at Elevated Temperature. J. Phys. Chem. 92, 3007-3011
174. Bielski, B.H.J., Cabelli, D.E., Arudi, R.L., Ross, A.B., 1985. Reactivity of HO_2/O_2^- radicals in aqueous solution. J. Phys. Chem. Ref. Data., 14, 1041-1100
175. Sarathy, S.M., Vranckx, S., Yasunaga, K., Mehl, M., Osswald, P., Metcalfe, W.K., Westbrook, C.K., Pitz, W.J., Kohse-Hoinghaus, K., Fernandes, R.X., Curran, H.J., 2012. A Comprehensive Chemical Kinetic Combustion Model for the Four Butanol Isomers. Combust. Flame, 159, 2028-2055
176. Lee, L.C., Slanger, T.G., 1979. Atmospheric OH Production - The $O(^1D)$ + H_2O Reaction Rate. Geophys. Res. Lett., 6, 165-166
177. Klaening, U.K., Sehested, K., Wolff, T., 1984. Ozone Formation in Laser Flash Photolysis of Oxoacids and Oxoanions of Chlorine and Bromine. J. Chem. Soc., Faraday Trans. 1, 80, 2969-2979
178. Pope, F. D., Nicovich, J. M., Wine, P. H., 2002. A Temperature-Dependent Kinetics Study of the Reaction of $O(^3P_J)$ with $(CH_3)_2SO$. Int. J. Chem. Kinet., 34, 156–161
179. Ledakowicz, S., Miller, J.S., Olejnik, D., 2001. Oxidation of PAHs in Water Solution by Ozone Combined with Ultraviolet Radiation. Int. J. Photoenergy., 3, 95-101
180. Mao, J. et al., 2010. Chemistry of Hydrogen Oxide Radicals (HOx) in the Arctic Troposphere in Spring. Atmos. Chem. Phys., 10, 5823-5838
181. Dunlea, E.J., Ravishankara, A.R., 2004. Measurement of the Rate

Coefficient for the Reaction of $O(^1D)$ with H_2O and Re-evaluation of the Atmospheric OH Production Rate. Phys. Chem. Chem. Phys., 6, 3333-3340

182. Gericke, K.-H., Comes, F.J., 1981. Energy Partitioning in the Reaction $O(^1D) + H_2O \rightarrow OH + OH.$: The Influence of $O(^1D)$ Translational Energy on the Reaction Rate Constant. Chem. Phys. Lett., 81, 218-222
183. Titov, V.A., Khlyustova, A.V., Naumova, I. K., Sirotkin, S.A. and Agafonov, A.V., 2020. Formation Rate and Energy Yield of Hydroxyl Radicals in Water under the Action of Gas-Discharge Plasma. Plasma Phys. Rep., 46, 472–475
184. Mozetič, M., Zalar, A., 2000. Recombination of Neutral Oxygen Atoms on Stainless Steel Surface. Appl. Surf. Sci., 158, 263-267
185. Stafford, L., Guha, J., Donnelly, V. M., 2008. Recombination Probability of Oxygen Atoms on Dynamic Stainless Steel Surfaces in Inductively Coupled O_2 Plasmas. J. Vac. Sci. Technol., A 26, 455-461
186. Singh, H., Coburn, J. W., Graves, D. B., 2000. Recombination Coefficients of O and N Radicals on Stainless Steel. J. Appl. Phys. 88, No.6
187. Chen, J. H., Davidson, J. H. 2002. Ozone Production in the Positive DC Corona Discharge: Model and Comparison to Experiments., Plasma Chem. Plasma Process., 22, 495-522
188. Peyrous, R., 1990. The effect of relative-humidity on ozone production by corona discharge in oxygen or air—a numerical-simulation. 2. Air., Ozone Sci. Eng., vol. 12, 41-64
189. NASA Panel for Data Evaluation, Evaluation Number 19 (2020). [Online]. Available: http://jpldataeval.jpl.nasa.gov/
190. Usm, H. S., 2015. Generation of various radicals in nitrogen plasma and their behavior in media. Phys. Plasmas, 22, 123506
191. Takamatsu, T., Uehara, K., Sasaki, Y., Miyahara, H., Matsumura, Y.,

Iwasawa, A., Ito, N., Azuma, T., Kohno, M., Okino, A., 2014. Investigation of reactive species using various gas plasmas., RSC Adv., 4, 39901-39905

192. Li, S.Z., Wu, Q., Zhang, J., Wang, D., Uhm, H. S., 2010. Development of an atmospheric-pressure homogeneous and cold Ar/O_2 plasma source operating in glow discharge., Phys. Plasmas 17, 063506
193. Khalaf, M. K., Agool, I. R., Muslim, S. H. A., 2014. Electrical characteristics and plasma diagnostics of (Ar/O_2) gas mixture glow Discharge., Int. J. Innov., 3, 113-119
194. Hickling, A., Ingram, M. D., 1964. Contact glow-discharge electrolysis. Trans. Faraday Soc.,60, 783-793
195. Minagawa, Y., Shirai, N., Uchida, S., Tochikubo, F., 2014. Analysis of effect of ion irradiation to liquid surface on water molecule kinetics by classical molecular dynamics simulation. Japan. J. Appl. Phys., 53, 010210
196. Attri, P., et al., 2015. Generation mechanism of hydroxyl radical species and its lifetime prediction during the plasma-initiated ultraviolet (UV) photolysis. Sci. Rep. 5, 9332
197. Lim, J., Hoffmann, M. R., 2019. Substrate oxidation enhances the electrochemical production of hydrogen peroxide., Chem. Eng., 374, 958-964
198. Liu, J., He, B., Chen, Q., Li, J., Xiong, Q., Yue, G., Zhang, X., Yang, S., Liu, H., Liu, Q. H., 2016. Direct synthesis of hydrogen peroxide from plasma-water interactions., Sci. Rep, 6. 38454
199. Dorranian, D., Alizadeh, M., 2014. Effect of negative oxygen ions on the characteristics of plasma in a cylindrical DC discharge., J. Theor. Appl. Phys., 8:122
200. Chen, J., Wang, P., 2005. Effect of relative humidity on electron distribution and ozone production by DC coronas in air. IEEE T PLASMA

SCI. 3, No.2

201. Porter, D., Poplin, M. D., Holzer, F., Finney, W. C., Locke, B. R., 2009. Formation of hydrogen peroxide, hydrogen, and oxygen in gliding arc electrical discharge reactors with water spray. IEEE Trans. Ind. Appl. 45, No.2
202. Herron, J.T., 1988. Evaluated chemical kinetic data for the reactions of atomic oxygen O(3P) with saturated organic compounds in the gas phase. J. Phys. Chem. Ref. Data., 17, 967-1026
203. Matsumoto, T., Wang, D., Namihira, T., Akiyama, H., 2012. "Non-Thermal Plasma Technic for Air Pollution Control". Chapters, in: Budi Haryanto (ed.),Air Pollution - A Comprehensive Perspective, IntechOpen.
204. Kolb, J. F., Joshi, R. P., Xiao, S., and Schoenbach, K. H., 2008. Streamers in water and other dielectric liquids. J. Phys. D: Appl. Phys. 41, 234007
205. Bologa, A., Paur, H.-R., Seifert, H., Woletz, K., 2011. Influence of gas composition, temperature and pressure on corona discharge characteristics. IJPEST, 5, 110-116